Fundamental Studies of Photocatalytic CO_2 Reduction on TiO_2

DISSERTATION

zur Erlangung des akademischen Grades eines Doktors der Naturwissenschaften

- Dr. rer. nat. -

vorgelegt der

Fakultät für Chemie der Universität Duisburg-Essen

von

M.Sc. Martin Dilla

aus Rheinberg

Max-Planck-Institut für chemische Energiekonversion (MPI CEC)

Mülheim an der Ruhr

2019

DOI: 10.17185/duepublico/70231
URN: urn:nbn:de:hbz:464-20190626-143117-6

Kannst du nicht allen gefallen durch deine Tat und dein Kunstwerk,
mach' es wenigen recht; vielen gefallen ist schlimm.

Friedrich Schiller (1797)

Die vorliegende Arbeit wurde vom 01.09.2015 bis zum 31.03.2019 in der Forschungsgruppe „Nanobased Heterogeneous Catalysis“ unter Betreuung von Herrn Prof. Dr. Robert Schlögl am Max-Planck-Institut für chemische Energiekonversion in Mülheim an der Ruhr angefertigt.

Vorsitzender: Prof. Dr. Georg Jansen

1. Gutachter: Prof. Dr. Robert Schlögl
2. Gutachter: Prof. Dr. Jennifer Strunk

Tag der mündlichen Prüfung: 24.06.2019

Danksagung

Herrn Prof. Dr. Robert Schlögl danke ich für die Möglichkeit meine Doktorarbeit am MPI CEC anfertigen zu dürfen. Ich bedanke mich für herausfordernde wissenschaftliche Diskussionen, die in besonderer Weise dazu beigetragen haben, meine Fähigkeiten zur kritischen Auseinandersetzung mit komplexen Systemen maßgeblich weiter zu entwickeln.

Frau Prof. Dr. Jennifer Strunk danke ich für die mehrjährige erfolgreiche Zusammenarbeit. Während ihrer Zeit als Forschungsgruppenleiterin am MPI CEC war ihr mir entgegengebrachtes Vertrauen, kreative Ideen zu entwickeln und zu realisieren, die Grundlage guter und eigenständiger wissenschaftlicher Arbeit. Ihr außerordentliches Interesse am Erfolg ihrer Mitarbeiter und das große Engagement bei wissenschaftlichen Diskussionen waren für mich immer sehr wertvoll.

Herrn Prof. Dr. Martin Muhler bin ich für die Leihgabe von Geräten zur Errichtung meines „Arbeitspferdes“, dem Photoreaktor, sehr zu Dank verpflichtet. Erst dadurch war es möglich neuartige Methoden zur Durchführung photokatalytischer Reaktionen zu erproben, die erheblich zur Qualität und Aussagekraft der durchgeführten Experimente beigetragen haben.

Den Mitgliedern der „Nanocat-Gruppe“ am MPI CEC gilt mein spezieller Dank. Der Teamgeist, das Engagement und die von großem Vertrauen geprägte Zusammenarbeit waren für mich immer von ganz besonderer Bedeutung. Das hervorragende Betriebsklima, die außergewöhnliche Kollegialität und die regelmäßigen kritischen Diskussionen von Ergebnissen haben maßgeblich zum Erfolg meiner Arbeit beigetragen. Jennifer, Simon, Ahmet, Niklas, Alina und Thomas: Ich danke Euch für eine unvergessliche Zeit.

Den Mitarbeitern der Werkstätten des MPI CEC bin ich zu großem Dank verpflichtet. Ohne die professionelle Arbeit des Teams der Geräteentwicklung, allen voran Herr Stephan Syring und Herr Thomas Schneider, wären ein sicherer Betrieb des Photoreaktors und die technische Zeichnung des Rohrwendelreaktors nicht möglich gewesen.

Der größte Dank gilt meinen Eltern und Großeltern. Sie standen mir während meines Studiums immer mit Rat und Tat zur Seite. Ohne diese fortwährende Unterstützung wäre meine Promotion sicherlich nicht so angenehm und sorgenfrei verlaufen.

Stephanie, dir danke ich im ganz besonderen Maß für das Verständnis, die Motivation und die Kraft, die du mir in dieser Zeit gegeben hast. Alexander, du hast mir, ohne es selbst schon wahrnehmen zu können, bei der Verarbeitung so manch anspruchsvoller Situation in der letzten Phase meiner Promotion, sehr geholfen.

Abstract

The present study is dedicated to gaining a better understanding of the photocatalytic CO_2 reduction on P25-TiO_2. Investigations on this highly complex process required designing reactor systems which allow photochemical experiments under conditions of highest purity. The development of procedures for the removal of carbonaceous impurities and photocatalytic activity studies under continuous flow conditions were realized as well. Within the presented studies it was possible to show that CH_4 is the main product of photocatalytic CO_2 reduction with H_2O. The activity is strongly dependent on the concentration of both reactants, the energy range and intensity of the light source, respectively. All these observations indicate that CH_4 is formed in a photoinduced reaction by CO_2 and H_2O. The determination of the apparent quantum yield further points out that photophysical effects, such as the excitation and recombination of charge carriers are potentially less relevant for the low efficiency of the overall product formation. It appears more likely that steps in the reaction mechanism, which could be also promoted by thermal energy, for instance in the formation or desorption of products, determine the rate of product formation. A further aim of this work was to clarify the fate of O_2 as the by-product of the overall CO_2 reduction. Under the assumption that CH_4 is formed in a photocatalytic process by the reactants CO_2 and H_2O it is consistent that O_2 is formed as the by-product. This aspect is commonly neglected by the scientific community. Standard CO_2 reduction experiments with bare TiO_2 as photocatalyst are however usually not accompanied by a detectable formation of gas phase O_2, implying that it has to be consumed someway. In fact, in the study presented here, it could be discovered that the presence of externally dosed O_2 inhibits the CH_4 formation. In order to investigate the absence of gas phase O_2 and the inhibiting effect of the supposed by-product in detail, TiO_2 was modified with H_2O oxidation co-catalysts. As these samples were active in H_2 and O_2 formation, the effect of improved H_2O oxidation properties on the CO_2 reduction was evaluated. It became apparent that the photocatalytic H_2O oxidation is actually not involved in the hydrogenation reaction of the CO_2 reduction on bare TiO_2. Furthermore, a stoichiometric reaction of TiO_2 seems to be associated with the absence of O_2. Consequently, the photocatalytic reduction of CO_2 on P25-TiO_2 cannot be described by a catalytic cycle. Moreover, the consumption of O_2 represents an important factor for the photocatalytic activity of TiO_2, since it prevents an inhibition of the CH_4 formation. The overall study is a contribution to an illustration of the complexity, the challenges and the limitations of investigations in the field of photocatalytic reactions with TiO_2. It is exemplified that progress in the research of photocatalytic CO_2 reduction for chemical energy storage can only be achieved by the development of significantly more complex systems.

Zusammenfassung

Die vorliegende Arbeit ist dem besseren Verständnis der photokatalytischen CO_2 Reduktion auf P25-TiO_2 gewidmet. Die erfolgreiche Erforschung dieses hochkomplexen Prozesses bedurfte der Entwicklung von Reaktorsystemen, die für photochemische Reaktionen unter hochreinen Bedingungen geeignet sind. Dazu zählte auch die Entwicklung von Methoden zur Entfernung von kohlenstoffhaltigen Verunreinigungen von der Oberfläche eines Photokatalysators und zur Durchführung von Aktivitätsmessungen unter kontinuierlichen Flussbedingungen. Im Rahmen dieser Arbeit konnte gezeigt werden, dass CH_4 das Hauptprodukt der Photokatalytischen CO_2 Reduktion mit H_2O ist. Die Aktivität in der CH_4 Bildung ist stark abhängig von den Konzentrationen der Reaktanden und der Energie bzw. der Intensität des eingestrahlten Lichtes. Diese Beobachtungen deuten auf die Bildung von CH_4, basierend auf einer lichtinduzierten Reaktion von CO_2 und H_2O hin. Die Bestimmung der apparenten Quantenausbeute zeigt, dass photophysikalische Prozesse, wie die Anregung und Rekombination von Ladungsträgern, möglicherweise weniger an der sehr niedrigen Effizienz der Produktbildung beteiligt sind. Eine Limitierung ist wahrscheinlich mehr auf Schritte im Reaktionsnetzwerk der CO_2 Reduktion zurückzuführen, die auch durch thermische Energie gefördert werden können. Die Bildung der Produkte aus den extrem stabilen Molekülen CO_2 und H_2O, sowie die Desorption von der Oberfläche des Photokatalysators sind als Beispiele zu nennen. Eine weitere wichtige Beobachtung dieser Arbeit ist, dass das Nebenprodukt O_2 nicht in der Gasphase des Photoreaktors detektiert werden konnte. Sowohl die Reduktion von CO_2 zu CH_4, als auch die Oxidation von H_2O sind Prozesse die O_2 bilden müssen. Tatsächlich konnte beobachtet werden, dass eine externe Zugabe von O_2 sogar eine Hemmung der CH_4 Bildung hervorruft. Die Abwesenheit von O_2 sowie die Hemmung der Produktbildung werden in der Literatur oftmals vernachlässigt. Dabei ist es von essenzieller Bedeutung die Abwesenheit dieses Reaktionsproduktes erklären zu können. In einer Studie unter zusätzlicher Verwendung von Co-Katalysatoren für die Oxidation von H_2O war es möglich, Eigenschaften der photokatalytischen Aktivität des TiO_2 genauer zu analysieren. Die erhaltenen Proben zeigten unter photokatalytischen Reaktionsbedingungen eine merkliche Aktivität in der Bildung von H_2 und O_2. Es wurde aber auch ersichtlich, dass die photokatalytische Oxidation von H_2O sehr wahrscheinlich nicht die wasserstoffliefernde Reaktion in der Bildung von CH_4 darstellt. Die Ergebnisse deuten zudem auf eine stöchiometrische Reaktion von TiO_2 mit O_2 hin, wodurch eine Freisetzung dieses Reaktionsproduktes möglicherweise verhindert wird. Eine solche Reaktion liefert einen entscheidenden Beitrag zur Vermeidung der inhibitierenden Eigenschaften des O_2 auf die Bildung von CH_4. In diesem Fall ist die lichtinduzierte Bildung von CH_4 auf P25-TiO_2 kein katalytischer Kreislauf. Insgesamt ist diese Arbeit ein Beitrag, der die Komplexität, sowie die Herausforderungen und Einschränkungen zur Erforschung der photokatalytischen CO_2 Reduktion aufzeigen soll. Es wird deutlich, dass ein Fortschritt in der Entwicklung von Ansätzen für die chemische Energiespeicherung, basierend auf photokatalytischer CO_2 Reduktion, nur durch ein deutlich komplexeres System als TiO_2 möglich sein wird.

Table of Contents

List of Symbols

Symbol	Denotation	Unit
AQY	Apparent Quantum Yield	%
E	Energy of an electron	eV
E_F	Potential of the Fermi level	eV
$E_{F,n}$	Quasi-Fermi-level of the electrons	eV
$E_{F,p}$	Quasi-Fermi-level of the holes	eV
$E_{F,S}$	Potential of the Fermi-level of the surface	eV
E^0_{Redox}	Standard redox potential	V
E_{vac}	Potential of the vacuum	eV
ΔG	Gibbs free Energy	kJ mol^{-1}
ΔH_f	Enthalpy of formation	kJ mol^{-1}
h	Planck Constant	J mol^{-1} K^{-1}
k_B	Boltzmann constant	J K^{-1}
n_e	Free electron density	
n_{filled}	Number of filled energy levels	
n_h	Free hole density	
n_i	Intrinsic carrier density	
n_{total}	Total number of energy levels	
P	Pressure	Pascal
T	Temperature	K
χ_s	Electron affinity	eV
Φ	Quantum yield	%
ϕ_m	Work function of the metal	eV
ϕ_{SB}	Potential of the Schottky Barrier	eV

List of Abbreviations

Abbreviation	Denotation
ATP	Adenosine triphosphate
AQY	Apparent quantum yield
BID	Barrier Discharge Ionization Detector
CB	Conduction Band
CF	Conflat Flange
DFT	Density Functional Theory
EPR	Electron Paramagnetic Resonance
FEP	Fluorinated Ethylene Propylene
FID	Flame Ionization Detector
GC	Gas Chromatograph
HOMO	Highest Occupied Molecular Orbital
HREELS	High Resolution Electron Energy Loss Spectroscopy
ID	Inner Diameter
IR	Infrared
LED	Light Emitting Diode
LUMO	Lowest Unoccupied Molecular Orbital
MFC	Mass Flow Controller
MS	Mass Spectrometer
NADPH	Nicotinamide adenine dinucleotide phosphate
ND	Neutral Density
NHE	Normal Hydrogen Electrode
OEC	Oxygen Evolving Center
QY	Quantum yield
SR	Surface Recombination
Sat	Saturator
TCD	Thermal Conductivity Detector
UV	Ultraviolet
VB	Valence Band
V_{OX}	Oxygen Vacancy
VR	Volume Recombination

1. Introduction

1.1 The Challenge of Energy Supply in the near Future

The massive use of fossil fuels for energy supply results in an increasing scarcity of the natural reservoirs. About 80 % of the German energy demand in 2016 was provided by fossil energy carriers e.g. oil, hard coal, lignite and natural gas.[1] The energy of fossil fuels is stored in chemical bonds and is commonly released by combustion processes. Thereby H_2O and CO_2 are formed as products of the total combustion. In 2016 the worldwide CO_2 emission was determined with 33.432 Gt, whereby Germany contributed to this enormous value by approximately only 1 %.[2] This human made excess CO_2 cannot be assimilated by the natural carbon cycle,[3] thus it accumulates in our atmosphere. In this way, the atmospheric CO_2 concentration increased from 278 ppm[4], at the beginning of the industrial revolution (around 1750) to 403 ppm[5] in October 2017. CO_2 is a greenhouse gas and is known to affect the climatic conditions and contributes to the global warming. In the long term, it is mandatory to refrain from irreversible burning of fossil fuels and CO_2 emission.[6] In order to meet the demand for energy in the near future, it is rather necessary to develop pathways for the utilization of renewable energy sources and to contribute to a more sustainable energy system. The use of wind power, water power and sun light will play an essential role in this enterprise. The annual global solar irradiation is estimated with $5.5 \cdot 10^6$ EJ[7], whereby the annual energy demand of humankind is estimated with $4 \cdot 10^2$ EJ.[8] Although the use of sun light is challenging due to the volatility and diluted intensity,[6] it becomes obvious that it bears an enormous potential for energetic use and chemical energy storage.[6,9]

1.2 Heterogeneous Photocatalysis

Photocatalysis is the approach to utilize the energy of (sun-) light for a chemical reaction. It is desirable to run a chemical reaction simply with the energy provided by the light and the help of a suitable photocatalyst which lowers the kinetic barrier a of specific reaction. However, a heterogeneous photocatalyst is a highly complex system which needs to exert miscellaneous properties to enable a redox reaction. These properties can be associated with four main functions. The first function is that of a photo absorber, which represents that the material provides charge carriers, under the absorption of photons with sufficient energy to induce an excitation. The second and the third function require an efficient separation of the charge carriers and their transport to the surface of the material, respectively. The fourth function is that of a heterogeneous catalyst. Therefore, it is essential that the material exposes active sites, which bind the reactants in a specific electronic and geometric manner to activate them for the desired charge transfer reaction. In the following these functions will be explained in a more extensive manner.

1.2.1 Physical Background of Semiconductors

Semiconducting materials appear to be suitable with respect to the first function, the absorption of photons and the generation of charge carriers, namely negatively charged electrons and positively charged holes. In general, the formation of electron-hole pairs and the electrical conductivity in solid materials are established by the electron distribution.[10] Every atom in a solid material contributes atomic orbitals for the formation of molecular orbitals. The number of atomic orbitals is equal to the number of molecular orbitals. As a consequence, the number of energy levels is similar as well. The energy differences are getting smaller, the more atoms are contributing to the particle, so that bands of continuous energy levels are created.[11] The Fermi-Dirac statistics describes the ratio between the number of filled energy levels (n_{filled}) and the total number of energy levels (n_{total}) as a function of the temperature (eq. 1.1):

$$\frac{n_{filled}}{n_{total}} = \frac{1}{1+e^{\frac{E-E_F}{k_B T}}} \qquad \text{(eq. 1.1)}$$

where k_B is the Boltzmann constant, E the energy of an electron and E_F the Fermi level. All electronic states filled at $T \approx 0$ K contribute to the valence band (VB) and the unoccupied states form the conduction band (CB). These bands are overlapped in case of a metal or be separated in insulators and semiconductors.[10,11] For the last two materials, there is a forbidden energy gap between the VB and CB which is referred to the band gap (Figure 1).[11] This energy gap, or rather the energetic difference between the VB and CB determines the optical absorption properties of the semiconductor. Another important parameter of these materials is the Fermi level E_F. It is located in the band gap and represents the electronic properties of a semiconductor (Figure 1).

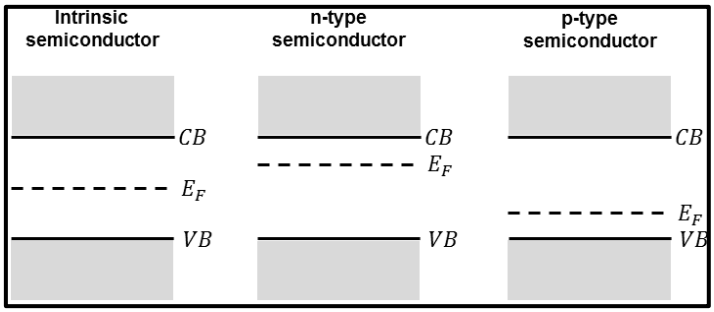

Figure 1: Position of Fermi level in intrinsic, n-type and p-type semiconductors.

From a thermodynamic point of view, it describes the electrochemical potential of electrons in a solid.[11,12] A semiconductor consisting of only one type of atom is termed as intrinsic semiconductor. In such materials, the Fermi level is approximately centered between the CB and VB. The position of the Fermi level can be influenced, for instance, by doping with foreign elements. In case the semiconductor is doped with an element which withdraws electrons from the VB a positive conductivity results.

Negative conductivity results if the doping element donates electrons to the CB. Those materials are termed p-type and n-type semiconductors, respectively, with Fermi-levels located closer to the VB and CB on the energy scale (Figure 1).

1.2.2 Thermodynamic Background and Basics of Photocatalytic Reactions

It is possible to excite electrons from the VB to CB, if the available thermal or spectral energy is greater than the band gap of the semiconductor (Figure 2, top right). Thereby, positively charged holes remain in the VB. In general, the optical transitions in semiconductors can be classified as direct and indirect.[13] The direct transition occurs with the required photon energy and without a change in momentum. In contrast the indirect transition requires an additional phonon.[13] In case of band gap excitation, the overall concentration of charge carriers is increased, leading to a non-equilibrated thermodynamic potential. Thus, two quasi-Fermi-levels related to the electrons $E_{F,n}$ and holes $E_{F,p}$ are required to adequately describe the resulting electronic properties of the semiconductor. (Figure 2, bottom).[11,14,15]

The concentration of majority carriers, consisting of namely electrons in case of n-type semiconductors and holes in case of p-type semiconductors, is not significantly increased due to the excitation. For this reason the $E_{F,n}$ corresponds almost to the Fermi-level of an n-type semiconductor in equilibrium (Figure 2, bottom).[11,16] The same is valid for the $E_{F,p}$ in a p-type semiconductor. However, the CB minimum and VB maximum are a frequently used approximation for the thermodynamic potential of electrons in n-type semiconductors and holes in p-type semiconductors. [16,17] The quasi-Fermi-levels align to E_F with increasing distance from the surface of the semiconductor (Figure 2, bottom).[11,16] This is due to the low penetration depth of photons into a semiconductor, so that the excitation is limited to the surface near region of the material.[16] In general, incomplete filled bands are responsible for the electrical conduction of a semiconductor and the concentration of quasi-free charge carriers and their mobility influences the charge transport in the CB and VB.[11]

After the formation of excited charge carriers they can migrate rather freely through the material, thereby they can undergo various recombination and trapping reactions (Figure 2, top left). For a photocatalytic reaction it is desired that the excited charge carriers become spatially separated and migrate to the surface of the semiconductor to undergo a charge transfer reaction with adsorbed species (Figure 2, top left). In order to achieve this, it is necessary that the band edges span the redox potentials of the desired reaction.[13] More precisely, the photogenerated electrons can only fall spontaneously to lower energy levels on the electrochemical scale. In this regard an electron can reduce an acceptor molecule under the prerequisite that the electrochemical potential for this reaction is less negative than the CB minimum (Figure 2, bottom). For an oxidation reaction it is necessary that the VB edge is more positive than the electrochemical potential. On the basis of kinetic barriers it is possible that an over potential for the oxidation or reduction reaction is required. An effective photocatalyst can reduce this over potential,

hence it assists to improve the rate of a specific reaction. Under these circumstances a semiconductor is also applicable for the second function of a heterogeneous catalyst. If a semiconductor is only capable for the function of a photoabsorber, it can be modified with a co-catalyst. This strategy helps to add active sites for either the oxidation or reduction reaction. Furthermore, a co-catalyst can intensify the charge carrier separation across the interface due to the transfer and storage of electrons or holes from the photoabsorber.[18]

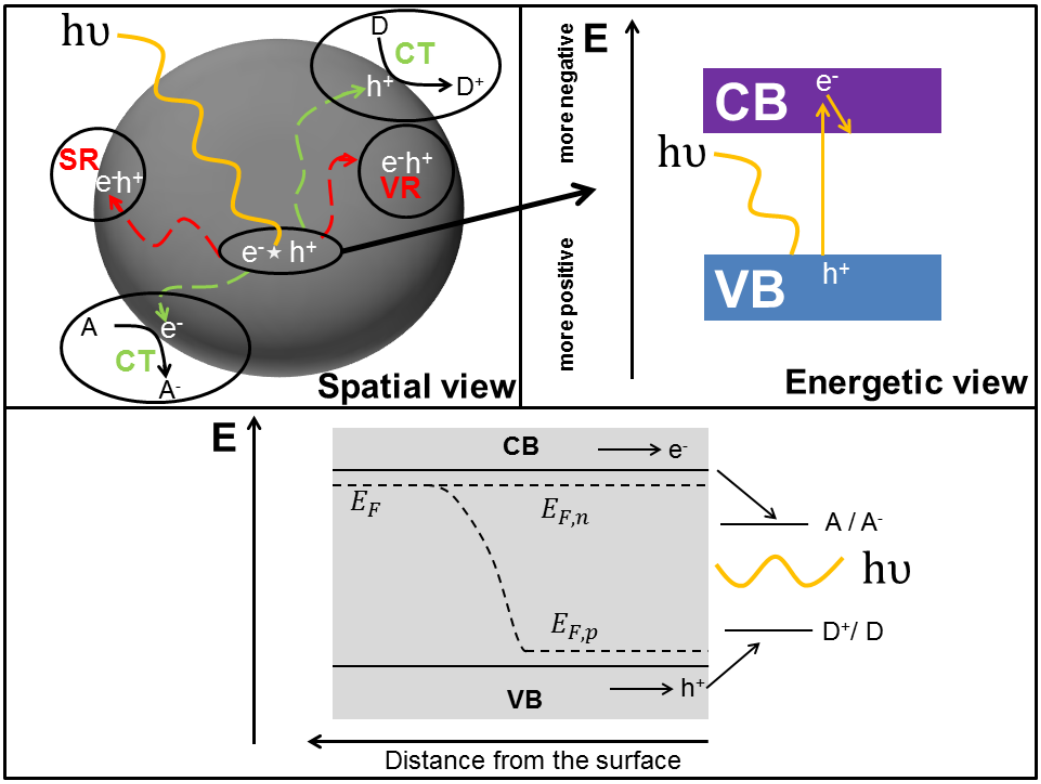

Figure 2: Schematic representation of the light induced events on a photocatalyst. Top left: Spatial view, CT = charge transfer, VR = volume recombination, SR = surface recombination. Top right: Energetic view, VB = valence band, CB = conduction band. Bottom: formation of quasi-Fermi-levels and charge transfer on the surface of n-type semiconductor as a function of the distance to the surface. E_F: Fermi-level, $E_{F,n}$: Quasi-Fermi-level of the electrons, $E_{F,h}$: Quasi-Fermi-level of the holes. Adapted from [17] (top left) and [16] (bottom).

Besides the charge transfer reaction to an adsorbed molecule, there also exists charge carrier recombination. Thereby opposite charges undergo a reaction which each other, whereupon their excited energy is lost for a catalytic reaction. The lifetime of a photogenerated electron-hole pair is therefore in the nanosecond range.[11] Time resolved spectroscopic studies revealed that about 90 % of charge carriers recombine rapidly after excitation.[19] In addition the charge carrier recombination is usually much faster than any charge transfer reaction. On this account the recombination events are the counterpart of the excitation reaction and lower the efficiency of a photocatalytic reaction. In the past many attempts have been tried to suppress the charge carrier recombination by improving the charge separation. Prominent examples are heterojunctions, supported charge traps and bulk doping.[19] Although the recombination of excited charge carriers is undesirable, it carries information on the charge carrier dynamics.[19,20] It is represented by the transfer of an electron from the CB edge or trapped state

to the VB. Recombination reactions proceed in the bulk and on the surface of a semiconductor (Figure 2, top left). These processes are termed volume (VR) and surface recombination (SR), respectively and are associated with the release of spectral and thermal energy.[11,20] The charge carrier concentration, their mobility, defect density, trapping properties and electrical fields influence the rate of recombination in a semiconductor.[11,17,20] A material dependent quantity of the recombination probability is the "diffusion length". It describes the average distance of charge carrier migration before a recombination event takes place.[17] In the end, only a very small amount of charge carriers is capable to escape from recombination to participate in a catalytic reaction. In this context, the quantum yield (eq. 1.2) depicts a number for the efficiency of a photoinduced reaction. It is defined as the ratio between the number of charge carriers, which are consumed for the formation of the desired product and the overall number of photons absorbed by the photocatalyst. It is hypothesized that each photon excites one electron-hole-pair.

$$\Phi(\%) = \frac{\text{number of electrons or holes}}{\text{number of absorbed photons}} \cdot 100 \qquad \text{(eq. 1.2)}$$

A further undesired reaction is when the excited charger carriers undergo oxidation and reduction reaction with the semiconductor itself. As the material is decomposed, this process is called photocorrosion. Whether a semiconductor performs photocorrosion reactions is also determined by the potentials of the particular reaction with regard to the band edge positions. If the potentials for the reaction are within the band gap, then photocorrosion is thermodynamically possible.[21]

1.3 TiO_2 as a Photocatalyst

After four decades of research in the field of photocatalysis, TiO_2 is still one of the most intensively studied materials, because it shows a relatively good efficiency in many photocatalytic test reactions,[22] it is cheap,[22] non-toxic, and it displays an outstanding stability against photocorrosion[11,23]. Specifically, solely the photocorrosion through holes is possible from the thermodynamic point of view, but the decomposition kinetics of this process is extremely slow.[21] Besides the significance of TiO_2 in photocatalytic research, it is also very famous in other applications, for instance as white pigment for cosmetics and paints, in gas sensors, corrosion-protective coatings and ceramics.[24] Furthermore it is used in heterogeneous catalysis as promotor, additive and supporting material.[24]

1.3.1 Crystal phases of TiO_2 and P25

Three major crystalline phases of TiO_2 are known, two of which are tetragonal, the rutile and the anatase phase and the brookite structure, which is orthorhombic. Furthermore, TiO_2 also exists in high pressure forms, namely the monoclinic baddeleyite-like form and the orthorhombic α-PbO_2-like form.[11] The rutile phase is the most common phase that appears in nature.[11] It is industrially synthesized from

ilmenite ($FeTiO_3$) by the chloride or sulfate process.[11] In the chloride process $FeTiO_3$ is chlorinated to $TiCl_4$ and further purified and oxidized to TiO_2. Alternatively, in the sulfate process $FeTiO_3$ is dissolved in sulfuric acid, whereby titanyl sulfate is formed and precipitated. Afterwards a calcination step to TiO_2 is conducted. The enthalpy of formation increases in the order $\Delta H_f(\text{rutile}) < \Delta H_f(\text{brookite}) < \Delta H_f(\text{anatase})$, while the surface energy reveals the reverse trend.[25] The latter induces an effect on the crystal formation especially for very small particles.[25] On this account the synthesis of pure phases can be limited by impurities consisting of the other phases.[26] At temperatures above 580 °C it is possible to transform anatase and brookite into the thermodynamic stable rutile phase.[27] The crystal structures of all three phases consist of Ti atoms surrounded by six O atoms in an octahedral coordination and the interconnection determines the crystal structure. For rutile, half of the octahedral gaps are filled with Ti with has a tetragonal body-centered unit cell on their part.[28] In direction of one lattice axis, long chains of TiO_6 octahedra are resulting which are connected by two edges (on opposite sides).[28] Additionally they are connected by the six octahedral edges and form a three dimensional network. In brookite and anatase, the arrangement of oxygen atoms can be described as cubic close-packed.[28] Half of the octahedral gaps are filled by Ti atoms in a way that each TiO_6 octahedron shares three and four edges, respectively to other octahedra.[28] Due to the formation of the different structures an octahedral distortion occurs. These specific distortions affect the thermodynamic stability as well as the optical and electronic properties of the material.[29-31] It should be noted that the conduction band edge does have mostly Ti 3d character and the valence band edge has O 2p character.[24]

A very prominent type of polycrystalline titania is AEROXIDE® TiO_2 P25 (abbreviated: P25). It is produced by Evonik Industries. In the past it was tried to determine the precise phase composition of P25, where it was found that it consists of anatase and rutile in the ratio of about 70:30 to 80:20.[28] Furthermore, some small amounts of amorphous phases have also been found.[32] Unfortunately, the exact character of interphase connection is not fully understood yet. It was proposed that P25 consists of a unique microcrystalline structure, where the anatase crystallites are in an intimate contact to an overlayer of rutile.[33] In contrast it was also hypothesized that P25 contains separated parts, where either the anatase or the rutile structure exists.[34-36] Clarification of the morphology and the structure-function relationship of P25 is an important step on the way to improve the knowledge of TiO_2 in photocatalytic reactions.

In general, the crystal structure of TiO_2 is commonly not ideal. Miscellaneous defects, for instance point defects, linear defects and planar defects can be found in TiO_2 structures.[11] Thereby, point defects, namely oxygen vacancies (V_{OX}) and Ti interstitials represent the most frequently appearing defects. Ti interstitials are formed under reductive conditions.[11] In this process, titanium ions are transferred from a lattice site to an interstitial site. Under thermal treatment, they tend to migrate from the surface to the bulk.[37] V_{OX} generation takes place under reductive conditions, as well. In addition to that, they can also be formed under illumination with UV light, under thermal treatment in vacuum, and by (non)- metal

doping.[38] The formation of a V_{OX} accompanies the presence of quasi-free electrons[11] and generation of Ti^{3+}.[38] In this process Ti 3d states with energies between 0.75 and 1.18 eV below the CB band minimum of the semiconductor become occupied. For this reason, Titania can be described as an n-type semiconductor.[16] However, there is no general consensus whether the Ti^{3+} states are localized or delocalized.[37] In the localized form the charge would reside at a few Ti or even a single Ti site. On the contrary, the delocalized form could be illustrated as an electron which is spread over an infinite number of Ti atoms.[37] As a consequence of the Ti^{3+} formation, the electronic structure and the charge transport properties are affected. More precisely, the band gap is narrowed, whereby the visible light response is increased, and the charge carrier recombination is slightly lowered due to an improved charge separation.[38] Furthermore, it appears that V_{OX}'s play an essential role in adsorption and activation of reactants for a catalytic reaction.[38] For instance, the Ti^{3+} next to the V_{OX} is supposed to act as an active site for the transfer of electrons to reactant molecules.[39,40] Moreover, the three crystal phases of TiO_2 have different enthalpies of formation for a V_{OX} in which rutile shows the highest enthalpy of formation followed by anatase and brookite, where it is comparably easier to create an oxygen vacancy.[41] Generally, an oxygen deficient TiO_2 crystal can be described by the formula TiO_{2-x}, where x represents the deviation from stoichiometry.

1.3.2 Charge Carrier Recombination, Dynamics and Trapping

Illumination of TiO_2 with photons of appropriate energy to overcome the band gap results in the formation of excited charge carriers. Due to the different band gaps of rutile (3.0 eV) and anatase (3.2 eV)[37] it is required to illuminate with photons of minimum wavelength of 412 and 386 nm, respectively. However, the photocatalytic efficiency of TiO_2 is limited by the fast recombination of charge carriers, which goes along with the release of heat and only limited emission of photons. [19,20,42] A recombination reaction occurs in the range of 1 ps on the surface to 20 ns in the bulk of TiO_2.[20] In contrast charge transfer reaction to adsorbed species is significantly slower. For instance the one electron transfer to an O_2 molecule takes about 10-100 µs.[20] In general it is questionable if the enormous amount of released energy due the recombination reaction does have an impact on chemical reactions occurring on the surface of TiO_2.[19] Such a mechanism is a contradiction to the widely believed charge transfer mechanism, in which the charge carriers need to migrate to the surface of the photocatalyst to participate in a chemical reaction.

After their formation in the bulk, they can either act as free carriers or they can undergo carrier phonon interaction, which is usually termed polaron.[19,43] To which extent charge carriers stay as free carriers or undergo polaron formation is not known.[37] Basically, it can be differentiated between small and large polarons. A small polaron is associated with structural deformations which range only over a small number of lattice sites. When the structural deformation spreads over a huge number of lattice sites, it is conversely termed large polaron. At the surface, the deformation of the crystal is less constricted than

in the bulk. As a consequence, the trapping energy at the surface is larger and charge carriers prefer to move from the bulk to the surface.[43] On this way the polaron has the option to undergo various types of trapping events. In general, trap states are localized both at the surface and in the bulk. The transfer of a charge carrier from one trap state to another is referred to as hopping and can be induced, for example, by thermal energy. A non-thermal trapping is also possible, however, it is determined by the optical properties of the trap state.[19] From the energetic point of view it can be discriminated between shallow and deep trap states.[42] The shallow trap state is located close to the CB edge, so that excitation to the CB or another trapping state is feasible with low amount of energy.[37] If the energetic depth is so large that a simple thermal excitation is not possible it is called a deep trap.[42] For this reason, it is assumed that shallow traps can improve, while deep traps reduce the photocatalytic activity.[42]

In the following the manifestation of charge carrier trapping in TiO_2 will be discussed on the atomic level. In the bulk of TiO_2, electrons are preferentially trapped at Ti^{4+} which then formally becomes Ti^{3+}.[43] Thereby, the electron loses potential energy, because the trap state is lower in energy than the CB.[19] Holes are trapped favorably at lattice oxygen (O^{2-}) which then formally becomes O^{-}. Recombination of the electron hole pair in the bulk is fairly probable, if the two charges are close to one another. At the anatase surface, trapping of electrons occurs preferentially at five-fold coordinated Ti_{5c}^{3+} (1.1) and trapping of holes at bridging oxygen O_{2c}^{-} or in case of a hydroxylated surface on isolated OH groups (1.2).[43] The trapping of holes on surface OH-groups also results in the formation of hydroxyl radicals.[18] Hence, a coexistence of trapped holes and hydroxyl radicals is possible.[18] Photogenerated hydroxyl radicals play an important role on TiO_2, since they are able to induce oxidation reactions of organic compounds adsorbed on the surface.[44]

$$Ti^{4+} - OH + e^{-} \longrightarrow Ti^{3+} - OH \quad (1.1)$$

$$Ti - OH + h^{+} \longrightarrow Ti - \dot{O}H^{+} \quad (1.2)$$

Furthermore, it was found that titanium and oxygen of one surface $Ti - OH$ group bear the possibility to trap an exciton (1.3).

$$Ti^{4+} - OH \xrightarrow{h\nu} Ti^{3+} - \dot{O}H^{+} \quad (1.3)$$

Especially the nature of surface trapped polarons and their interaction with adsorbed species raises some questions. Fundamentally, there are two possible ways how charge carriers undergo a reaction with adsorbed species. In the direct case the charge carriers are transferred to the adsorbed species, while in the indirect case, the charge carriers are trapped before they are transferred to an adsorbed species. It is still not clear if the charge carriers undergo a direct or indirect reaction with adsorbed species. For

mechanistic studies of photocatalytic reactions, it is mandatory to know which species are able to trap electrons and holes.[43]

1.3.3 Band Bending

The electrochemical potential of the band edges in a semiconductor can deviate if one considers them from the bulk to the surface. Only in case of a fully stoichiometric surface and without any adsorbates, the potentials would be equal.[45] In general, deviations from stoichiometry, differences in the electrochemical potentials at phase boundaries as well as adsorption and desorption processes of molecules induce a redistribution of the electronic charges within the TiO_2 particle.[46] As a consequence of this, the bands are bent. The band bending influences the separation and migration of charge carriers in the semiconducting material and across the interface to adsorbed molecules or a co-catalyst.[19] For this reason, band bending is a meaningful concept in photoelectrochemistry and photocatalysis as it helps to understand and predict the behavior of charge carriers.

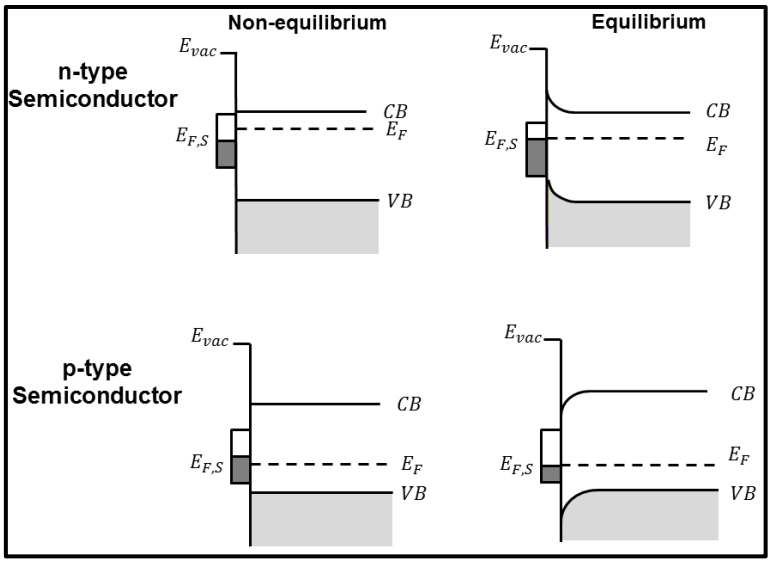

Figure 3: Surface-state-induced band bending. $E_{F,S}$: Fermi-level of the surface, E_{vac}: vacuum potential. Adapted from [47]

In case of an intrinsic semiconductor the bands are flat, as the Fermi-level is equal for the bulk and the surface and no charge transfer occurs between the surface and the bulk. For an n-doped semiconductor, the Fermi-level of the surface ($E_{F,S}$) is lower in energy than the Fermi-level of the bulk ($E_{F,}$) resulting in a non-equilibrated state (Figure 3, top left). In order to reestablish equilibrium conditions, electrons start to migrate from the bulk to the surface. Thereby, the potentials of E_F and $E_{F,S}$ align and the bands are bent upwards (Figure 3, top right). Such phenomena induced by doping are termed surface-state-induced band bending. For a p-type semiconductor the electrons will move from the surface to the bulk and downward band bending results (Figure 3, bottom right). It needs to be stressed that the Fermi-level is almost independent of the bulk dopant concentration due to the large difference between surface states ($\sim 10^{15}$ cm^{-2}) and bulk dopant states ($\sim 10^{8} - 10^{12}$ cm^{-2}).[47] Moreover, the number of surface states

is determined by the type of surface structure of the semiconductor, thus it affects the surface-state-induced band bending as well.[47] Under this circumstance, one semiconductor can show different bending behavior in the different crystalline phases. However, the direction of band bending strongly depends on details of the surface composition.[47] In case of TiO_2 the surface contains lots of defects in the form of V_{OX}'s. The formation of the vacancy is accompanied by an electron transfer from O 2p to Ti 3d. This unpaired electron in Ti 3d shows a donor-like behavior.[19,20,24] For this reason the bands are bent downwards on TiO_2 surfaces.

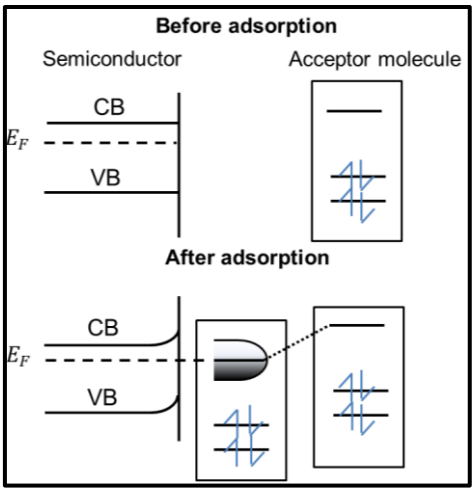

Figure 4: Band bending due to adsorption of an acceptor molecule. Adapted from [45]

A meaningful aspect for the evaluation of the photocatalytic activity is the band bending induced by adsorption. The adsorption of a reactant molecule on the surface of a photocatalyst is a prerequisite for the initiation of the catalytic reaction. When an acceptor molecule approaches to the surface of TiO_2, an unoccupied molecular orbital shifts downwards when it interacts with the solid (Figure 4).[45] In this way the molecular orbital of the adsorbate is broadened due to Heisenberg's uncertainty principle. At the same time electrons are transferred from TiO_2 to the adsorbed molecule so that an electrical field is generated. Thus, a Helmholtz layer is formed and the bands are bent upwards in the surface near region (Figure 4).[45,47] For a donor molecule, electrons are transferred to the semiconductor, whereupon a downward band bending occurs.[47] The resulting band bending caused by adsorption of donor and acceptor molecules is influencing the charge carrier transfer properties in a photocatalytic reaction. On the one hand side an upward band bending due to the adsorption of an acceptor molecule reduces the probability that excited electrons are transferred from the semiconductor to the adsorbed species. On the other hand side upward band bending facilitates the transfer of holes from the semiconductor to the adsorbed molecule.[45] It is obvious that adsorption induced band bending affects the efficiency of charge carrier transfer in a photocatalytic reaction.

Another parameter which causes charge carrier migration and band bending is when a semiconductor is brought in contact with a metal. This is a significant factor, since it can improve the activity of a metal

modified semiconductor. Once a semiconductor is in contact with a metal, electrons start to migrate according to the difference in work function of the two materials.[47] The work function describes the energy which is necessary to excite an electron from a solid material to an adjacent vacuum. Here, the difference in work function at metal-semiconductor interfaces represents the driving force for the charge carrier migration across the interface, thus the extent of band bending. The direction of charge carrier flow is a decisive factor for the activity of a photocatalyst. If the work function of the metal is larger than that of TiO_2, electrons are transferred from the semiconductor to the metal.[47] Therefore, the metal becomes negatively charged and an electrical field is generated. An electron which is transferred to the metal experiences repulsion due to the negatively charged Helmholtz layer of the metal. As a consequence, the potential energy rises up and the bands are bent upwards.[47] The electron transfer ceases, as soon as the Fermi level of the metal and the semiconductor ($E_{F,m}$ and $E_{F,s}$) are aligned.[47]

$$\phi_{SB} = \phi_m - \chi_s \qquad \text{(eq. 1.3)}$$

In this process a Schottky barrier ϕ_{SB} is formed. It is defined as the difference between the work function of the metal and the electron affinity of the semiconductor (eq. 1.3). This barrier can serve as an electron trap, hence it prevents electrons and holes from recombination. If the work function of the semiconductor is larger than that of the metal no Schottky barrier is formed and the electron transfer direction is reversed. However, most of the metal work functions are larger than that of TiO_2, so that the latter occurs less frequently.

The region in which the band bending prevails is termed space charge region. It can be differentiated between three types of space charge regions (Figure 5). If electrons are transferred to an adsorbate or a metal, then fewer electrons are available in the surface region of the semiconductor. As a depletion of charge carriers takes place, the bands are bent upwards and the space charge region is called depletion layer (Figure 5, left). In contrast, if the electrons are accumulated in the semiconductor and the bands are bent downwards, the space charge region is called accumulation layer (Figure 5, middle). The third form is the inversion layer. It can be generated, for example, when the electrons are depleted in the surface near region below the intrinsic level (n_i). Then the n-type conductivity is converted to p-type in the surface near region. The formation of an inversion layer is depicted in the middle of Figure 5, right.

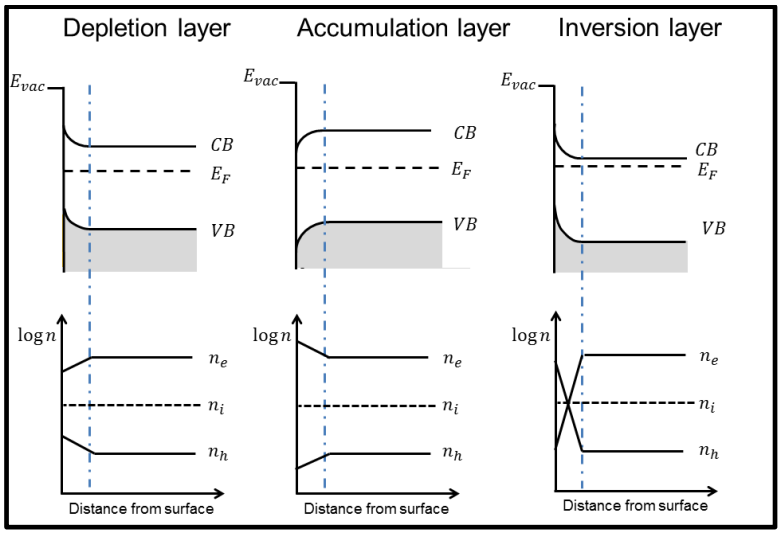

Figure 5: Types of space charge region. n_e: free electron density, n_h: free hole density, n_i: intrinsic carrier density. Adapted from [47]

1.3.4 Photocatalytic Activity

Most of the studies in photocatalysis are dealing with rutile and anatase phases, while the brookite phase is rarely investigated.[22] A potential reason is the difficulty to synthesize brookite as a phase pure material.[22] Due to impurity phases of rutile and anatase in brookite crystals, which are formed during the synthesis, it becomes rather difficult to evaluate the true activity of this phase. In many test reactions it appears that anatase is more active than rutile.[48] Differences in the activity of the two phases are mainly attributed to the electronic and optical properties. The VB edges of both crystal phases are roughly at the same position. However, the position of the CB edge differs due to different band gap energies. The band gap of rutile with 3.0 eV is smaller than that of anatase with 3.2 eV.[43] Thus, the anatase phase does have a more negative CB edge compared to rutile.[48] For this reason the excited electrons are more reductive which is advantageous with regard to the overpotential of a reduction reaction. Furthermore, the charge carrier recombination kinetics also affect the activity of anatase and rutile. The electronic transitions in rutile might be characterized as direct.[49] In contrast anatase is an indirect semiconductor. For this reason a strong electron phonon-coupling influences the recombination.[50] In addition, anatase shows a more pronounced surface band bending, resulting in a steeper potential compared to rutile, so that the charge separation is improved in anatase.[51] According to that it was found that in rutile only the surface near holes can migrate efficiently to the surface, so that the bulk recombination is dominating.[51] For these reasons, the rate of charge carrier recombination in anatase might be lower than in rutile and therefore the lifetime of excited charge carriers is improved.[49] An extended life time of these charge carriers increases the probability to participate in a surface catalytic reaction before they recombine. Next to the investigation of the pure TiO_2 phases in photocatalytic research, polycrystalline materials are also very popular, because they often show a better performance in many test reactions compared to the single phase. One of the most frequently used polycrystalline phases in photocatatlytic research is P25.[34] Especially its outstanding activity might be

one of the reasons, why P25 is common as a reference and benchmark material.[32] On this account it is desirable to get knowledge about the structure-function relationship of the interconnection between anatase and rutile, which could contribute to a better understanding of the photocatalytic activity of TiO_2.[34] It is hypothesized that the superior activity of P25 is based on an improved charge separation due to the transfer of charge carriers between the anatase and rutile phase.[32] As a result of this charge carrier transfer, they can escape from recombination, thus their life time is enhanced and the probability to participate in a photocatalytic reaction is improved as well. Furthermore it is assumed that the charge carrier transfer proceeds very fast.[51] Until now there is no consensus about the direction of charge carrier transfer between the phases.[51] According to the band edge positions of anatase and rutile, it would be expected that the electrons are transferred from the anatase to the rutile phase (Figure 6 A). This observation has been made in several studies.[33,52,53] However, other research groups found the reverse charge carrier transfer direction to occur.[52,54] Such a transfer could be realized by an electron transfer from higher-level rutile CB states to anatase lattice trapping sites (Figure 6 B).[52,54] Subsequent to this, the electrons migrate to anatase surface trap states.[52,54] In this scenario the visible light response, due to the smaller band gap of rutile, could also extend the excitation of charge carriers more into the visible region. Admittedly, an improved charge separation might not be the only reason for explaining the activity of P25. It was also assumed that the formation of interfaces between anatase and rutile could result in exposure of highly active sites.[51,52]

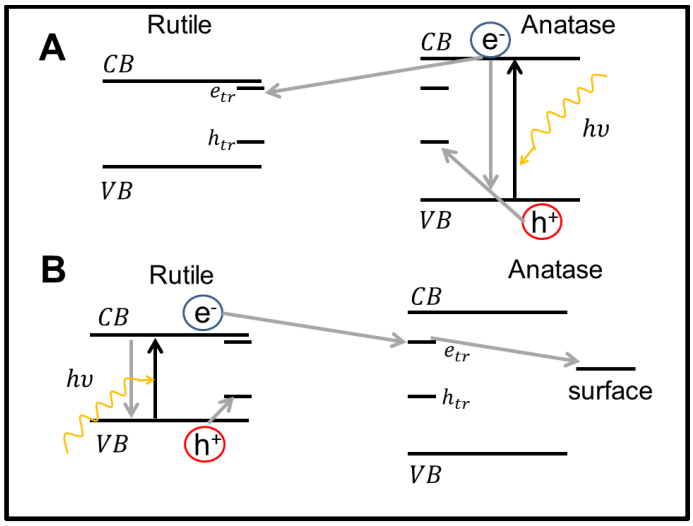

Figure 6:A: Model of P25 activity where charge separation occurs on anatase and rutile acts as an electron sink. B: Model of P25 activity of a rutile antenna and subsequent charge separation. Adapted from [54]

1.4 CO_2 Reduction and H_2O Oxidation for Chemical Energy Storage

In regard of the environmental consequences of the massive use of fossil fuels, namely its scarcity and the accumulation of CO_2 in our atmosphere, it becomes desirable to make use of this greenhouse gas as a raw material. Namely in a solar driven chemical conversion to higher energy compounds, like CO,

HCOOH, CH_3OH and CH_4.[17,19] Such products are often termed "solar fuels"[55]. They can be combusted or used in fuel cells and allow to close the carbon cycle.[17] On this account solar fuels could help to contribute to a more sustainable energy system. Furthermore, solar fuels could also be used as a feedstock for chemical synthesis, replacing fossil fuels in this application.[17]

1.4.1 The Biological Photosynthesis as a Role Model

The most famous process driving the reduction of CO_2 and oxidation of H_2O is the biological photosynthesis. It is a light driven process which converts light energy into chemical energy. The creation required about three billion years and is a milestone in the evolution of life on earth as it produces O_2 and biomolecules, such as carbohydrates ($C_m(H_2O)_n$). The overall photosynthesis can be divided in two complementary processes, namely the light dependent oxidation of H_2O and the light independent reduction of CO_2.[56] Consequently protein-complexes such as the photosystem I and II have the primary function to utilize the energy provided by the sun light for biological energy storage.[57]

Oxidation of H_2O to O_2 is realized by the photosystem II. The catalytic core of photosystem II is a tetramanganese-calcium cluster ($CaMn_4O_5$), which represents the oxygen evolving center (OEC).[57] The OEC catalyzes the oxidation of H_2O by cycling through five meta-stable states. For that photons with an energy of about 1.8 eV are used, which corresponds to red light.[56] Photons with higher energy are also absorbed, but internal conversions by light harvesting pigments degrade their energy to that of red light, whereby heat is released.[56] The energy provided by the splitting of H_2O is stored in the form of ATP (Adenosine triphosphate) and NADPH (Nicotinamide adenine dinucleotide phosphate).[57,58] Both ATP and NADPH are required for the fixation of CO_2 in the dark reaction.[56,58] The overall reaction is referred to as the Calvin-cycle and includes three phases, the carbon fixation, the reduction and the regeneration.[58] The fixation of CO_2 is conducted by Ribulose-1,5-bisphosphate and additional energy is provided by photosystem I,[56,59] leading to the formation of 3-Phosphoglyceric acid. The carboxylic group (-COOH) of 3-Phosphoglyceric acid is then reduced to a carbonyl group (-CHO), so that 3-Phosphoglyceraldehyde is formed. In this reaction ATP and NADPH are consumed.[58,59] A part of this aldehyde serves as intermediate for the formation of carbon hydrates, for instance, glucose, sucrose, lipids and proteins. In addition 3-phosphoglyceraldehyde and ATP are also used for the regenerative formation of Ribulose-1,5-bisphosphate.[59] The consumed amounts of NADPH and ATP are also regenerated to close the catalytic cycle.[59] Under consideration of the light dependent and the dark reactions, the overall reaction equation to, for instance, glucose can be written as:

$$6\,CO_2 + 6\,H_2O \longrightarrow C_6H_{12}O_6 + 6\,O_2 \qquad (1.4)$$

For each electron which is utilized from H_2O oxidation to reduce CO_2 the absorption of two photons with sufficient energy is required. This is the consequence of the combination of two photosystems.[56]

The photosystem II uses the light to run the extraction of electrons and protons from H_2O and the photosystem I utilizes the light to provide additional energy for the CO_2 fixation.[56,57] Consequently, the formation of one O_2 or the fixation of CO_2 requires the energy of at least eight photons corresponding to the red light.[56] The formation of a glucose molecule, with an energy content of 2813 kJ/mol requires the absorption of at least 48 photons with a wavelength of 680 nm.[56]

In general the efficiency of the biological photosynthesis with solar light into biomass is below 1 %.[60] Although the number appears to be small, it needs to be stressed that the loss of energy is mainly based on the degradation of higher energy photons for driving a significant number of reactions associated with the metabolism, reproduction and survival of the photosynthetic organism.[56] Overall it shows that photosynthetic organisms are extremely proficient to utilize the energy provided by the sun to ensure their viability. For this reason the natural photosynthesis is likely the best, although probably also the most complicated role model for the development of strategies for the formation of renewable energy sources.

1.4.2 Photocatalytic CO_2 Reduction

In the past different ways have been investigated in order to reduce CO_2 in solar driven processes. This means homogeneous approaches with, for instance, metal complexes of Ru and Re and heterogeneous approaches with solid-liquid or solid-gas interfaces using semiconductors like TiO_2 or ZnO as the photocatalyst.[17] In general it can be discriminated between pure photocatalytic and photoelectrochemical approaches. The latter represents the integration of both electrocatalysis and photocatalysis. In case of photoelectrochemical experiments, an external bias is used for facilitating the separation of photoexcited charge carriers while the overpotential is reduced due to the extra light illumination.[61] Primarily, this work focuses on the heterogeneous pure photocatalytic approach. The scientific interest in heterogeneously catalyzed CO_2 reduction increased since the initial report of Inoue et al.[62] in 1979. They tested various semiconductors in the CO_2 reduction resulting in the formation of HCHO and CH_3OH. There are also existing reports dealing with the formation of CH_4, C_2H_6 and CO as possible products of CO_2 reduction.[63-65] However, the yields were extremely low. In the past various strategies for improving the activity have been tried. Most of the modifications try to achieve an increase in the visible light absorption properties, for instance by (non-)metal ion doping.[20,66] Furthermore, suppression of the charge carrier recombination is another goal of photocatalyst modification.[67] Another approach is the use of plasmon-active particles, for instance Au and Ag.[68-70] However, many studies dealing with a variety of photocatalysts, with quite different activities and selectivity were published within the last three decades of research in this field. It needs to be stressed that it was impossible to make any significant breakthroughs in the efficiency.[71] The rate of product formation is still far away from any application on the industrial scale.[72] A major issue is the poor knowledge about the details of this highly complicated reaction on the molecular level. Especially the reaction mechanism

might be a key parameter for the development of efficient photocatalysts. It has been suggested that improving the photocatalytic CO_2 reduction is only achievable if there would be an in-depth understanding of the reaction mechanism.[17]

The CO_2 reduction, for instance, to CH_4 is represented in reaction (1.5). In this process the oxidation state of the carbon atom changes from +4 to -4, for which 8 electrons have to be transferred. At the same time, two C=O double bonds are cleaved and the formation of 4 C-H bonds takes place.

Reduction: $$CO_2 + 8\,H^+ + 8\,e^- \longrightarrow CH_4 + 2\,H_2O \qquad E^0_{Redox} = -0.24\,V \qquad (1.5)$$

Oxidation: $$2\,H_2O \longrightarrow O_2 + 4\,H^+ + 4\,e^- \qquad E^0_{Redox} = +0.82\,V \qquad (1.6)$$

Overall Reaction: $$CO_2 + 2\,H_2O \xrightarrow{hv,\ photocatalyst} CH_4 + 2\,O_2 \qquad (1.7)$$

However, apart from the CO_2 reduction, a second reaction which delivers electrons to be transferred is required. Moreover, it becomes obvious from reaction 1.5 that a source of hydrogen is needed for the hydrogenation reaction. On the basis that H_2 does not naturally exist and its synthesis is usually based on fossil fuels,[71] it would be useful, in the ecological sense, to use H_2O as the hydrogen source. Using of H_2O requires that it can be split in order to make use of the hydrogen. Therefore, H_2O needs to be oxidized (1.6). The products of this reaction are O_2, H^+ and electrons. It needs to be considered that the reactions 1.5 and 1.6 are in reference to the normal hydrogen electrode (NHE). The potentials are calculated from half-cell electrochemical measurements at pH 7.[17,63] The overall CO_2 reduction to CH_4 can therefore be represented by reaction 1.7.

1.5 Obstacles in Photocatalytic CO_2 Reduction

1.5.1 Thermodynamics of Photocatalytic CO_2 Reduction

The attempt to perform a chemical reaction with CO_2 and H_2O is in fact challenging, because these molecules are thermodynamically extremely stable. This is why CO_2 reduction and H_2O oxidation, respectively require a significant input of energy. The overall photocatalytic CO_2 reduction with H_2O (1.7) does have a change in Gibbs free energy of $\Delta G = +818\ \mathrm{kJ/mol}$. On this account the reaction is thermodynamically uphill. However, a reaction is only catalytic by definition, when the change in Gibbs free energy is negative ($\Delta G < 0$). Hence, the CO_2 reduction and H_2O oxidation are not true catalytic processes. Nowadays it is common practice to use the term photocatalytic, but it would be more reasonable to use the term photosynthetic.[17] For this reason CO_2 reduction is an example of the term "artificial photosynthesis".[73]

1.5.2 Activation of CO_2 and H_2O on TiO_2

The stability of the CO_2 molecule and the low electron affinity[17,74] causes its low tendency to participate in a chemical reaction. From the thermodynamic point of view, proton coupled multi- electron reactions are more favorable in comparison to single electron reductions, because they result in the formation of thermodynamically stable products.[17] Reaction (1.5) is an example of such a reaction. Until now there is no evidence of the existence of such concerted multi-electron transfer processes.[18] Alternatively, it is conceivable that the reactions are conducted in a series of one electron transfer processes.[17] Considering that the CO_2 reduction proceeds by a series of one-electron-transfer processes, then the first step (1.8) will be a severe obstacle.[75,76]

$$CO_2 + e^- \longrightarrow C\dot{O}_2^- \qquad E^0_{Redox} = -1.9\,V \qquad (1.8)$$

An important prerequisite for charge carrier transfer is an adequate symmetry and overlap of the molecular orbitals. It has been found by Indrakanti et al.[77] that the orbital overlap is only sufficient, when the surface contains V_{OX}'s. The extra electron of the Ti^{3+} species can be transferred to the CO_2 molecule and $C\dot{O}_2^-$ is formed. The anion of CO_2 is thermodynamically metastable, but kinetically stabilized.[78] Thus, it has an average lifetime of 60-90 µs and can be identified with spectroscopic methods.[78] Another important factor for the addition of an electron is breaking the symmetry of the linear CO_2 molecule due to the repulsive forces of the free electron pairs of the oxygen atoms. As a consequence the $C\dot{O}_2^-$ has a bent structure. This conformation is highly unfavorable and therefore the LUMO of the CO_2 molecule is located at a high energy.[78] Without a specific interaction of CO_2 with the photocatalyst and lowering of this potential, virtually no conduction band edge of any known semiconductor exhibits adequate potential to allow the first one-electron transfer. A study of Freund and Roberts[78] states that changes in the optimal O-C-O bond angle of 180 °, does have an impact on the energy of molecular orbitals. More precisely, the LUMO of CO_2 decreases with the bond angle, thus the electron affinity increases.[78] Hence, it is conceivable that the adsorption on TiO_2 results in the formation of a partially charged and bent structure of CO_2. Such an interaction between the photocatalytst and the reactant may improve the transfer of electrons. In general, there are a number of adsorption modes of CO_2 on TiO_2 (Figure 7). Thereby, Lewis acidic Ti sites and basic lattice oxygen are interacting with the Lewis basic oxygen and Lewis acidic carbon atom of CO_2, respectively and linear and bent adsorption modes are resulting. The formation of a bent mode is favored on defective TiO_2 surfaces.[77]

It can be also noticed by regarding the adsorption modes that further species with a bent structure can be formed (Figure 7). These adsorbates are carbonates and bicarbonates. The bicarbonate structures include an OH group, while the carbonates do not. Both Ti and O can be involved in the adsorption of carbonates. In case that adsorption originates from one surface atom, the species is named monodentated

carbonate. Bidentated carbonates are bound to the surface of the substrate with two covalent bonds. For this reason these adsorbates might also play a role in the mechanism of photocatalytic CO_2 reduction. Until now there is no general consensus which of the CO_2 adsorption modes is sufficiently activated for a CO_2 reduction. It is still under debate if either adsorbed CO_2 or carbonates are the initial step in product formation of photocatalytic CO_2 reduction on TiO_2.

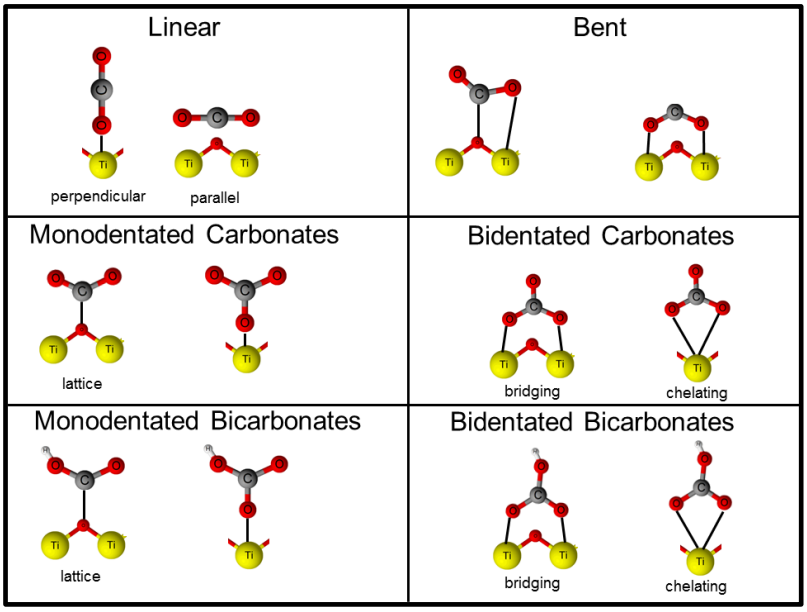

Figure 7: CO_2 and carbonate adsorption modes on TiO_2. Adapted from [38]

The second reactant H_2O does also have a specific interaction with the surface of TiO_2. On a defect free surface, H_2O is mainly adsorbed as a molecule.[79] In the presence of V_{OX}'s, H_2O is predominantly adsorbed in a dissociative manner.[79] Thereby, the V_{OX} is replenished and two surface OH-groups are formed. It has been initially proposed by Salvador[80] that the oxidation of the surface OH-groups (1.9) may appear as the initiating step of H_2O photooxidation.

$$Ti - O - H + h^+ \longrightarrow Ti - O^{\cdot} - H \tag{1.9}$$

$$Ti - O - Ti + H_2O + h^+ \longrightarrow Ti - O^{\cdot} \cdots H - O - Ti + H^+ \tag{1.10}$$

In contrast Nakamura an co-workers[81,82] suggested that a nucleophilic attack (1.10) of the H_2O molecule on the surface trapped hole might be more likely for the initiation of H_2O oxidation. Such a reaction can be described as a Lewis-acid-base type reaction and therefore the energetics and kinetics compared to the charge transfer reaction of (1.9) are different. In a DFT based study of Li and Selloni[83] it was further verified that the nucleophilic attack is more favored on rutile compared to anatase. This is mainly due to the high activation barrier on the anatase phase.[83]

1.5.3 Literature Review – Mechanism of Photocatalytic CO_2 Reduction

The photocatalytic reduction of CO_2 on TiO_2 is based on a multitude of steps. In general, the reaction pathway includes the following steps: adsorption of the reactants on TiO_2, activation of the adsorbed reactants by photogenerated charge carriers, formation of intermediates on the catalyst surface, conversion to final products, desorption of products and the regeneration of the catalyst.[72]

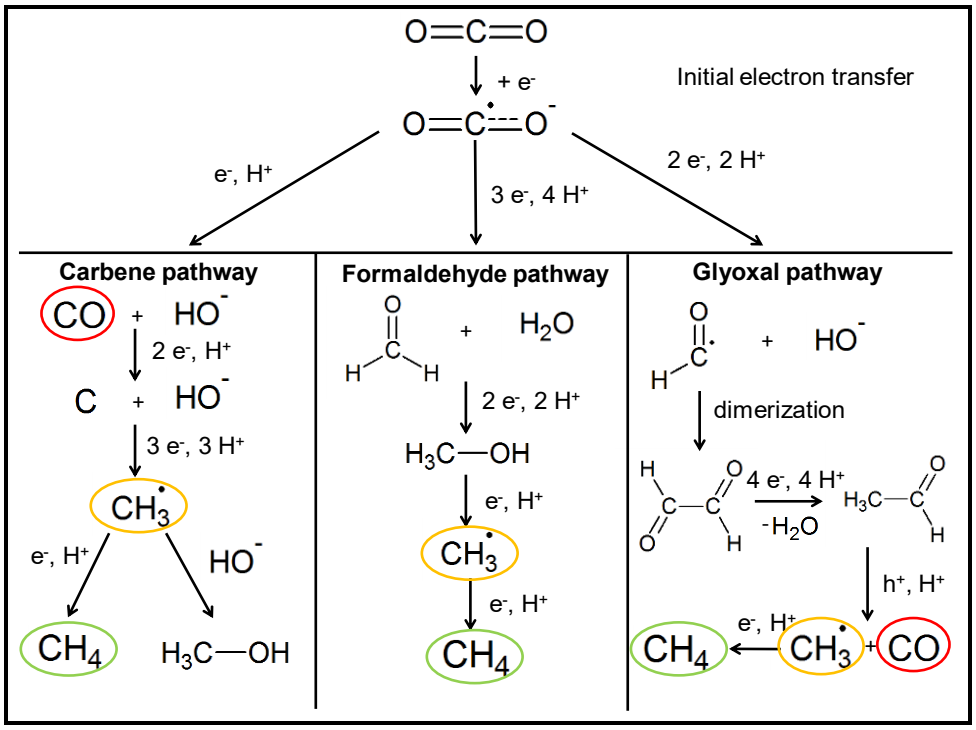

Figure 8: Carbene, formaldehyde and glyoxal pathway.[17,64,84]

The mechanism of product formation in photocatalytic CO_2 reduction is not understood. It is still a matter of debate how the product formation is realized on the molecular level. It is desirable to identify intermediates and the reaction pathway, so that kinetic barriers related with slow steps can be improved.[72] In the literature different mechanisms are proposed for the formation of CH_4.[17,64,84] But none of these has been supported with sufficient evidence to be generally accepted by the scientific community. Three different pathways (Figure 8) and scientific reasons for their limited validity are presented in the following. These mechanisms have one similarity. The product formation starts with a one electron transfer to the CO_2 molecule. On the basis of this initial step, the carbene pathway assumes CO to be an intermediate of the photocatalytic CO_2 reduction leading to CH_4 (Figure 8). However, it has been found that CO is not consumed in a photocatalytic reaction when TiO_2 is used as the photocatalyst.[72] So it appears unlikely that CO is an intermediate of a consecutive reaction on TiO_2. Another mechanism presumes methanol and formaldehyde as intermediates of the photocatalytic CO_2 reduction (Figure 8). Unfortunately, it was figured out that these species have no electron affinity, thus it is unlikely that these molecules will accept electrons. Consequently, they will be not further reduced

to CH_4.[64] Furthermore, it has been observed that these molecules tend to be decomposed to CO_2, CO and H_2 under photocatalytic reaction conditions.[72] This is potentially due to the favorable hole consuming oxidation reaction.[72] To conclude, it appears implausible that these species are relevant for the photocatalytic formation of CH_4. A further mechanistic consideration is the participation of C_2 intermediates in the product formation of photocatalytic CO_2 reduction. The first C_2 mechanism has been published already in 1981 by Amatore et al.[84]. In a study by Shkrob et al.[64] the appearance of C_2 intermediates has been further investigated. They suggested the formation of ethanedial from two formyl radicals as the first C_2 intermediate on the way to CH_4 (Figure 8). Unfortunately, it has been observed that ethanedial and other C_2 intermediates, which contain carboxyl or aldehyde groups also tend to be decomposed to CO_2, CO and H_2 under photocatalytic reaction conditions.[72] In contrast, C_2 molecules containing a methyl group, for instance acetaldehyde, showed significant formation of CH_4.[72] To sum up, there is a need for further research to obtain information about the product formation and intermediates of the photocatalytic CO_2 reduction on TiO_2.

1.5.4 Literature Review – Fate of O_2 in Photocatalytic CO_2 Reduction

The stoichiometry of CO_2 reduction leading to CH_4 (1.7) presupposes the formation of O_2. Both reactions the reduction of CO_2 and the oxidation of H_2O, are processes where O_2 is formed as the second reaction product. However, with some exceptions[85-89] the reports of CO_2 reduction focus mainly on the formation of carbon related products, but less attention is paid to the fate of O_2 as the by-product. It is often not included to the analysis or absent in the product distribution. By definition a reaction is catalytic, when all reactants are converted to the final products and desorb from the surface afterwards. In a stoichiometric reaction, however, the catalyst is not involved. In order to verify if the photocatalytic CO_2 reduction is a true catalytic cycle, it is of fundamental interest to clarify what happens to every product species. In this case it is essential to better understand how O_2 and O-derived intermediates interact with TiO_2. It is furthermore interesting to investigate which further reactions with reactants, products and the photocatalyst are possible with O_2 under illuminated reaction conditions. In general, three pathways which could be relevant for the absence of O_2 in the product distribution of photocatalytic CO_2 reduction are conceivable. First of all, the H_2O oxidation reaction, which comprises the transfer of four holes per O_2 molecule, is a complex process associated with significant overpotentials.[90] If no external bias or sacrificial agent is used and the process in driven purely photocatalytically, kinetic limitation might be accountable.

Secondly, molecular oxygen does have miscellaneous ways to undergo reaction with TiO_2. The reduction of O_2 to the superoxide radical ($O_2^{\bullet-}$), for instance, is thermodynamically possible, because the redox potential of this reaction (1.11) is less negative than the CB edge of TiO_2.[91]

$$O_2 + e^- \longrightarrow O_2^{\cdot -} \qquad E^0_{Redox} = -0.137\ V \qquad (1.11)$$

It has been observed that this reaction occurs after O_2 has been chemisorbed on TiO_2.[92] It can be differentiated between two $O_2^{\cdot -}$ adsorption modes, namely the α-O_2 and the β-O_2, which coordinate side-on and end-on to the surface of TiO_2, respectively. Carter et al.[93] found evidence that α-O_2 enables the replenishment of V_{OX}'s. Thereby an oxygen adatom is formed as well. A study of Ishibashi et al.[94] investigated the O_2 reduction on TiO_2 under the influence of UV light irradiation. The formation of $O_2^{\cdot -}$ has been observed under the applied reaction conditions.[94] Furthermore, the authors argued that $O_2^{\cdot -}$ has a relatively low mobility on the surface of TiO_2 and is immediately deactivated by transferring one electron back to TiO_2 as soon as the irradiation ends.[94] Nakamura et al.[95] investigated the O_2 reduction on TiO_2 films in the liquid phase. In addition to the formation of $O_2^{\cdot -}$ it was found out that the formation of surface superoxo, surface peroxo, surface hydroperoxo, hydroperoxo radical and hydrogen peroxide takes place.[95] These reactions involve the accessibility of electrons and H^+.

The backward reaction which is represented by the oxidation of for instance CH_4 might count as a third possible reason for the absence of O_2 under illuminated reaction conditions. Highly reactive hydroxyl radicals, formed on TiO_2 in the H_2O oxidation process and also $O_2^{\cdot -}$ could play a role in the backward reaction of CO_2 reduction.

1.5.5 Characteristics of Photoreactors and Experimental Design

The basis to obtain reliable data of photocatalytic CO_2 reduction experiments is strongly associated with the design of the photoreactor and the choice of experimental conditions. Performing activity studies of a photocatalyst without former pretreatment in order to remove impurities is meaningless. It is to be expected that the surface of semiconductor based photocatalysts supplies small amounts of adsorbed carbonaceous impurities.[65,70,72] They originate mostly from solvents and sacrificial agents during the sample synthesis or modification, for instance the deposition of a metal co-catalyst.[70] In addition carbonaceous impurities can also adsorb from the environment. The exact type of these species and especially their behavior under photocatalytic reaction conditions is often not known. They may desorb or undergo a charge transfer reaction on the photocatalyst. Isotope labelled $^{13}CO_2$ experiments are one option to differentiate if product formation originates from CO_2 or from impurities. A study by Yang et al.[96] dealing with isotope labelled $^{13}CO_2$ reduction on Cu(I)/TiO_2 verified the formation of products from impurities. Although the amounts are in fact very low, they can have a substantial effect on the experimental results, since the formation rate due to impurities is often in the range of products from the photocatalytic process of interest.[72] Hence, the actual rate of CO_2 reduction is overestimated, which results in wrong experimental data. On this account it must be considered that impurities can be generally responsible for the appearance of products similar to those of CO_2 reduction. Therefore it is

essential to realize experiments under conditions of highest purity. Only a surface without contaminants is the basis for product formation from CO_2. One reasonable option to remove carbonaceous impurities from the sample is calcination, but as the only pretreatment step it is usually not sufficient to achieve the required purity. The group of Mul[65] were the first introducing a procedure based on illumination under moist Helium, to remove impurities prior to the activity study. Such conditions allow the oxidation of organic molecules due to photogenerated charge carriers. The cleaning process is continued until no more carbon containing species leave the sample. At the same time the cleaning process is a blank experiment, which controls if all experimental conditions are similar to those of the activity test except for the presence of CO_2. When the cleaned sample is used for the test reaction, all formed products can be assigned to CO_2 reduction.

The development of a reactor is associated with versatile considerations and limitations to realize experimental conditions to obtain reliable and, in particular, objective scientific information. Basically it can be differentiated between batch and flow type reactors. In batch systems the reactants are added to the reactor beforehand to the reaction. In the following the reactor is sealed and after starting the reaction, only the chemical processes are able to change the molecular composition of the investigated atmosphere. However, such mode of operation allows accumulation of products and opens the opportunity of having undesired backward and consecutive reactions. In contrast continuous flow reactors lower the possibility of those reactions, as the concentration of the product molecules is kept low due to the permanent exchange of the atmosphere. Especially when mechanistic details are the object of interest it is useful to minimize backward and consecutive reactions, thus the application of continuous flow experiments is the more advantageous approach. A specific parameter influencing the continuous flow conditions is the geometry of the reactor, since it also determines the illumination conditions. On the one hand side, it is desired to have a maximized interaction between the reactants and the photocatalyst, to get optimal adsorption and desorption dynamics of the participating molecules. On the other hand side, the illuminated area inside the reactor should be as large as possible to maximize the extent of photoexcitation. In many cases it is not possible to accomplish both requirements with one reactor geometry.

After decades of photocatalytic research an enormous number of reactors and experimental procedures for activity studies has been developed and tested. On this account it is a challenge to compare rates of the same reaction on a certain photocatalyst in different photoreactor set-ups. The illumination geometry, light intensity, type of light source, thermal effects due to the illumination, the geometry and operating mode of the reactor are decisive factors for the overall reaction rate. It needs to be emphasized that all these factors originate from the engineering viewpoint of experimental design and not from the catalytic properties of the photocatalyst. On the basis that there is no general agreement about how to perform photocatalytic experiments, it became a common procedure to use commercially available materials as a reference photocatalyst. One prominent example is P25. Another important issue is that

most of the photoreactors are limited to batch mode operation, since the low product formation rates require the accumulation of product molecules in order to meet the detection limit of the analytics. Appropriate analytical devices are highly sensitive mass spectrometers (MS) and gas chromatographs (GC). However, only the MS is capable of conducting isotope labelling experiments, since the GC is insensitive to the mass of a molecule. The mass spectrometer is a suitable choice especially when the reactor is operated under continuous flow conditions, while the GC can be used for both batch and continuous flow reactors. When it comes down to evaluating the activity of a powdered sample, the rate is often related to the mass of the photocatalyst. Admittedly, the low penetration depth of the incident light beam into semiconductors results in only a very small amount of the sample participating in photoexcitation. As a consequence, the fraction of actual photoactive material varies strongly due to the reactor geometry and the illumination conditions. For this reason the performance of the photocatalyst is not reproduced properly. It would be best if the rate could be determined related to the illuminated surface area. However, doing so requires knowledge about the exact illuminated surface area, which is not easy to determine. On this account comparing activities by relating the rate of a photocatalyst to the mass is only then an option, when the study is performed under the same experimental conditions in the same set-up. In addition, performing experiments under exactly the same approach allows investigating the influence of different reaction parameters such as the concentration of reactant molecules, or the intensity of light.

1.6 Aims and Outline of the Thesis

Due to the low product formation rate of photocatalytic CO_2 reduction it is a challenge to obtain information about this highly complicated reaction on the molecular level. For this reason most of the research effort is spend in the development of modification strategies or finding suitable alternative photocatalysts in order to improve the yields. However, this approach is associated with a poor understanding of the fundamentals of this reaction and the evaluation of the observations made is often based on assumptions, because basic knowledge is missing. TiO_2 is still among the most active system reported for this process, so understanding the fundamentals of this reaction is of great relevance for further research in this field. Therefore, the present work is a detailed examination on details of product formation in photocatalytic CO_2 reduction on TiO_2. Furthermore the validity of the assumptions made in the past will be critically scrutinized. This work is dealing, on the one hand side, with the verification if the CH_4 formation is actually based on a photocatalytic process of the reactants CO_2 and H_2O on TiO_2. More specific it is elucidated if the CH_4 formation depends on the concentration of the reactants. Furthermore, it is investigated how the product formation is influenced by the energy and the intensity of light. On the other hand side, the fate of O_2 as the by-product in photocatalytic CO_2 reduction is examined. It is one of the most important issues in the entire context, as it allows clarifying if the observed activity is based on a catalytic cycle or a stoichiometric reaction with the photoabsorbing

material. This knowledge can contribute to better understand the origin of product formation and the associated photo-physical and chemical processes. Furthermore this understanding can help to create a basis for an appropriate development of strategies to make progress in the field of photocatalytic CO_2 reduction.

2. Experimental

2.1 The Photoreactor Set-up and Components

All experiments of this thesis were performed with a home-made photoreactor set-up, which allows performing activity studies of powdered samples in gas-phase photocatalytic reaction under conditions of highest purity. The most important components of the high-purity-gas-phase photoreactor, namely the reactors, the light sources and the gas chromatograph are explained in detail. In 2.1.4 the overall set-up is described as a whole, in order to illustrate how the particular devices are assembled to perform activity studies.

2.1.1 Continuous Flow Reactors: Overflow- and Flow through Type (Tubular Reactor)

For this work two different types of reactors were developed. In the following, the most important characteristics and the associated capabilities and limitations of these reactors for investigating photon driven reaction will be elucidated.

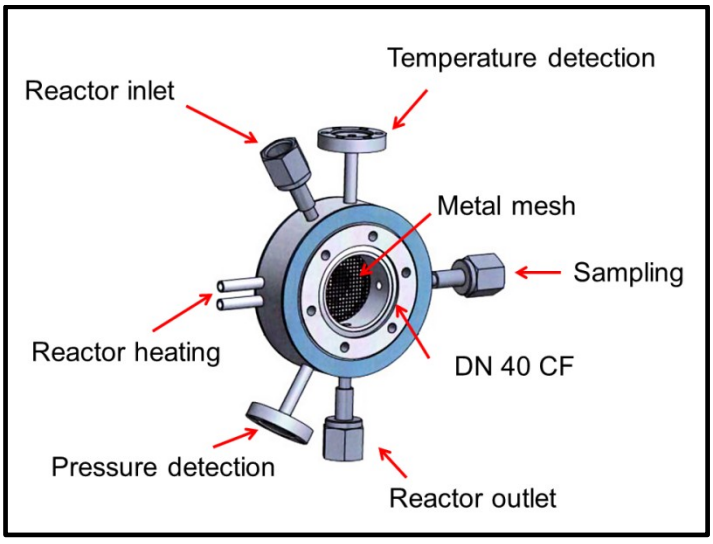

Figure 9: Schematic drawing of the overflow reactor and its connections.

The overflow reactor is made from stainless steel which is usually used for ultra-high vacuum applications. It includes various connections for different purposes. Figure 9 depicts a schematic illustration of this reactor. On the top side is a DN 40 CF connection for sealing the reactor with a lid. The lid (not shown in Figure 9) is a view port flange containing a quartz glass to enable light irradiation of the sample. Two DN 16 CF connections are installed for temperature and pressure detection. Furthermore, there are one gas inlet and two outlets realized by VCR® connection. Two of them are

used as the inlet and outlet of the reactants, products and inert gas molecules, respectively. The second outlet is needed for sampling purposes. Two small pipes on the left side of the reactor (Figure 9) are used for water based heating of the double walled reactor. The sample is placed in a quartz vessel on a mesh in the center of the reactor (Figure 9). The reactor can be operated either in batch mode, as well as in flow mode for the whole duration of the activity test. Such a type of reactor allows illuminating the sample from the top, whereby a large portion of surface area can be excited. However, the interaction between the gas-phase and photocatalyst placed in the quartz vessel is comparably low.

The second reactor type, a tubular continuous flow through reactor, is made from a 1/8' fluorinated ethylene propylene (FEP) tube. Due to the inner diameter of 2.1 mm it is feasible to fill the tube with powdered photocatalyst, so that a fixed bed is obtained. Swagelok connections and Teflon tape are used to connect the tubular reactor with the overall set-up. In this way it is possible to channel a gas flow through the fixed bed, significantly increasing the interaction between the gas-phase and photocatalyst compared to the overflow reactor. As FEP is transparent for the UV light, an illumination of the photocatalyst inside the tube can be realized from the outside. Due to the flow conditions the reactor is further termed as tubular reactor.

2.1.2 Light Sources

In this work different light sources are utilized in order to realize the optimal illumination conditions for the overflow and flow through reactor, i.e. a 200 W Mercury arc lamp (Hg/Xe) and high power UV LEDs.

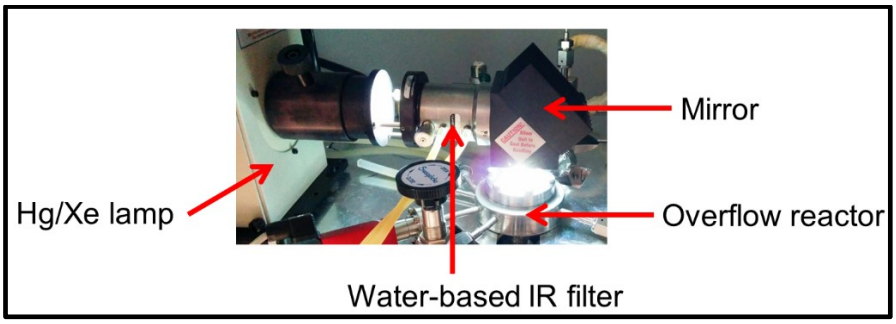

Figure 10: On top-illumination of the overflow reactor with the 200 W Hg/Xe lamp.

The 200 W Hg/Xe lamp (Oriel Instruments) is used for the illumination of the overflow reactor (Figure 10). This light source emits photons in the UV, the visible and near infrared range. A water-based filter is used for the removal of the IR radiation from the spectrum to prevent sample heating (Figure 10). The light beam of the Hg/Xe is directed to the reactor by a mirror (Figure 10), so that on-top illumination is realized. The Hg/Xe lamp does have the advantage that various light filters, for instance neutral density (ND) filters and cut-off filters, can be applied to the light beam pass. The use of ND filters allows changing the intensity of the overall light spectrum. In addition the use of cut-off filters makes it possible

to illuminate the sample with only a certain energy range of the overall light spectrum, for instance only the UV fraction.

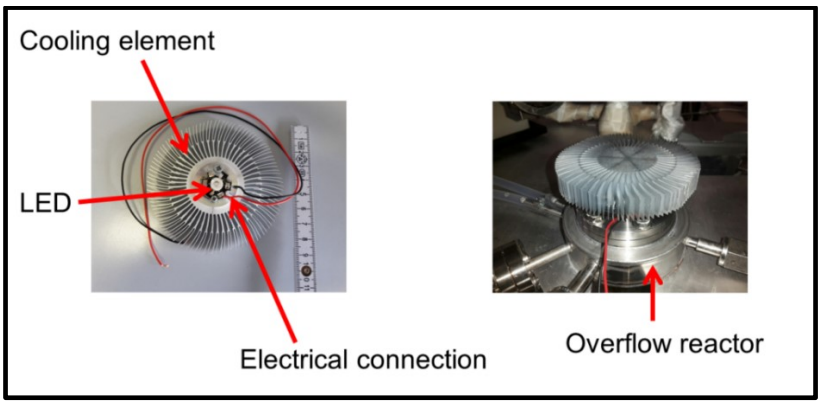

Figure 11: Left side: Single LED mounted on cooling element. Right side: On-top illumination of the overflow reactor with the single LED.

The overflow reactor can be also illuminated with a single high power UV LED. These single LEDs are mounted on a large cooling element in order to dissipate the heat evolved during operation (Figure 11, left side). The cooling element with the attached LED is placed on top of the reactor lid so that the photons are directed onto the photocatalyst inside the overflow reactor (Figure 11, right side).

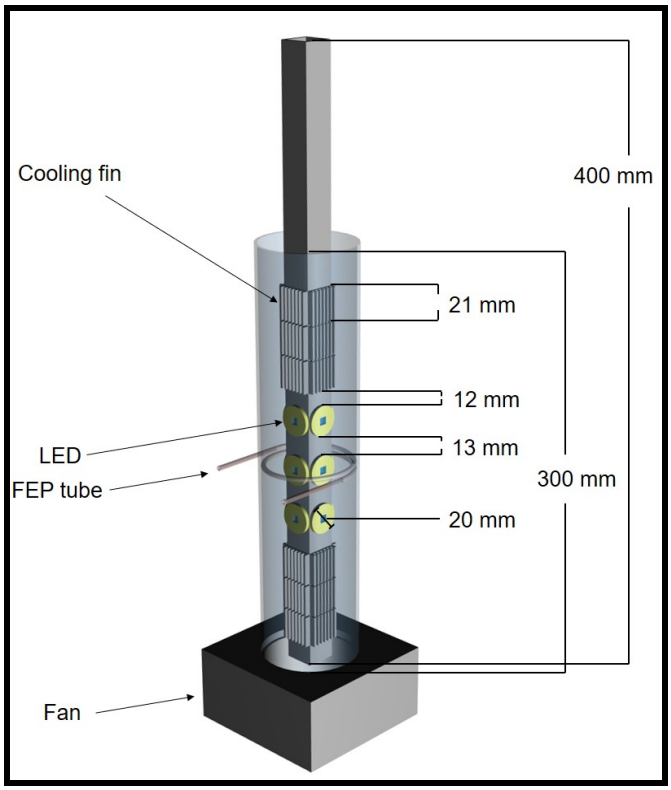

Figure 12: Schematic illustration of the LED bar and air cooling.

The illumination of the tubular reactor is implemented by a home-made immersion LED bar, made from a square aluminum profile (Figure 12). Three high power LEDs emitting photons with a wavelength of

365 nm are mounted to each of the four sides of the aluminum stick, amounting to a total of 12 LEDs with an overall power of 10 W. The LEDs are electrically connected in series. Under operation conditions the LEDs evolve a significant amount of heat, so that they reach the maximum operating temperature within a few minutes. Therefore, cooling fins and an air fan with a volumetric flow rate of 90 m^3/h were installed to dissipate the heat (Figure 12). A Teflon tube was installed around the aluminum bar in order to shield the light source and to direct the air stream along the LEDs (Figure 12).

2.1.3 Gas Chromatograph

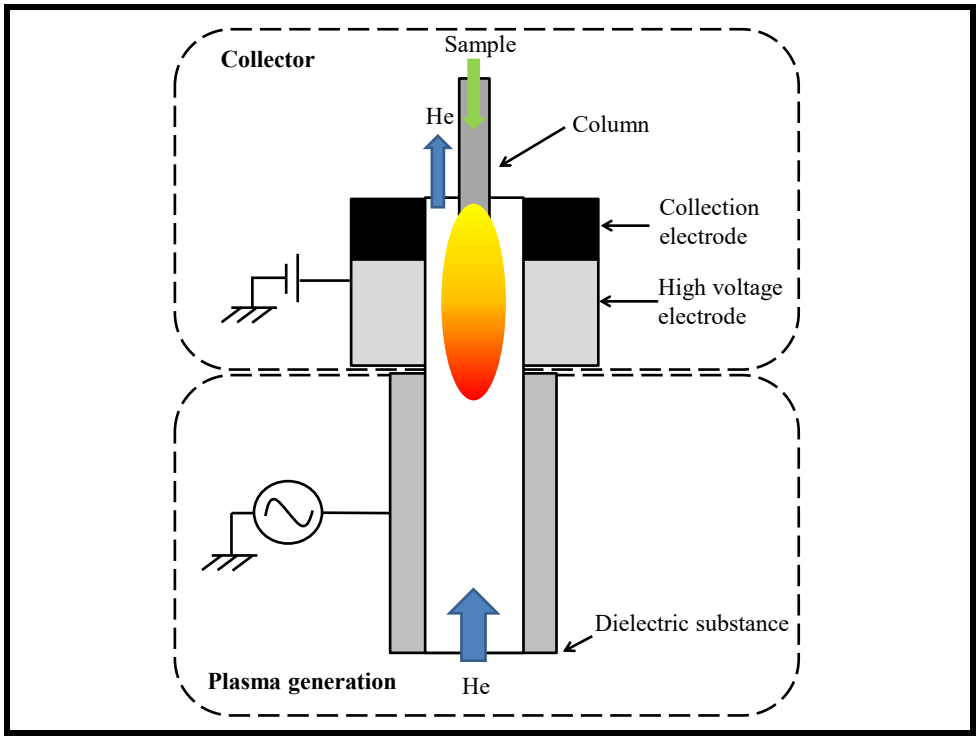

Figure 13: Schematic illustration of the barrier discharge ionization detection system.

Product analysis is performed with a Shimadzu TRACERA GC 2010 plus. This GC allows gas phase analysis in the 0.01 ppm range. The reason for this exceptional sensitivity is based on the plasma based barrier discharge ionization detection system (BID). Such a detector is twice as sensitive as a flame ionization detector (FID) and 100 times more sensitive than a thermal conductivity detector (TCD). A BID consists of two main sections (Figure 13). In the first section, the plasma is generated and the second is the controller section, where detection of sample molecules takes place. In the plasma generation section three electrodes are installed. A high voltage is applied to the central electrode. The non-equilibrium He plasma is generated by electrical discharge of the dielectric barrier by the applied high voltage. The meta-stable condition of the He plasma is used for the ionization of the sample molecules. As soon as the meta-stable He plasma returns to its ground state, photons are emitted. These photons have enough energy to ionize the sample molecules, which are amplified and accumulated by the collector. The voltage value is the quantity to be measured for the BID system. Detectable components

of this GC comprise CH_4, C_2H_6, CH_3OH, CO, O_2, H_2 and the reactants CO_2 and H_2O. On the basis of this high sensitivity, the BID is a suitable analytical device for an application in photocatalytic CO_2 reduction experiments under continuous flow conditions.

2.1.4 High-Purity-Gas-Phase Photoreactor Set-up

Figure 14 depicts a flow diagram of the complete photoreactor setup for photocatalytic CO_2 reduction. In addition to the previously introduced devices the overall set-up includes a gas supply, saturators, a cryostat and a vacuum pump. Basically, the set-up consists of two separated systems (set-up 1 and set-up 2). Each of the two individual set-ups includes one of the two reactors introduced in 2.1.1 of this chapter. The tubular reactor is installed in the first set-up, while the overflow reactor is placed in the second set-up. For the gas supply, four mass flow controllers (MFC) are installed. Two of them are connected to He 6.0 (99.9999 % He) gas cylinders. The other two MFCs are used for dosing of diluted CO_2 in He gas mixtures as the reactant gas. As the setup provides only one gas supply, a 4-port VICI® Valco valve (Figure 14) is installed to dose the desired gas flow to the particular set-up. All tubes are made from stainless steel and the connections are realized by VCR® or Swagelok® fittings. The cryostat is connected by three-way valves to the jacket of the overflow reactor in order to heat or cool it (Figure 14). Another important feature of the cryostat is the adjustment of the particular temperature inside the saturator for enrichment of the gas-phase with H_2O. For this purpose the cryostat is connected to the metal coil inside the saturators (Sat 1 and Sat 2 in Figure 14). They are metal-sealed and made from stainless steel. The H_2O vapor pressure is used to estimate the H_2O concentration in the overall gas flow. This is performed with the Antoine equation (eq. 2.1) and the three temperature-dependent dimensionless parameters A, B and C (Table 1).

$$\mathrm{P} = 10^{\mathrm{A}-\frac{\mathrm{B}}{\mathrm{T}+\mathrm{C}}} \qquad \text{(eq. 2.1)}$$

Table 1: Dimensionless parameters of Antoine equation for temperature range 273-303 K.[97]

A	B	C
5.40221	1838.675	-31.737

The vapor pressure *P* of the water in the saturator can be calculated for a given temperature. A division by the ambient pressure yields the fraction of water in the gas phase (eq. 2.2). When the water is at room temperature, the saturation of gaseous water in the gas flow is 2.3 %. If the saturator is cooled down to 5 °C, the saturation of gaseous water is only 0.86 % (approximately 8600 ppm). Both values are calculated for ambient pressure. Condensation of water in the piping is avoided by heating the pipes to 120 °C with heating tapes.

$$\varphi = \frac{P}{P^0} \cdot 10^6 \qquad \text{(eq. 2.2)}$$

The illumination of the capillary reactor in set-up 1 is realized by the immersion lamp, while set-up 2 uses the 200 W Hg/Xe lamp. The water-based IR filter of the 200 W Hg/Xe lamp in set-up 2 is cooled by the cryostat. A pump is used to evacuate the sampling unit (Figure 14) and the sample loop of the GC. Thereby, the pressure difference between the sample loop and the reactor is the driving force of sampling. The pressure inside the reactor is equal to the ambient pressure under continuous flow reaction conditions, so that there is always a driving force to fill the evacuated sample loop. The analysis of the gas phase in the two set-ups is conducted with one GC. This GC is installed in vicinity of the second set-up. On this account the gas flow of set-up 1 is directed to the sampling unit of set-up 2 to be analyzed.

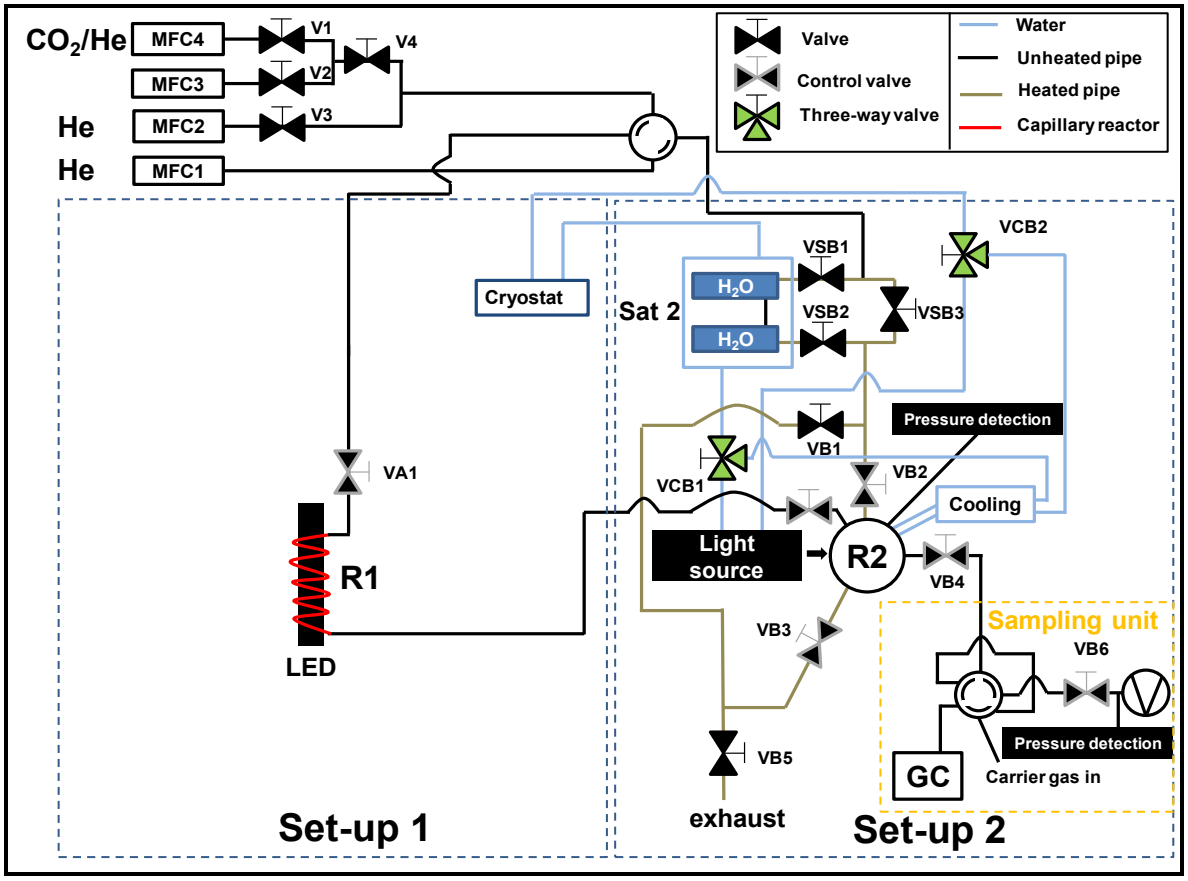

Figure 14: Schematic illustration of the set-up for CO_2 reduction.

2.2 Experimental Methods

2.2.1 Gas Chromatographic Measuring Program

The online analysis of the gas-phase during photocatalytic experiments with only one injection into the GC requires a complex measuring program. The GC is therefore provided with two columns, a Porapak column (PoraPLOT Q) and a molecular sieve (CP-Molsieve 5A). The investigated gas mixtures can include CO_2, CO, CH_4, H_2O, O_2 and H_2. It is necessary to use a molecular sieve to separate H_2, O_2, N_2, CO and CH_4, since these molecules do not have enough interaction to be separated by the Porapak

column. The latter is used for separation of H_2O and CO_2. At run time of the analysis the GC needs to switch the carrier gas flow between the two columns to enable separation of the particular molecules. This is realized by a 6 port VICI® valco valve. It can set the molecular sieve on- and offline (Figure 15). Another 6 port valco valve is used for the injection of the sample into the column (Figure 15). The GC uses He 6.0 as the carrier gas.

GC program sequence:

1. Minute 0: sample loop is loaded (Event 2, Figure 15). The temperature of the columns is initially at 30 °C.
2. Minute 0.01: sample loop is flushed with the carrier gas and the sample molecules flow into the Porapak column (Event 1, Figure 15).
3. Minute 0.06: carrier gas is in the Porapak column (Event 2, Figure 15) and molecular sieve is online (Event 4, Figure 15). Due to the low interaction of CH_4, CO, H_2 and N_2 with the Porapak column they arrive quickly at the molecular sieve.
4. Minute 4: The first molecules are leaving the Porapak column. It should be avoided that these species arrive at the molecular sieve. Therefore the molecular sieve is set offline (Event 3, Figure 15) and the molecules leaving the Porapak column get detected. Simultaneously, the restrictor is set online to enable continuous gas flow properties. At the same time the first heating ramp is initiated whereby the temperature of the columns is increased from 30 °C up to 160 °C (heating rate: 20 °C/min) (Figure 16). This procedure facilitates desorption of CO_2 and H_2O molecules from the column. After reaching the maximum temperature it is held for 6 minutes. Then the temperature is decreased to 60 °C (cooling rate: 40 °C/min).
5. Minute 21: molecular sieve is set online (Event 4, Figure 15). Separation of the molecules which arrived before minute 4. The second heating ramp starts and the temperature is increased again to 160 °C (heating rate: 10 °C/min) and held for one minute. Finally the sample molecules are detected by the BID.
6. Minute 32: The measuring program ends, the oven of the GC is cooled down to 30 °C and the position of the valco valves is set to the initial states. A new analysis can be conducted as soon as the initial temperature is reached.

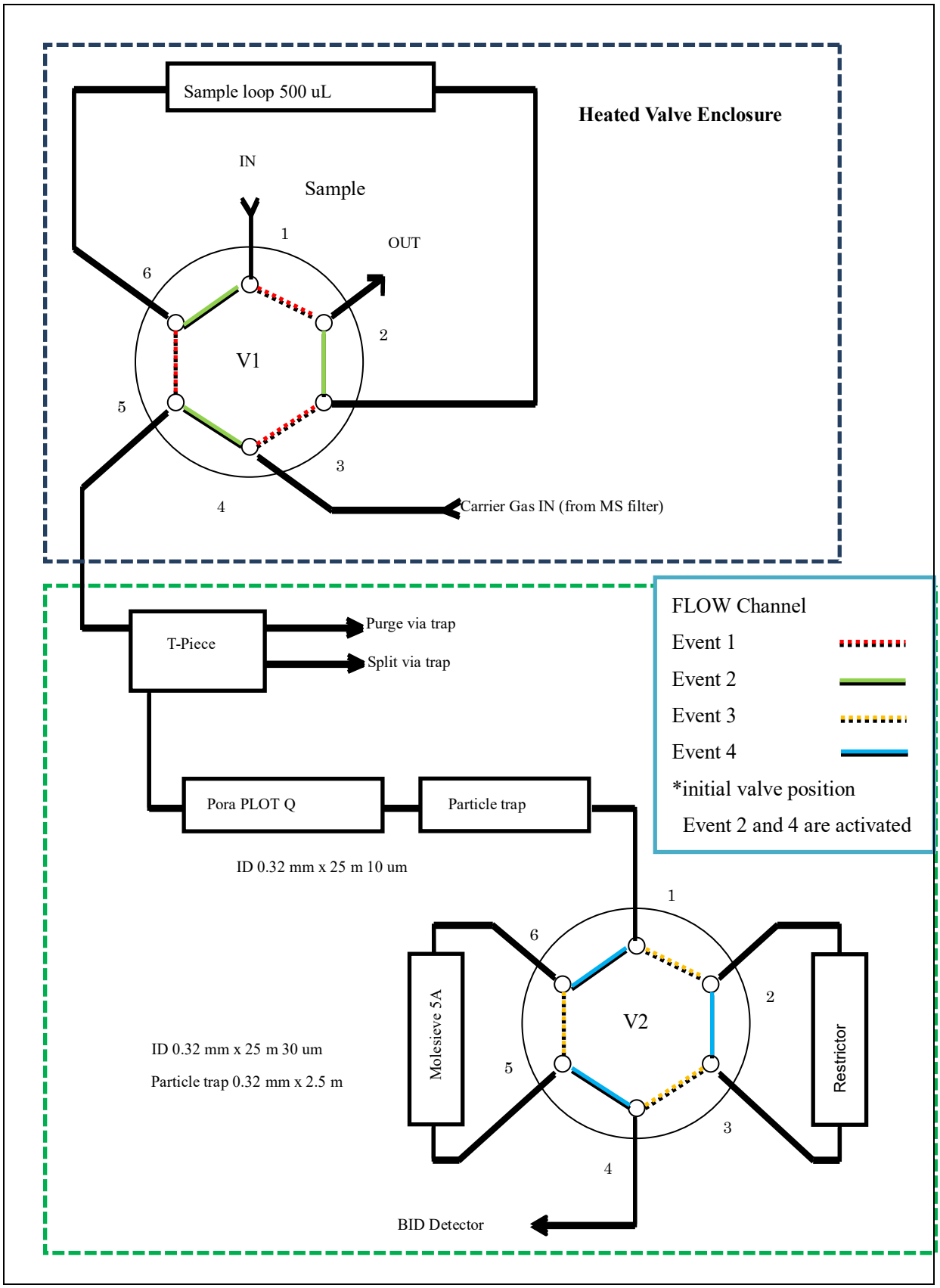

Figure 15: Event 1-4 of the GC program.

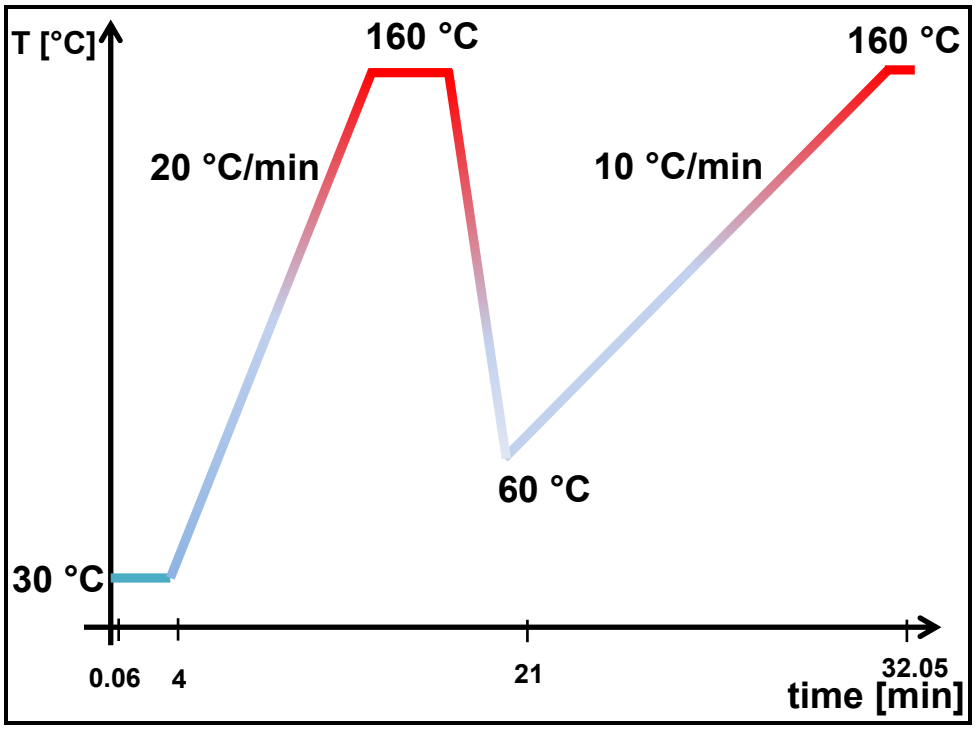

Figure 16: Temperature program of the GC measuring program.

2.2.2 Calibration of the GC for Qualitative and Quantitative Analysis

In this work gas chromatography is used for qualitative and quantitative analysis of the reaction gas atmosphere in the photoreactor. In order to implement this, it was necessary to calibrate the GC with CO_2 and H_2O as the reactants, and CH_4, H_2 and O_2 as the probable products, respectively. Calibration was conducted by a dilution series with each of these molecules. For this purpose, highly diluted gas mixtures of CO_2 (1000 ppm), CH_4 (100 ppm), H_2 (100 ppm) and O_2 (100 ppm) with He 6.0 were used. The calibration gas cylinders were connected to the MFC 4 and a continuous flow of the gas mixture and pure He from MFC 2 (Figure 14) for specific dilution was flushed through the reactor until a steady-state of gas phase composition was reached. Then a GC analysis of the actual gas-phase was conducted and the retention time of each molecule was checked for qualitative analysis. The integrated peak area in the resulting chromatogram was then related to the adjusted concentration in the gas flow. This procedure was carried out with four different concentrations of each molecule, so that in the end a linear slope was obtained. For quantitative analysis, the gradient of this slope was used as the calibration factor, allowing to convert the integrated peak area of the specific molecule to its concentration in the gas flow. An overview about the calibration equation and retention time of all investigated molecules is given in Table 2. In contrast, calibration of H_2O was performed with the help of the stainless steel saturator of the photoreactor set-up 2 (Figure 14). The amount of H_2O in the He gas-flow from MFC 2 was adjusted by the temperature according to the Antoine-equation (eq. 3). The calibration equation of H_2O is also given in Table 2. On the basis of the concentration and the adjusted gas flow rates it becomes feasible to calculate the molar flow rate. The unit of the molar flow rate is $\mathrm{mol/min}$.

Table 2: Overview of the calibrated molecules, their retention time and calibration equation for quantitative analysis with y = concentration [ppm],a = calibration factor, x = integrated area.

Molecule	Retention time [min]	Calibration equation $y = a \cdot x$	Coefficient of determination R^2
CO_2	7.3	$y = 8.7 \cdot 10^{-4} \cdot x$	0.99979
CH_4	26.5	$y = 6.2 \cdot 10^{-4} \cdot x$	0.99986
O_2	23.5	$y = 1.7 \cdot 10^{-3} \cdot x$	0.99957
H_2	22.5	$y = 2.5 \cdot 10^{-3} \cdot x$	0.99999
H_2O	18.1	$y = 2.5 \cdot 10^{-3} \cdot x$	0.99272

2.2.3 Removal of Carbonaceous Impurities and Continuous Flow CO_2 Reduction

Each sample is calcined in order to remove carbonaceous impurities before studying the activity in photocatalytic CO_2 reduction. After calcination the sample is weighted into a quartz vessel. It is taken great care of a fine distribution of the powder sample on the bottom of the vessel, fully covering it with the photocatalyst. 70 mg of P25 TiO_2 are enough to fulfill this requirement sufficiently. The quartz vessel is then placed in the center of the reactor. Subsequently, the reactor lid is put on top of the reactor and fastened by six screws. As a consequence of introducing the sample, large amounts of O_2 and N_2 diffuse into the reactor. To flush out all the air in the reactor, a He gas flow is dosed to the reactor, by setting the flow rate of MFC 2 to 35 mL/min. Since the purging of the reactor requires about 3 hours, it is useful to introduce the sample the day before starting the photocatalytic study. After purging out the air it is necessary to purify the sample from the residual carbon-containing species. The cleaning step is performed in the high-purity gas-phase photoreactor right before the CO_2 photoreduction experiment. It is performed under continuous flow conditions and at ambient pressure. A flow of 5 mL/min He (gas purity 99.9999 %), with traces of H_2O (< 100 ppm) is flushed through the reactor under illumination. More water will actually be present, since the P25 powder, coming in contact with ambient air during sample filling, is expected to be covered by adsorbed multilayers of physisorbed water.[98] GC measurements are performed every 45 minutes to monitor the cleaning progress. As soon as the concentrations of products of the cleaning reaction are sufficiently decreased, CO_2 is added to the feed as well. This means that the flow rate of He (MFC 2) is set to 0 mL/min and the flow rate of the CO_2 in He mixture (MFC 4) is set to 5 mL/min. From this point of time CO_2, H_2O and He are flushed through the reactor so that the CO_2 reduction under continuous flow conditions takes place. The interval of conducting GC analyses is kept at 45 minutes. Such an approach allows guaranteeing that the sample is

actually cleaned from impurities and product formation originates only from CO_2 reduction. At the same time it is allows to follow product formation as a function of the CO_2 flow rate.

3. Quantitative Evaluation of CH_4 Formation in the Steady State

Abstract

In this study photocatalytic CO_2 reduction on TiO_2 P25 was investigated for the first time under high-purity continuous flow conditions with gas chromatographic (GC) online detection of the main product CH_4. The thorough photocatalytic cleaning procedure in humid helium prior to all measurements was conducted under continuous flow too and we were able to monitor the decrease of carbonaceous contaminant concentration. On addition of CO_2 to the feed under illumination, an increase in CH_4 concentration was observed, which clearly follows the increase in CO_2 concentration in the reactor. It was also demonstrated that CH_4 formation ceases as soon as the lamp is switched off, providing clear evidence for the formation of CH_4 from CO_2 in a photoinduced process. It was shown that higher CO_2 concentration accelerated CH_4 formation under steady-state conditions up to a certain optimum. Higher CO_2 concentrations lead to a decrease in CH_4 formation. This observation is tentatively assigned to a limited availability of photogenerated charge carriers at the TiO_2 surface, or a lack of suitable catalytically active sites. Traces of O_2 in the reactor completely hinder CH_4 formation, implying that the lack of concomitant oxygen evolution observed in previous measurements on TiO_2 is likely beneficial for the overall process. This study represents a first step towards performing true steady-state kinetic studies of photocatalytic CO_2 reduction.

The main content of this chapter is published in ChemCatChem **2017**, 9, 696-704 as "Photocatalytic CO_2 Reduction Under Continuous Flow High-Purity Conditions: Quantitative Evaluation of CH_4 Formation in the Steady-State", M. Dilla, R. Schlögl, J. Strunk.

3.1 Introduction

During the last decades of research in the field of photocatalytic CO_2 reduction, the modification photocatalysts has been tested to accomplish higher product yields. Most of the modification strategies were aimed at increasing the visible light absorption or improving the charge carrier recombination properties.[20,66,67] Possibly, the key issue for photocatalyst improvement is the understanding of the mechanism of photocatalytic CO_2 reduction.[99] The mechanistic steps on the molecular level are not well understood and controversial.[63,64,84,100] In general, the reaction pathways include the following steps: adsorption of the reactants on TiO_2, activation of the adsorbed reactants by photogenerated charge carriers, formation of intermediates on the catalyst surface, conversion to final products, desorption of products and the regeneration of the catalyst.[38] The exact nature of the intermediates or the kinetics of the elementary steps, however, are still not understood. It might be that the product formation cycle includes kinetic barriers linked to slow steps not yet identified.[72] Understanding the product formation mechanism of photocatalytic CO_2 reduction is desirable,[101,102] since this would enable selective modification of the photocatalyst or the reaction conditions to accelerate the rate of product formation.

The activity of a photocatalyst and the effect of reaction conditions on the product distribution are usually tested with home-made photoreactor set-ups. As a consequence, a variety of set-ups and reaction conditions for testing photocatalysts in CO_2 reduction can be found in literature. Thus, it becomes difficult to compare activity results of samples which were tested in different set-ups.[17] In principle the photocatalytic CO_2 reduction can be conducted in the liquid phase and in the gas phase.[71] Slurry reactors are often used for liquid phase experiments.[103] However, performing the photocatalytic CO_2 reduction in gas-phase reactors offers a number of advantages compared to liquid phase reactors. Gas-phase reactors enable investigation under conditions of highest purity by using equipment which is originally designed for high vacuum set-ups. Another advantage is that the second reactant, H_2O (steam), can be added to the photocatalyst in arbitrary amounts and in absence of dissolution phenomena.[72,102] Gas-phase photocatalytic CO_2 reduction can be conducted in flow and in batch mode, but as a result of the very small product yields obtained, many previous studies employed batch-mode operation.[65,71,72,102] During a batch mode CO_2 reduction, the gas phase necessarily remains inside the reactor. Thus, it is assumed that only the photoreaction itself can change the concentration of the reactants within the reaction volume. As they do not leave the reactor, intermediates and products desorbing from the sample can readsorb and can take part in another photoreaction such as hydrogenation reactions or even re-oxidation to CO_2. On these grounds, it is desirable to perform the photocatalytic CO_2 reduction under continuous flow conditions of CO_2 and H_2O (steam) with shorter contact times between catalyst and reacting gas phase. Readsorption phenomena and consecutive reactions of intermediates and products might then occur to a lesser extent. However, the rate of product formation is often considered to be too low for continuous flow conditions[71], so that concentration of products is likely inadequate for accurate quantification. For this reason, the number of reports performing CO_2 reduction in flow mode is so far

limited. For instance Zhao et al.[104] and Li et al.[105] performed continuous-flow photocatalytic CO_2 reduction experiments with Ag/TiO_2 nanocomposites and Cu/TiO_2, respectively. They used a gas chromatograph as the analytical device. Zhao et al. found that Ag/TiO_2 composites show significant activity in the formation of CO and H_2, however, methanol was used as a hole scavenger in this study to increase product yields.[104] In the study by Li et al., Cu_2O species on TiO_2 were identified to increase the selectivity of CH_4 formation under photocatalytic reaction conditions, but CO remained the main product. In Ref. [105], although blank test without CO_2 are reported, it is not clear whether samples were photocatalytically cleaned prior to use. A thorough cleaning procedure before CO_2 reduction experiments is an essential step. Otherwise carbon-containing species, which originate from the synthesis procedure or subsequent modification, might be located on the surface of the sample and can contribute to the product formation. Total yields and thus also product formation rates would then be overestimated. So, apart from sufficient amounts of products for analysis, the need for conditions of highest purity is always another challenge in photocatalytic CO_2 reduction. Evidence for the actual formation of the products from CO_2 as reactant can only be obtained if the presence of any other compound as source for product formation is clearly ruled out.[65,102] Since a gas-chromatograph used for gas analysis is not sensitive to the mass of a compound, isotope labelling is not an option in this case.

In this study we used a gas-phase photoreactor set-up for CO_2 reduction experiments with TiO_2 P25 and conduct experiments in continuous flow mode under conditions of highest purity for the first time. For the experiments of this study it was required to identify adequate measurement conditions to enable product analysis and performing experiments under steady-state conditions. The used reactor design and choice of reaction conditions allowed performing both, the photocatalytic cleaning and CO_2 reduction consecutively in the same set-up. This new approach enables investigation of product formation exclusively from CO_2 feed. Furthermore, the effect of different CO_2 concentrations on the product formation rate was investigated. In addition, a pulse of O_2 was given to the feed to shed some light on the impact of the presence of this molecule in the gas phase on CH_4 formation in photocatalytic CO_2 reduction.

3.2 Experimental

3.2.1 Sample Pretreatment and CO_2 Reduction

70 mg of P25 have been employed for each CO_2 reduction experiment. Each sample has been calcined in synthetic air at 400 °C for 3 h prior to use. After introducing the sample into the reactor, the removal of carbonaceous species is conducted. This cleaning step is performed under continuous flow conditions and at ambient pressure. H_2O enriched He (purity 99.9999 %) is flushed (5 mL/min) through the reactor while the light source irradiates the sample. GC measurements are performed all 45 minutes to monitor the cleaning progress. As soon as the concentrations of products of the cleaning reaction are sufficiently

decreased, CO_2 was added to the feed as well. From that point of time CO_2, H_2O and He are flushed through the reactor so that the CO_2 reduction under continuous flow conditions takes place. After five consecutively performed GC measurements, the illumination source is turned off. After 45 minutes in the dark a final GC measurement is performed.

The continuous flow CO_2 reduction experiments were performed with 100, 500, 1000, 7000 and 15000 ppm CO_2. Two sets of experiments were performed: In one set, all measurements have been performed with fresh 70 mg of TiO_2 originating from the same package. In the other set, the same 70 mg batch of TiO_2 was used for all experiments, but the sample was cleaned from residual hydrocarbons after each reaction. Using the exact same sample for all experiments ensures constant irradiation conditions and therefore comparability between the separate CO_2 reduction experiments. However, a deactivation of the TiO_2 sample might not be accounted for. This can be prevented when a new sample is used each time, but then one has to accept that the irradiation conditions will necessarily change due to a differing orientation of powder particles within the sample dish. Since it cannot be decided a priori which set will yield the better results, both versions were tried and compared in this study.

A further part of this study concerns the influence of O_2 on the product formation. In this experiment, a small pulse of O_2 was given to the feed in the initial phase of CO_2 reduction, so that CO_2, H_2O, O_2 and He were available in the reactor. As a result of the O_2 pulse dosing and the flow conditions, the concentration of O_2 consequently decreases over the time, thus it becomes possible to evaluate the influence of a changing O_2 concentration on product formation.

Notably, although the concentration of H_2O in the feed was continuously set to 8600 ppm in all measurements, the recorded H_2O concentration in the reactor effluent was reproducibly as low as $\approx$ 400 ppm. While the exact reasons for the decrease are still unknown, we tentatively assign it to adsorption of water on the sample itself and the reactor walls. Preliminary experiments under batch reactor conditions (not shown for brevity) showed that CH_4 formation is independent of the exact H_2O concentration as long as H_2O is present in excess to the amounts of CH_4 produced. An excess with respect to reaction stoichiometry (CO_2:H_2O=1:2 for CH_4 formation) is not required. If the reactor is operated in batch mode, even adsorbed water multilayers on TiO_2 in almost complete absence of water in the gas phase were still sufficient to allow CH_4 formation, although with 30 % lower yields. In the future the effect of H_2O concentrations on the product formation will be investigated in detail under flow conditions, but this is outside the scope of the current study.

3.3 Results

3.3.1 Photocatalytic Cleaning of P25

Figure 17 shows a photocatalytic cleaning reaction with P25 over a time period of 6.75 hours. The initial 0.5 ppm of CO_2 in the first GC measurement (=0.1 nmol/min) indicate that the He purging gas of 99.9999% purity contains about 0.5 ppm CO_2. The concentrations of CO_2 and CH_4 increase in the gas-phase of the reactor after the light source is started. CO_2 likely originates from desorption of species such as carbonates due to light irradiation as well as photocatalytic decomposition of hydrocarbon impurities. The concentrations of CO_2 and CH_4 decrease within the course of time and become fairly stable after 3 hours of irradiation (Figure 17). During the first 3 hours of cleaning it appears likely that the formation of CH_4 is the result of both CO_2 reduction with the available CO_2 in the gas-phase and reactions of carbon-containing species on the surface of the sample. The latter is expected to be the predominant factor.[65] After 3 hours of UV-Vis light irradiation, almost all impurities on the surface of the sample are removed. Consequently, the effluent amount of CH_4 must be predominantly the result of photocatalytic CO_2 reduction. For this reason the CO_2 reduction experiments of this study are conducted subsequent to the cleaning reaction without a break of irradiation. This approach ensures that the course of CH_4 formation can be controlled as a function of the added concentration of CO_2 and avoids, for the most part, that hydrocarbon impurities are counted as products of CO_2 reduction.

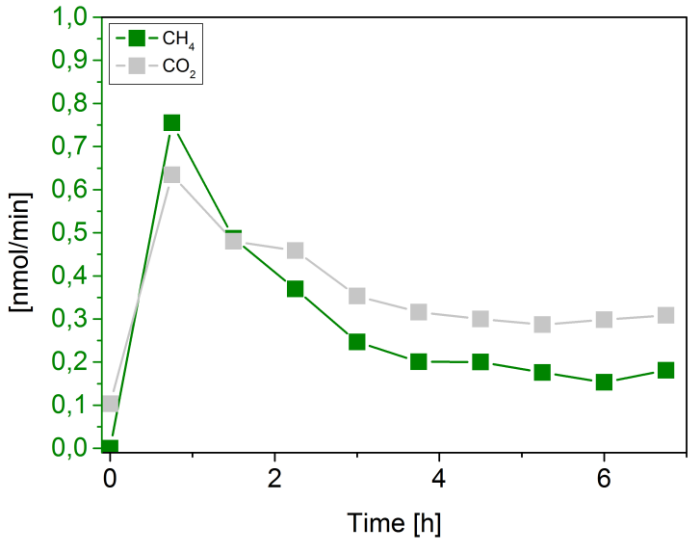

Figure 17: Photocatalytic cleaning procedure of P25, irradiation time: 6.75 h, lines are included in order to guide the eye.

3.3.2 Photocatalytic CO_2 Reduction under Continuous Flow Conditions

In Figure 18 the photocatalytic cleaning and CO_2 reduction (1000 ppm CO_2) is shown. Please note that CH_4 concentrations are shown on a different scale (left axis) than the CO_2 concentrations (right axis).

At 0 hours the gas atmosphere in the reactor consists of He and H_2O. After the first measurements the light source was switched on so that the photocatalytic cleaning reaction was started. In the following four measurements of the photocatalytic cleaning procedure, it can be observed that CH_4 appears in the gas-phase of the reactor. The concentration of CH_4 decreases after the second measurement and remains constant from the third measurement, similar to what has been observed in the separate flow cleaning (Figure 17). After 3 hours of photocatalytic cleaning, the CO_2 reduction experiment was initiated by addition of CO_2. In Figure 18 it can be clearly seen that the CH_4 concentration then scales with the CO_2 concentration in the reactor. After 6.75 h the light source was turned off. In the subsequent measurement the CH_4 concentration is significantly lower and almost equal to the value observed prior to CO_2 addition (measurement after 3 h).

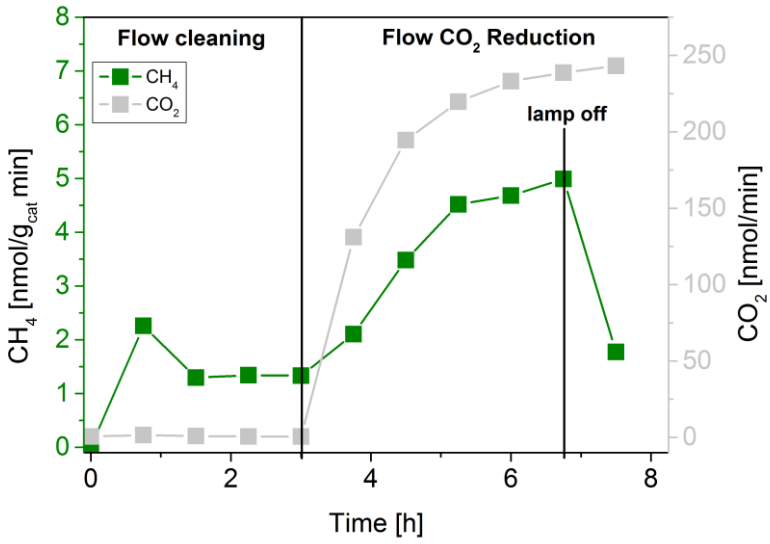

Figure 18: Photocatalytic CO_2 reduction under continuous flow conditions with 1000 ppm CO_2 (amounting to a flow of 238 nmol/min), photocatalytic cleaning: 3 h, CO_2 reduction: 3.75 h, lines are included in order to guide the eye.

However, after 6.75 h under irradiation the CO_2 concentration still showed an increasing tendency (Figure 18). The same observation can be made for the CH_4 concentration. So it was not possible to measure CH_4 formation under steady-state conditions in this measurement. It was necessary to optimize the experimental parameters. For this purpose, the CO_2 flow was initially set to 25 mL/min, to enable a fast increase of the reactant concentration as a result of the rapid gas phase purge. After 30 minutes, the CO_2 flow was set to 6 mL/min comparable to the previous experiment. The chronology of GC measurements remained unchanged.

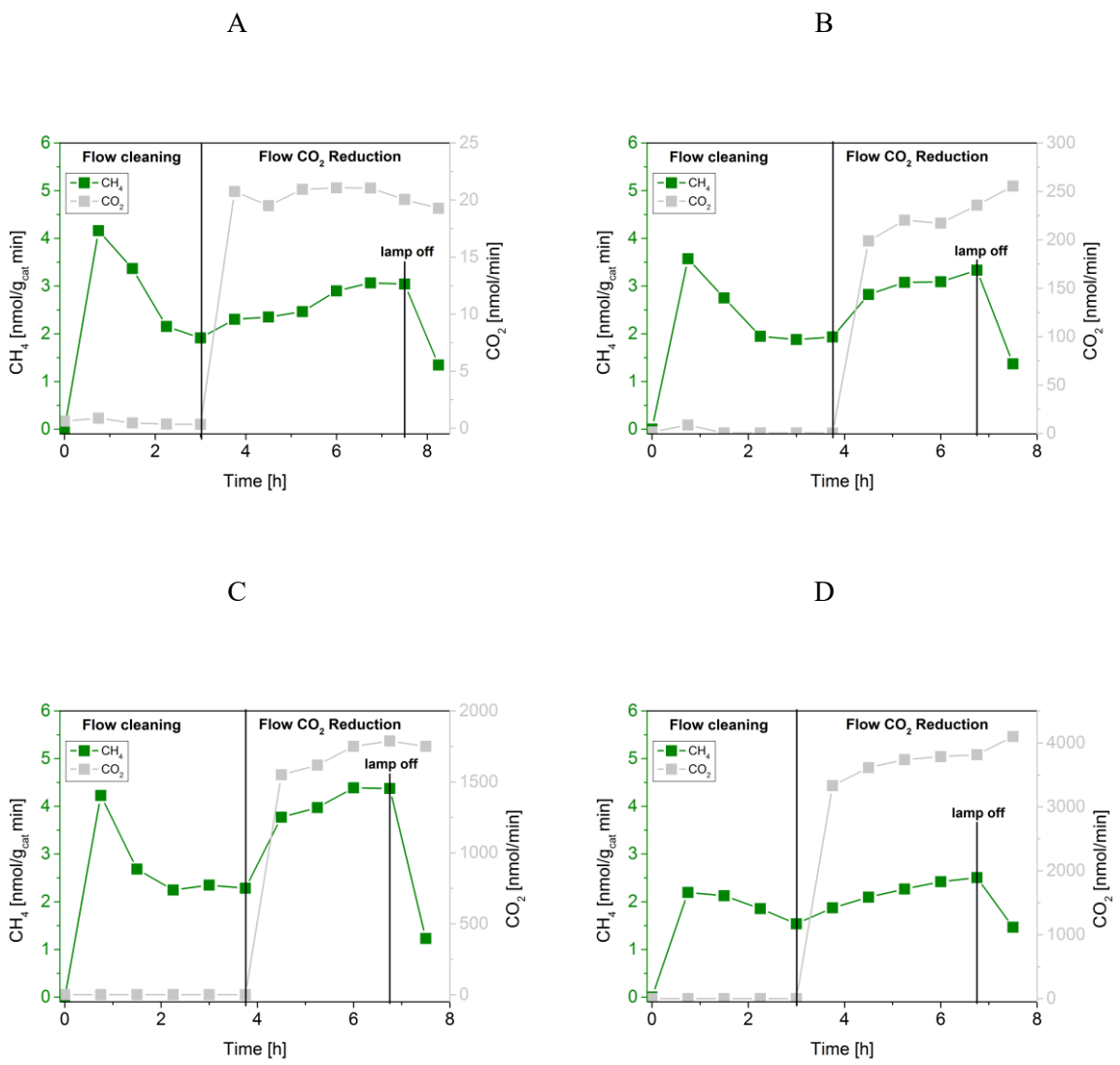

Figure 19: Photocatalytic CO_2 reduction under continuous flow conditions with A: 100 ppm CO_2 (amounting to a flow of 19 nmol/min), photocatalytic cleaning: 3 h, CO_2 reduction: 3.75 h. B: 1000 ppm CO_2 (amounting to a flow of 238 nmol/min), photocatalytic cleaning: 3.75 h, CO_2 reduction: 3 h. C 7000 ppm CO_2 (amounting to a flow of 1775 nmol/min), photocatalytic cleaning: 3.75 h, CO_2 reduction: 3 h. D: 15000 ppm CO_2 (amounting to a flow of 3500 nmol/min), photocatalytic cleaning: 3 h, CO_2 reduction 3.75 h. Lines are included in order to guide the eye.

Figure 19 A-D shows the CO_2 reduction experiments with the same sample filling and optimized reaction conditions. The CO_2 concentration was set to 100, 1000, 7000 and 15000 ppm, respectively. Measurements were conducted in the order (1) 15000 ppm, (2) 1000 ppm, (3) 7000 ppm, (4) 100 ppm. From Figure 19 A-D it can be clearly seen that the CO_2 concentration rises close to the nominal concentration in the feed stream within the first 30 minutes of the reaction run. The CO_2 concentration becomes almost stable in the following measurements. These experimental conditions allowed observing CH_4 formation under near-steady-state conditions for the measurements with 100 and 7000 ppm CO_2, at least for the last two GC measurements of each experiment before the lamp was turned off. It needs to be emphasized that true steady-state conditions can only be achieved when all products of a catalytic cycle fully desorb from the sample after their formation, so that the catalytic cycle is actually completed. In the experiments of this study, however, it was not possible to detect O_2 as

stoichiometrically required by-product of photocatalytic CO_2 reduction, which will be described below. For this reason, the term "near-steady-state" is used to describe the constant CH_4 formation under continuous feed of CO_2. For the measurement with 1000 ppm CO_2, the two measurements performed after 5.25 and 6 h of measurement displayed a stable CH_4 concentration increased slightly again in the last measurement after 6.75 h. As the changes are small, it is assumed that the measured CH_4 concentration does not differ significantly from that hypothetically observed in near-steady-state. This is not the case for the measurement with 15000 ppm CO_2, for which the concentration of CH_4 still increases significatnly in each measurement.

A long term experiment was thus conducted with 15000 ppm CO_2 in the feed (Figure 20). The experimental approach is similar to the experiments shown in Figure 19. The CO_2 flow was initially set to 25 mL/min for the first 30 minutes of CO_2 reduction. Then the CO_2 flow was set to 6 mL/min and GC measurements are performed all 45 minutes. A fresh batch of 70 mg TiO_2 was used for this measurement. It can be clearly seen that the CH_4 concentration increases from 4.5 h to 8.25 h (Figure 20) and becomes stable for the following 3 h. Thus, it was possible to measure CH_4 formation over a period of 3 h under near-steady-state conditions. The CH_4 concentration decreases slightly from 10.5 to 11.25 h. It was not possible to clarify which circumstances lead to the decrease of product formation. It appears reasonable that a deactivation of the photocatalyst, for instance by loss of active sites, generation of species which cannot contribute to the product formation, or the accumulation of oxygen-derived species, affected the rate of CH_4 formation. These species may occupy active sites and prevent the activation of CO_2 for a photocatalytic CH_4 formation, or contribute to the re-oxidation of formed products. Notably, the concentration reached in the steady state is very similar to the concentration reached in the last point of the measurement shown in Figure 19 D, so this point was likely measured right before steady state was reached.

In Figure 21 (green line) the CH_4 concentration after 6.75 h of UV-Vis light irradiation as a function of the CO_2 concentration is shown for the set of measurements with the same 70 mg TiO_2 sample for all measurements, as discussed above (Figure 19). The measurement with 15000 ppm CO_2 is included but not connected to the other data points since it is not clear if steady state was reached (Figure 19, D). It is not possible to use instead the data from Figure 20, because a different sample filling was used. The CH_4 concentration is strongly affected on variation of the CO_2 concentration between 0 and 1000 ppm. However, a further increase to 7000 ppm CO_2 does not increase the formation of CH_4 significantly.

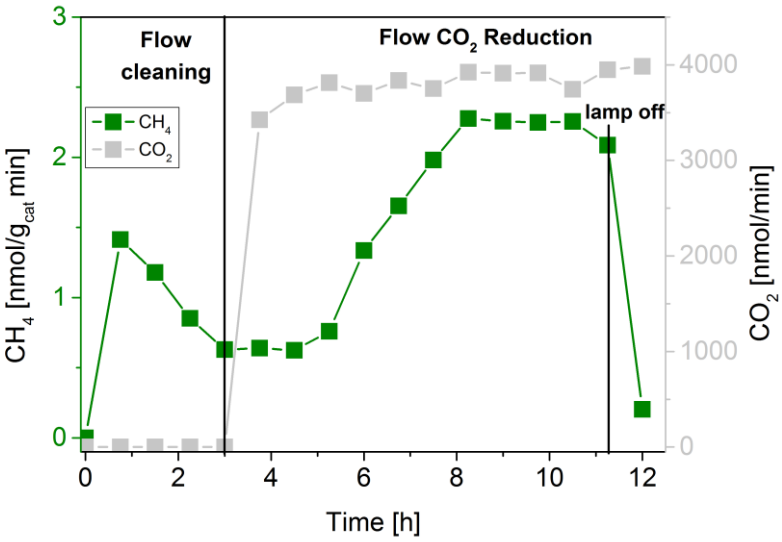

Figure 20: Long-term photocatalytic CO_2 reduction experiment under continuous flow conditions with 15000 ppm CO_2 (amounting to a flow of 3500 nmol/min), photocatalytic cleaning: 3 h, CO2 reduction: 8.25 h. Lines are included in order to guide the eye.

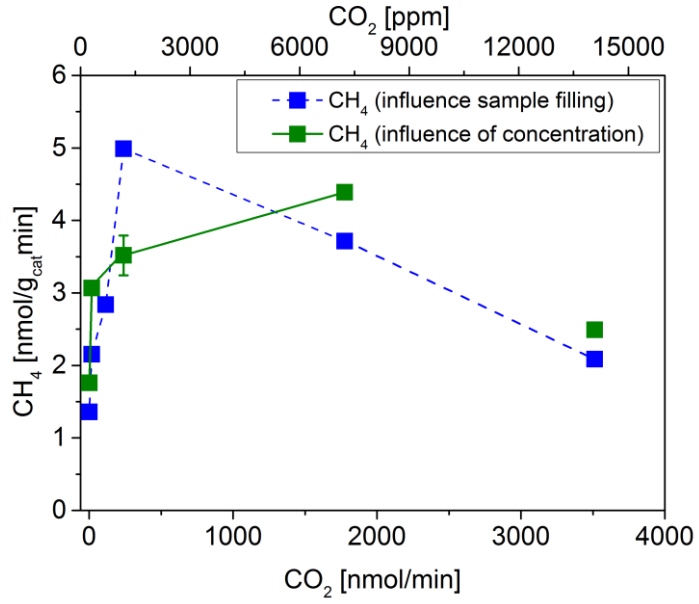

Figure 21: Photocatalytic CO_2 reduction under the influence of different sample filling (blue line) and constant sample filling (green line). Lines are included in order to guide the eye.

The CH_4 formation was also investigated under the influence of differing sample fillings, that is, using a fresh batch of 70 mg of TiO_2 for each measurement. In this curve, the result of the long term experiment with 1.5% CO_2 (Figure 20) is included. In Figure 21 (blue line) it can be observed that the CH_4 formation is influenced significantly by the sample filling. The CH_4 concentration at 100 and 7000 ppm CO_2 is lower than observed in the previous measurement, whereas the CH_4 concentration at a CO_2 concentration of 1000 ppm is significantly higher (Figure 21, blue line) than the results using the same sample (Figure 21, green line). The sample orientation determines the light reflection properties and the portion of

surface area of the photocatalyst oriented towards the light source, so that only the exposed surface area is irradiated by the light source. Additionally, the penetration depth of UV-Vis light is limited to a few portions of a millimeter,[106] so that only a small part of the sample is excited by the light source. Consequently, the number of photogenerated charge carriers available for product formation decreases with the irradiated sample surface. For this reason, sample fillings with a smaller light-exposed surface area exhibit a lower photocatalytic activity. From the results of the present study, the use of the same sample filling for all measurements thus appears to yield the more reliable data.

3.3.3 Influence of O_2 on the Product Formation in Photocatalytic CO_2 Reduction

In another experiment of this study, the influence of O_2 on the product formation of photocatalytic CO_2 reduction was evaluated (Figure 22). For this purpose a pulse of O_2 and a continuous flow of CO_2 were simultaneously given to the reactor after 3 hours of photocatalytic cleaning. The data point at 3.75 h hours shows that the CO_2 concentration increased to 320 ppm within the first 45 min of irradiation and purging (Figure 22). At the same time the O_2 concentration is 25 ppm and decreases over the course of time as a result of the flow conditions. The concentration of CH_4 decreases from 3 to 3.75 h. This trend continues until 4.5 h. It appears that the photocatalytic formation of CH_4 is inhibited in the presence of O_2 in the reactor gas atmosphere. The CH_4 concentration then rises as soon as the O_2 concentration was below 5 ppm (Figure 22).

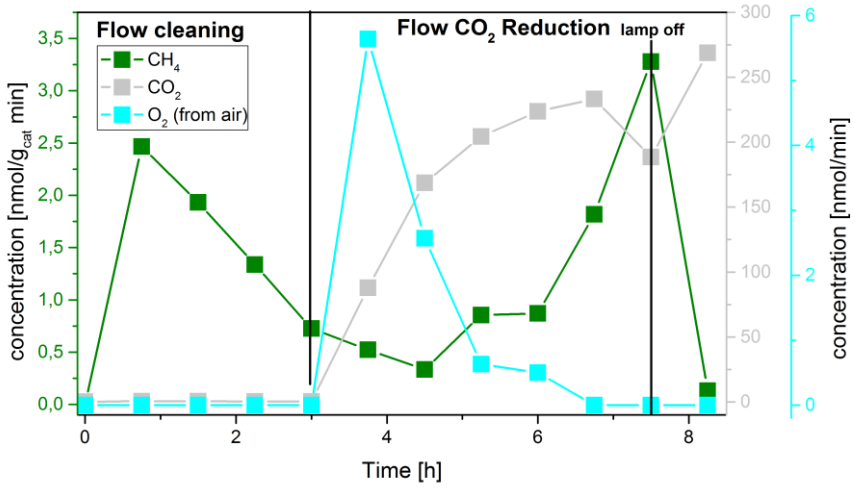

Figure 22: Photocatalytic CO_2 reduction under the influence of O_2 pulse dosing. Lines are included in order to guide the eye.

3.4 Discussion

3.4.1 Flow Cleaning

The results of the photocatalytic cleaning procedure (Figure 17) clearly show that carbonaceous impurities present on the sample surface can either be hydrogenated (to CH_4) or oxidized (to CO_2) during the photocatalytic cleaning in humid helium. Furthermore, while it appears that about half a ppm of CO_2 is present in the ultrapure helium purge gas, we find no indication for the presence of any CH_4. So, the purge gas can be clearly ruled out as source of species falsely identified as reaction products. The flow cleaning procedure can also be considered an improved process for sample cleaning, because it significantly reduces the time required for the whole experiment compared to multiple batch cleanings that required an evacuation or purge procedure in between. Similar to the observations made in the batch cleaning, CH_4 concentration cannot be brought down to absolute zero. This is may be both an effect of the 0.5 ppm CO_2 present in the feed gas and some minor residual hydrocarbons that still degrade with extremely slow kinetics. However, it is clear that constant and very low concentrations can be reached, which can be taken as a baseline in the subsequent CO_2 reduction experiments.

3.4.2 Photocatalytic CO_2 Reduction in Flow Mode

Conducting the photocatalytic CO_2 reduction under continuous flow conditions (Figure 18) showed that the concentration of effluent CH_4 increases with the concentration of CO_2 during the purging process of the reactor under irradiation. Notably, the CH_4 concentration rises above the baseline reached during cleaning right away on addition of CO_2 to the reactor. The concentration of CO_2 becomes fairly stable with time and the concentration of CH_4 reveals the same trend. Furthermore, as soon as the illumination stops, no further CH_4 was formed. All those observations are clear evidence that CH_4 is the true product of photocatalytic CO_2 reduction on P25. The fact that CH_4 formation requires UV-Vis light proves that its formation is a photoinduced catalytic process.

3.4.3 Influence of CO_2 Concentration on the CH_4 Formation

It has been observed that CH_4 formation by CO_2 reduction is strongly influenced by the CO_2 concentration. The formation of CH_4 increases considerably if the gas-phase CO_2 concentration is below 1000 ppm (Figure 21). Between a CO_2 concentration of 1000 and 7000 ppm, the CH_4 concentration barely increases, and it appears to decrease again if CO_2 concentrations are higher, although our results are not unambiguous in this respect. This needs to be addressed in future studies. The obtained results indicate that either the availability of suitable catalytic active sites or the amount of available charge carriers at the surface of TiO_2 limit the overall reaction rate, as will be outlined below.

Any photocatalyst needs to perform the functions of a photoabsorber and that of a heterogeneous catalyst. Regarding the former, light needs to be absorbed in the semiconductor and charge carriers with sufficient reduction and oxidation potential need to be created and migrate to the surface. With respect to the latter, the material needs to have suitable exposed active sites that bind the reactant favorably and provide the appropriate electronic and geometric structure to lead to the formation of the desired product. Similar to the well-known elementary steps in classical heterogeneous catalysis, the elementary processes at the active site can likely be classified as adsorption, reaction, and desorption steps. The adsorption of the reactant is an important event of a photocatalytic reaction[107], as it facilitates the activation of the reactants so that charge carrier reaction can occur. The surface of TiO_2 provides various sites for CO_2 adsorption. It is known that CO_2, for instance, adsorbs on Ti^{4+} surface atoms, bridging oxygen atoms and oxygen vacancies (V_{OX}).[108-110] Thereby, various types of adsorption modes involving linear and bent CO_2 occur. Additionally, formation of mono- and bidentate carbonates and bicarbonates takes place.[109] However, the CO_2 adsorption mode and site that are active for a photocatalytic conversion to CH_4 remain unknown. The variation of the CH_4 formation with CO_2 concentration may imply that the availability of suitable adsorption sites is a limiting factor in the product formation once CO_2 concentration increases to values above 1000 ppm (Figure 21). A further increase of the CO_2 concentration then results in saturation of the active sites and the product formation cannot be enhanced. Likewise, it is possible that an increasing partial pressure of CO_2 in the gas-phase of the reaction atmosphere results in CO_2 adsorption modes that are not suitable for a photocatalytic reduction reaction. So, they either do not contribute to CH_4 formation, or the number of active sites may even be decreased due to occupation with insufficiently activated species.

A further limiting factor of product formation may be found in the function of TiO_2 as photoabsorber and source of charge carriers, that is, in the concentration of photoexcited charge carriers reaching the surface. After their formation in the bulk, photogenerated electrons and holes need to migrate to the surface of the sample to catalyze a redox reaction. During this transfer they can undergo various trapping and recombination events.[43] Only a small part of the charge carriers reaches the surface and can be transferred to an adsorbed species. Consequently, product formation will be limited by the available concentration of charge carriers under certain conditions. In this study, it is possible that the charge carrier concentration limits the product formation once the CO_2 concentration is above 1000 ppm. As a consequence, the concentration of available reactants on or near the surface might then be higher than the concentration of surface charge carriers. We cannot distinguish between either of the two possibilities – limiting number of catalytic active sites or photogenerated charge carrier – based on the results of the present study alone. Thus, further studies of CO_2 adsorption and light intensity variation are in progress to clarify this issue.

3.4.4 Influence of O_2 on the Product Formation of Photocatalytic CO_2 Reduction

In this study, it was not possible to detect O_2 as a by-product of photocatalytic CO_2 reduction. The stoichiometry of the CO_2 reduction leading to CH_4, however, requires the formation of O_2 (1.7). As a result of the use of a GC for product analysis, the presence of O_2 can only be excluded for the gas phase. A potential reason for the absence of O_2 or O-related molecules in the gas phase may be that they remain bound to the photocatalyst after their formation instead of being desorbed. CH_4 formation is obviously not negatively influenced by such species during the time periods studied in this work, because it is clear that a steady formation can clearly be reached and no major deactivation phenomena are observed. The location and fate of O_2 as by-product of photocatalytic CO_2 reduction will be investigated in future work.

The present study reveals, however, that O_2 present in the gas phase inhibits the product formation, a process that would necessarily occur once the by-product O_2 would be released into the gas-phase. Formation of CH_4 is only detected after O_2 disappeared from the gas phase (Figure 22). It is conceivable, in general, that the presence of gas-phase O_2 promotes the backward reaction of CO_2 reduction, that is, hydrocarbon oxidation. In addition to this effect, a potential reason can be found in the adsorption properties of O_2 onto TiO_2. A defective surface of TiO_2 provides adsorption sites for O_2.[93] The O_2 adsorption on TiO_2 is energetically favorable compared to the adsorption of CO_2. For this reason, CO_2 may compete with O_2 for adsorption sites on TiO_2, in which case the adsorption of CO_2 on the surface of TiO_2 may be hindered in presence of O_2. In that case, it cannot undergo a photocatalyzed reaction anymore, so a restricted adsorption of CO_2 would inhibit product formation.

Furthermore, the adsorption of O_2 onto TiO_2 enables reaction, for instance, with oxygen vacancies (V_{OX}) leading to their replenishment.[111,112] In literature it is often stressed that reactions with CO_2 necessarily involve the formation of the $CO_2^{-\cdot}$ anion[77,78,113] by a one electron transfer reaction that has been proposed to be initiated by Ti^{3+} centers located at V_{OX}.[39,77,114] Although we cannot confirm yet if this is really a relevant elementary step relevant in the product formation mechanism, a replenishment of V_{OX} by gas-phase O_2 may decrease the number of active sites. Consequently, the overall activity of the photocatalyst is then reduced due to loss of active sites.

Another photocatalytic reaction of O_2 on TiO_2 is the one-electron transfer to form the superoxide radical ($O_2^{-\cdot}$). This reaction is thermodynamically possible, because the redox potential of this reaction (1.11) is less negative than the CB edge of TiO_2.[91] Additionally, the formation of $O_2^{-\cdot}$ (1.11) is thermodynamically favorable in comparison to the one electron transfer to a CO_2 molecule (-1.9 V)(1.8), which should not be possible at all on TiO_2 or any other semiconductor.[18] One-electron reduction of molecular oxygen reduces the number of photogenerated electrons available for CO_2 reduction. Our observations may then be explained by considering that the consumption of photogenerated electrons

for CO_2 reduction starts only after all O_2 molecules are converted to $O_2^{-\cdot}$ or flushed out of the reactor, respectively.

Whereas we unable to clarify this issue on the basis of the current results, it is clearly shown that the (likely atomic) oxygen species formed during photocatalytic CO_2 reduction react differently than dioxygen added to the gas phase. This may be a result of the inability of the formed O-species to take up more electrons (if the oxygen atoms remain anionic in the 2- oxidation state), or the storage of such O-related species at sites that do not affect CO_2 adsorption. From our current point of view, however, it appears to be beneficial that the by-product oxygen is not liberated as molecular O_2 into the gas phase concomitantly to CO_2 reduction to CH_4. Should this be the case, product yields would be further decreased. In contrast, when using TiO_2 as photocatalyst the development of reaction-regeneration process may be the preferred option, in which first CO_2 reduction to CH_4 occurs for a certain reaction time, and then the photocatalyst is regenerated to remove the bound oxygen species by a process yet to be developed.

3.5 Conclusions

In the current investigation further evidence was collected that the formation of CH_4 on TiO_2 truly originates from photocatalytic reduction of CO_2. The removal of carbonaceous contaminants in a flow cleaning prior to photocatalytic CO_2 reduction was clearly demonstrated. Whereas small traces of CO_2 ($\approx$ 0.5 ppm) were detected in the helium purge gas, no CH_4 was found. During the cleaning procedure CH_4 formation, both from contaminants and the CO_2 in the purge gas, was reduced down to a constant baseline of less than 1 ppm. CH_4 concentration then increased as soon as CO_2 was introduced into the reactor, and the increase in concentration mirrored the increasing in CO_2 concentration in the reactor during the purging process. As soon as the lamp was switched off, CH_4 formation ceased and the concentration returned to the baseline, which is clear indication for its formation in a photoinduced process. Measurements with constant concentration of CO_2 revealed that a steady state CH_4 formation can be reached in less than 4 hours of photocatalytic CO_2 reduction. From a comparison of the (near)-steady state CH_4 concentration as function of the CO_2 concentration it became clear that CH_4 formation is significantly accelerated for CO_2 concentrations up to 1000 ppm, but a further increase in CO_2 concentration has no beneficial effect or may even decrease the CH_4 yield. Based on the results, either the amount of available catalytic active sites or the number of photogenerated charge carriers reaching the TiO_2 surface appear as likely limiting factors for CH_4 formation. A possible negative trend observed for high concentrations of CO_2 may also be attributed to the formation of inactive surface species that block active sites. These issues will be addressed in further studies. Addition of an oxygen pulse to the gas phase completely hinders the formation of CH_4, which can only be initiated once O_2 levels in the gas phase have decreased to below 5 ppm. This is likely caused by a competition between O_2 and CO_2 for adsorption sites and/or charge carriers. The oxygen species inevitably formed as by-product of

photocatalytic CO_2 reduction, do not appear in the gas phase, so it is assumed that they remain on or inside the photocatalyst. As the achieved steady-state CH_4 formation and the results of the long term measurement clearly show, those oxygen species do not cause a pronounced inhibiting effect within the reaction times studied here. It is thus beneficial for CH_4 yields that oxygen is not evolved into the gas phase. Process concepts for CO_2 reduction may instead consider reaction-regeneration operation, in which CH_4 and O_2 are evolved alternatingly instead of concomitantly.

4. Influence of Light Intensity and H_2O Concentration

Abstract

The present study deals with fundamental investigations on the effect of light energy and intensity on the photocatalytic reduction of CO_2 on TiO_2 P25 under high purity continuous flow conditions. In accordance with previous works, gas chromatographic (GC) online detection identified CH_4 as the main product of photocatalytic CO_2 reduction. It was found that the product formation is dependent on the light intensity, which verifies that CH_4 is formed in a photon induced process on TiO_2. A variation of the light intensity revealed that charge carrier recombination is more strongly enhanced compared to the charge transfer reaction to adsorbed species. On these grounds, the rate of CH_4 formation increases only by the square root of the light intensity. Furthermore, product formation is predominantly a UV photon driven process. A further part of this study investigated the effect of H_2O on the CH_4 formation. The photocatalytic removal of carbon-containing species and the CO_2 reduction can already proceed with traces of adsorbed H_2O, whereas a continuous flow of gaseous H_2O results in an inhibition of product formation. Based on our study, we can identify highly promising routes for photocatalyst improvement.

The main content of this chapter is published in ChemCatChem **2017**, 9, 4345-4352 as "Photocatalytic CO_2 Reduction Under Continuous Flow High-Purity Conditions: Influence of Light Intensity and H_2O Concentration", M. Dilla, A. Mateblowski, S. Ristig, J. Strunk.

4.1 Introduction

In general a photocatalyst is a highly complex system which has to perform two functions. The first function is that of a photoabsorber. Absorption of photons with energy greater than the band gap results in the formation of charge carriers with sufficient oxidation and reduction potential for the relevant reaction.[13] In addition it is required that the charge carriers have adequate mobility, to migrate to the surface of the material. Thereby, the charge carriers can undergo various recombination and trapping events which lowers their life time and mobility, respectively.[17,43] The second function is that of a heterogeneous catalyst, which means that the material exposes active sites for the specific photoreaction. These sites need to provide appropriate adsorption properties for the reactant so that the particular charge transfer reaction can proceed.[17,115] Gaining a fundamental knowledge especially about the photoinduced processes is required.

The light-induced excitation of a photocatalyst with one photon of sufficient energy results in the formation of one electron-hole pair. Such a reaction represents a first order reaction.[116] In contrast the recombination reaction is a second order reaction,[116,117] since two carriers of opposite charge are needed for the reaction to proceed. With increasing light intensity the excitation is enhanced, thus the concentration of excited charge carriers increases as well. Consequently, the recombination kinetics is also influenced by the light intensity. Over a certain range of low light intensities, the rate of a photoreaction increases linearly.[118] However, the higher the light intensity, the higher is the influence of the recombination reaction, so that the rate can only be increased by the square root of the light intensity.[117-121] To the authors knowledge there is no systematic study on the effect of light intensity on the product formation in photocatalytic CO_2 reduction with TiO_2 under continuous flow conditions. On these grounds, the intensity of light has been varied in this study to obtain information on the productivity of photocatalytic CO_2 reduction under steady state conditions. In addition, further sets of experiments of photocatalytic CO_2 reduction were conducted with either UV or visible light, to discriminate if the product formation is purely UV-light induced. Photocatalytic CO_2 reduction with increased reactor temperature was also investigated. This study allows gaining a fundamental understanding on the influence of light and elevated temperatures on the product formation of photocatalytic CO_2 reduction. Additionally, optimization of illumination conditions to run this reaction more efficiently was attempted.

In our previous study[122] the effect of CO_2 concentration on product formation of photocatalytic CO_2 reduction was investigated. It was observed that the product formation can be increased with the CO_2 concentration, but only up to a continuous flow of < 240 nmol/min (1000 ppm).[122] A further increase of the CO_2 concentration did not increase the product formation significantly. This observation was attributed to the limited concentration of available charge carriers and active sites for CO_2 reduction on the surface of the photocatalyst, respectively.[122] Additional to the presence of the reactant CO_2, a source

of hydrogen for the hydrogenation reaction to CH_4 is required. For this purpose H_2O can be used. It is commonly believed that photocatalytic splitting of H_2O needs to proceed to utilize the hydrogen atoms of this molecule for the generation of C-H bonds. From the thermodynamic point of view the photocatalytic H_2O splitting should be possible on TiO_2. However, the hole-consuming H_2O oxidation reaction is kinetically limited owing to a significant overpotential.[123] Thus the activity of H_2O splitting without using sacrificial agents or an external bias is rather low.[123] For mixtures of pure CO_2 and H_2O, reaction stoichiometry of the photocatalytic H_2O oxidation half reaction (1.6) and thus of overall CO_2 reduction (1.7) require the formation of O_2.

However, O_2 is often not found as a product of these two processes.[122,124,125] The absence of O_2 in the product spectrum makes it seem questionable if the photocatalytic H_2O splitting is involved in photocatalytic CO_2 reduction, or if any other source of hydrogen, for instance surface hydroxyl groups, is relevant in the product formation. For this reason the participation of photocatalytic H_2O splitting as hydrogen delivering reaction in the formation of CH_4 was a second focus of the present study. Finally, the experiments in this work aimed at finding optimal conditions to run the photocatalytic CO_2 reduction with higher productivity, revealing inevitable limitations of photocatalysts based on bare TiO_2.

4.2 Experimental

4.2.1 Sample Pretreatment and CO_2 Reduction

70 mg of P25 have been utilized for each CO_2 reduction experiment. Prior to the activity test, P25 was calcined in synthetic air at 400 °C for 3 h in order to remove carbon-containing impurities originating from the sample synthesis and the environment. This thermal pretreatment is necessary, since these carbon-containing species can contribute to the product formation leading to an overestimated activity of the sample. However, the thermal pretreatment is not sufficient to remove all of these carbon-containing species. For this reason the sample still needs to be further purified under photocatalytic reaction conditions. This cleaning step is performed inside the high-purity gas phase photoreactor in a gas phase containing only He and H_2O. The CO_2 reduction experiment is started once the concentration of products of the cleaning procedure (CH_4 and CO_2) is sufficiently low.

Due to inevitable aging effects of the Hg/Xe light sources, and potential slightly differing performance of the installed filters, light intensity was determined prior to each experiment. All reported light intensities thus apply to the exact measurement they are reported for.

The experiments with either UV or visible light were performed with a continuous flow of 7000 ppm CO_2 in He (1700 nmol/min). Absorption of the UV and visible part of the lamp spectrum was performed with Schott GG400 and UG11 (size 50 mm x 50 mm x 3 mm) colored glass filters, respectively. The

GG400 absorbs light with wavelengths smaller than 400 nm. The Schott UG11 filter removes light with wavelengths larger than 400 nm from the light beam. With the latter, UV radiation is in principle still transmitted, but the intensity of UV light is significantly attenuated. Although the lamp spectrum of the 200 W Hg/Xe lamp contains about 32% of UV light, the filter reduces the light intensity to ~11% of its corresponding value without filter, demonstrating that the filter also significantly attenuates the UV portion of the lamp spectrum. The total light intensity in this measurement (aged Hg/Xe lamp + 25% ND filter + Vis-Filter) amounted to only 0.012 W/cm^2. For these experiments additionally a 25% ND filter was used to protect the colored glass filters from thermal damage due to the illumination with the Hg/Xe lamp. A fresh sample of P25 was used for each of the two runs.

The experiments with different light intensities are conducted with only one sample of P25. From our previous work,[122] it is known that the sample filling influences the exposed portion of surface area, thus the activity of the sample.[122] On this account, using only one sample of P25 ensures equal illumination conditions. The intensity of the light was adjusted by ND filters and the resulting light intensity which hits the sample surface was measured by a Thorlabs PM100D actinometer with a S305C measuring cell. In these experiments the photocatalytic CO_2 reduction was performed under continuous flow of 1000 ppm CO_2 in He (250 nmol/min). The light intensity was adjusted to 0.17 (100 %), 0.092 (50 %), 0.041 (25 %), 0.023 (10 %), 0.012 (5 %) and 0.003 W/cm^2 (1 %) of the incident light intensity of the (aged) Hg/Xe lamp. The measurements were performed in the order (1) 0.17 W/cm^2, (2) 0.092 W/cm^2, (3) 0.023 W/cm^2, (4) 0.041 W/cm^2, (5) 0.003 W/cm^2, (6) 0.012 W/cm^2, in order to rule out apparent trends from consecutive measurements. After each activity test the sample was cleaned under photocatalytic conditions. Thereby, no ND filters were used to realize an efficient removal of carbonaceous intermediates of the previous CO_2 reduction experiment. All experiments under variation of the spectral range (=light energy) and light intensity, respectively, were performed with a nominal H_2O flow rate of 24 nmol/min (~100 ppm).

Studies of thermal effects were carried out using the cooling/heating mantle of the photoreactor. Temperature control was achieved using a Lauda Proline RP845 thermostat filled with pure water. Heating is thus limited to ~75°C. It is possible to record only the temperature of the heating mantle. The CO_2 reduction experiments for the investigation of thermal effects were performed with a continuous flow of 7000 ppm CO_2 in He (1700 nmol/min). No H_2O was dosed to the reactor, so that only the adsorbed H_2O residues on the surface of the photocatalyst can participate in the CO_2 reduction. For reference, one pure thermal reaction was carried out at 60°C without irradiation.

For the study of the effect of H_2O on the product formation of photocatalytic CO_2 reduction, experiments with a continuous flow of 7000 ppm CO_2 in He (1700 nmol/min) and variable H_2O partial pressure were executed. The product formation was investigated under the influence of large (~6000 ppm H_2O, 1400 nmol/min), small (~100 ppm H_2O, 24 nmol/min) and no H_2O dosing. The content of H_2O in the gas-

phase was adjusted by splitting the gas flow in two parts. One part of the gas flushed through the saturator while the other bypassed it. Both flows were combined before entering the reactor. This approach enables to saturate the gas flow with very small amounts of H_2O.

4.3 Results

4.3.1 Photocatalytic CO_2 Reduction under the Influence of different Light Energies

Figure 23 shows photocatalytic CO_2 reduction under the influence of light with wavelengths larger than 400 nm. For this experiment a 25 % ND and UV absorbing filter were introduced to the beam path of the illumination source, resulting in an overall light intensity of 0.67 W/cm^2. The two filters were installed after 3.75 h of photocatalytic cleaning, when the sample was sufficiently cleaned. After 45 minutes of visible light illumination, it can be observed that the CH_4 formation rate at the end of photocatalytic cleaning decreased significantly. At 4.5 h the CO_2 dosing was initiated. In the following three GC measurements (5.25 to 6.75 h) no CH_4 formation was observed. It appears that product formation from CO_2 is completely hindered under the applied illumination conditions with only visible light. After 6.75 h (Figure 23) the UV absorbing filter was removed from the beam path, to illuminate the photocatalyst with the whole spectrum of the lamp (ND filter still installed). The light intensity was determined to be 1.06 W/cm^2 in this measurement. Under these conditions it was possible to detect significant CH_4 formation. This result clearly shows that UV light is essential for the product formation of photocatalytic CO_2 reduction.

In a control experiment the CO_2 reduction was performed with pure UV light (Figure 24). After 3.75 h of photocatalytic cleaning with adequate removal of carbon residues, the ND and UV transmitting filters were introduced simultaneously into the beam path (Figure 24). In the last GC measurement of photocatalytic cleaning at 4.5 h no CH_4 has been detected. In the further course of the experiment the CO_2 flow was initiated. Then, contrary to the experiments shown in Figure 23 some CH_4 formation was indeed observed in the GC measurements from 5.25 to 6.75 h. No visible light hits the sample, which provides evidence that visible light is less relevant for the reaction. The observed difference in CH_4 formation rate can be most likely attributed to the transmission properties of the UV transmitting filter and the aging of the lamp, rather than an influence of visible light (see above). Since the intensity of UV light impinging on the sample is lowered, the activity of the photocatalyst is reduced, too. CH_4 formation increases once the UV transmitting filter was removed (7.5 and 8.25 h), in accordance with expectations.

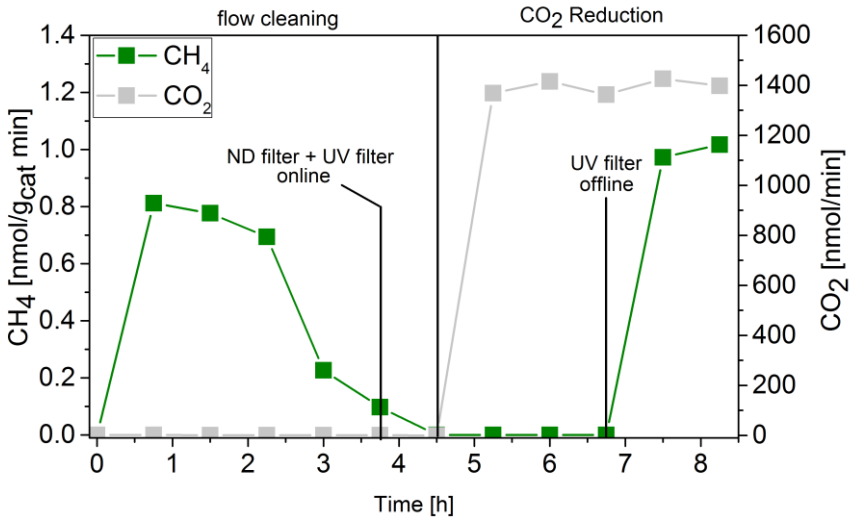

Figure 23: Photocatalytic CO_2 reduction under continuous flow conditions with UV absorbing filter. Photocatalytic cleaning (0 to 4.5 h). CO_2 reduction with wavelengths of 400-700 nm (4.5 to 6.75 h) and CO_2 reduction with complete lamp spectrum (6.75 to 8.25) CH_4 concentrations are shown on a different scale (left axis) than the CO_2 concentration (right axis).

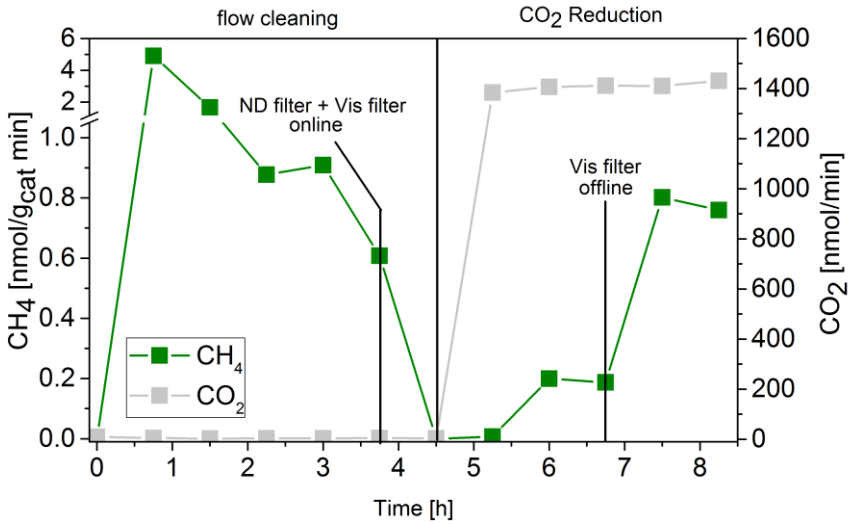

Figure 24: Photocatalytic CO_2 reduction under continuous flow conditions with UV transmitting filter. Photocatalytic cleaning (0 to 4.5 h). CO_2 reduction with wavelengths of 200-400 nm (4.5 to 6.75 h) and CO_2 reduction with complete lamp spectrum (6.75 to 8.25). CH_4 concentrations are shown on a different scale (left axis) than the CO_2 concentration (right axis).

4.3.2 Photocatalytic CO_2 Reduction under the Influence of different Light Intensities

Figure 25 shows the CO_2 reduction experiments with 0.17 (100 %), 0.092 (50 %), 0.041 (25 %), 0.023 (10 %), 0.012 (5 %), 0.003 W/cm^2 (1 %). Compared to the previous paragraph, the light intensity during the use of the 25 % ND filter is significantly lower. This difference in the two sets of experiments can be traced back to the decreasing light intensity of Hg/Xe lamps with increasing hours of operation. The experiments of the previous paragraph were performed with a relatively new illumination source with fewer hours of operation, whereas the experiments in this paragraph were performed with a relatively older lamp with many hours of operation.

From Figure 25 A-F it can be obviously seen that CH_4 concentration increases as soon as CO_2 is flushed through the reactor. After a certain number of GC measurements the CH_4 concentration stabilizes. Each CO_2 reduction experiment in Figure 25 was conducted until stabilization of the CH_4 formation was approached. Although oxygen formation is not observed, we attribute the stable CH_4 formation rate to a "near steady state", as it was explained in the previous chapter. The CH_4 formation rates at the end of each experiment (Figure 25) were used to evaluate the influence of the light intensity on the photocatalytic CO_2 reduction. The Figure 25 (E) and (F) present the results of CH_4 formation from CO_2 reduction at lowest light intensities. On first glance, it may appear that no CH_4 is formed from CO_2, since the amounts formed at the end of the experiments (7.75 h) do not exceed those at the end of the cleaning procedure (4.25 and 3.75 h, respectively). However, it needs to be considered that the rate of product formation from hydrocarbon impurities to CH_4 also decreases significantly at lower UV light intensities (Figure 24). In Figure 25 (E) it becomes clear that in fact "no" CH_4 is formed from impurities at such low light intensity (measurement at 5.25 h). From Figure 25 A-F it can also be seen that the light intensity influences the time until a stable CH_4 formation is reached. For the experiment with 0.17 W/cm^2 CH_4 formation becomes almost stable after 3.75 h. In the experiment with 0.092 W/cm^2 the stable CH_4 formation was reached after 90 minutes of CO_2 reduction. A further decrease of this period to 45 minutes was observed by conducting the CO_2 reduction with 0.023 and 0.041 W/cm^2. In contrast, the experiments with 0.012 and 0.003 W/cm^2 (Figure 25) show that the establishment of a stable CH_4 formation requires about 2.25 h. The reasons for these observations are still unknown.

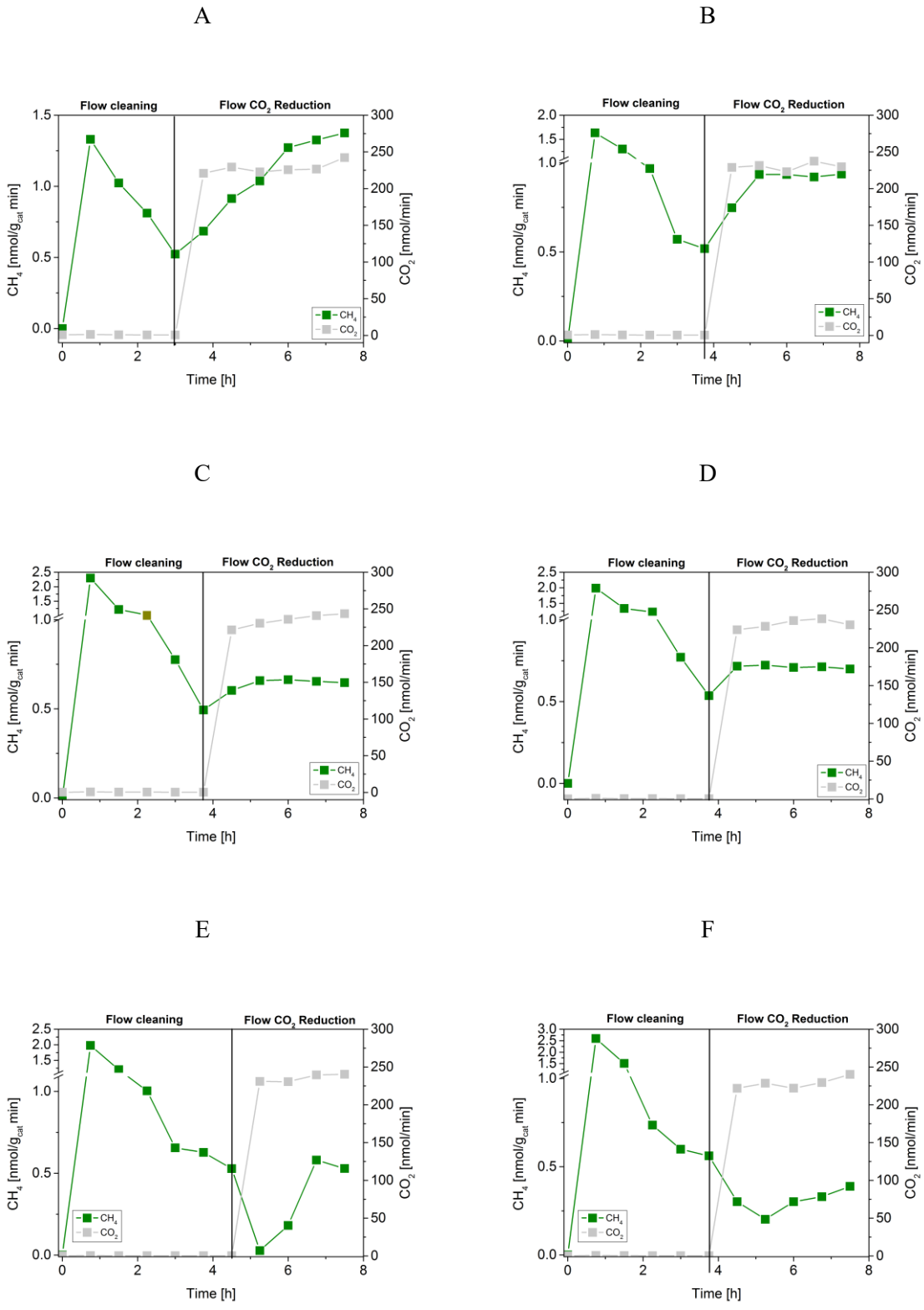

Figure 25: Photocatalytic CO_2 reduction under continuous flow conditions with light intensity of A: 0.17 (100 %), B: 0.092 (50 %), C: 0.041 (25 %), D: 0.023 (10 %), E: 0.012 (5 %), F: 0.003 W/cm^2. CH_4 concentrations are shown on a different scale (left axis) than the CO_2 concentration (right axis).

It is clear from Figure 26 that the product formation is significantly enhanced if the light intensity varies between 0 and 0.023 W/cm^2. A further increase of the light intensity shows further enhancement of the CH_4 formation, but the increase of the rate is less significant than at lower light intensities.

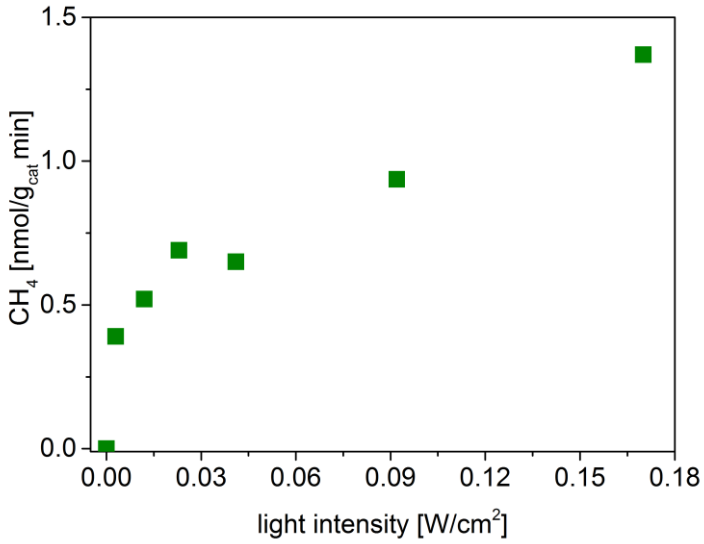

Figure 26: Photocatalytic CO_2 reduction under the influence of different light intensities.

4.3.3 Influence of Thermal Effects

A B

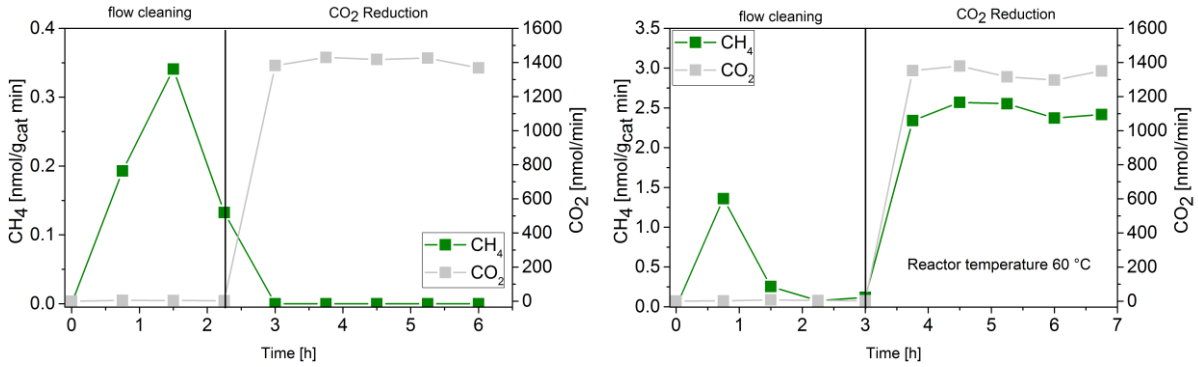

Figure 27: A: CO_2 reduction under continuous flow conditions. Reactor temperature 60 °C. Thermal cleaning from 0 to 2.25 h. CO_2 reduction from 2.25 to 6 h. B: Photocatalytic CO_2 reduction under continuous flow conditions with complete lamp spectrum. Reactor temperature 60 °C. Photocatalytic cleaning (0 to 3 h). CO_2 reduction (3 to 6.75 h). CH_4 concentrations are shown on a different scale (left axis) than the CO_2 concentration (right axis).

Figure 27 A displays the results of a pure thermal reaction of CO_2 and H_2O on TiO_2. Clearly, CH_4 is not formed at all, excluding locally occurring pure thermal effects (e.g., because heat released upon recombination) as the predominant reason for product formation. On the other hand, as evidenced by the results reported in Figure 27 B, thermal effects can indeed enhance CH_4 formation. On heating the reactor to 60°C, as the reaction is performed und irradiation, the amount of CH_4 formed is almost twice as high as observed under comparable reaction conditions at room temperature (Figure 27 A). This

indicates that the reaction, although predominantly light induced, contains classical catalytic reaction steps as rate-determining step(s) that are expectedly improved by higher temperature, according to the well-known Arrhenius-type description of the reaction rate of elementary steps. To verify whether a simple improvement in the (associative) desorption of CH_4 is responsible for the observation of improved product yield, a sample was heated to 75°C after pure photocatalytic CO_2 reduction has been performed (Figure 28). The lack of any CH_4 desorption under these conditions rules out this explanation.

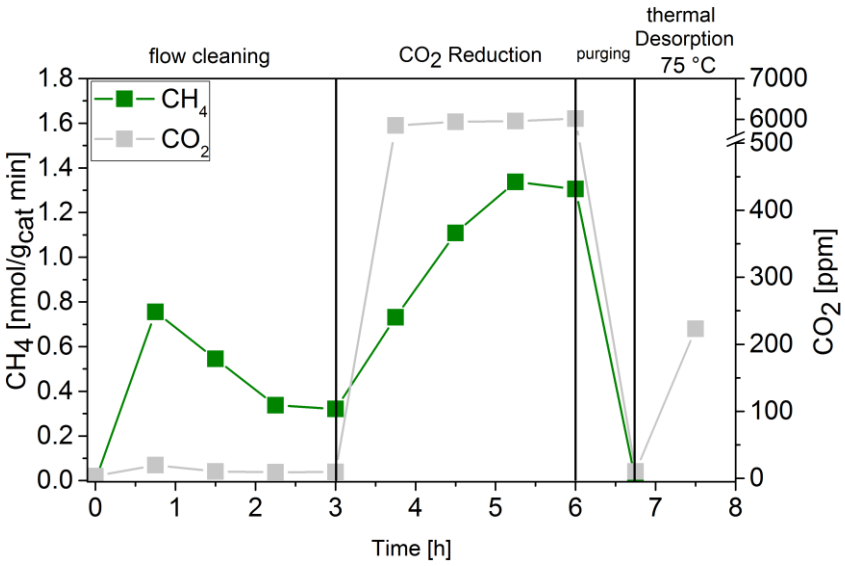

Figure 28: Studies of possible rate-limiting effects of CH_4 desorption. Photocatalytic CO_2 reduction was performed for 6 h at room temperature. After 45 min of purging in flow mode at room temperature, the reactor was heated to 75°C in batch mode. CH_4 desorption is not observed in this period.

4.3.4 Photocatalytic CO_2 Reduction under the Influence of different H_2O Concentration

To determine the effect of H_2O, product formation of photocatalytic CO_2 reduction was conducted under varying H_2O partial pressure in the reactant gas feed. Thereby all the other parameters, for instance the CO_2 flow and the illumination conditions remained unchanged. At first the photocatalytic cleaning procedure and the CO_2 reduction were performed without any additional dosing of H_2O (Figure 29) to verify if the physisorbed H_2O residues on the surface of the photocatalyst are sufficient to run the photocatalytic processes.

It is expected that the sample provides H_2O for a photocatalytic conversion, since the surface of TiO_2 is able to adsorb H_2O at room temperature.[126,127] It has been suggested that under ambient conditions, oxide surfaces might be covered with up to 20 layers of water.[98] From Figure 29 it is clear that the formation of CH_4 as the product of photocatalytic cleaning and further on as the product of photocatalytic CO_2 reduction took place. This result indicates that both processes can be performed with

the H_2O residues located on the surface of the photocatalyst. From 7.5 h onwards, the CH_4 formation rate decreases, most likely, this change in the product formation is a consequence of the lack of the hydrogen source for CO_2 reduction due to the absence of H_2O dosing.

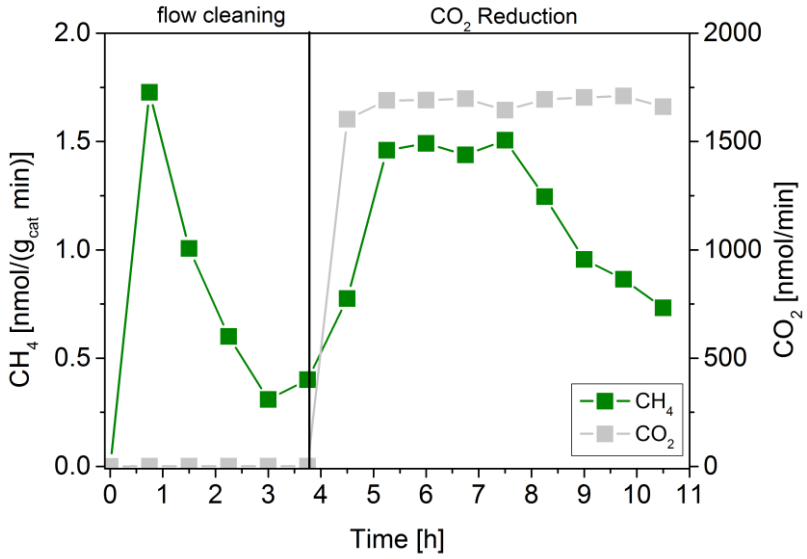

Figure 29: Photocatalytic CO_2 reduction under continuous flow conditions without additional dosing of H_2O. Photocatalytic cleaning (0 to 3.75 h); CO_2 reduction (3.75 to 10.25 h). CH_4 concentrations are shown on a different scale (left axis) than the concentration of CO_2 (right axis).

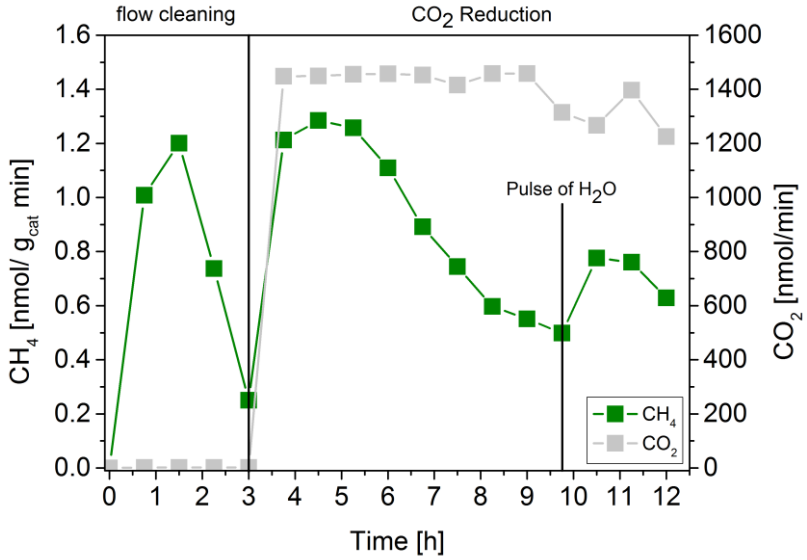

Figure 30: Photocatalytic CO_2 reduction under continuous flow conditions with pulse dosing of H_2O. Photocatalytic cleaning (0 to 3 h). CO_2 reduction (3 to 12 h). H_2O Pulse dose after 9.75 h. CH_4 concentrations are shown on a different scale (left axis) than the concentration of CO_2 (right axis).

On the basis of this experiment, attempts to examine the participation of gaseous H_2O in the product formation of photocatalytic CO_2 reduction were made. Therefore, the conditions of the former experiment (Figure 30) were applied a second time, but this time a pulse of H_2O was given to the reactor

as soon as the product formation was significantly decreased (Figure 30). An increase in product formation can be observed after the pulse of H_2O was given to the reactor. This finding reveals the participation of H_2O dosed from the gas phase in product formation from photocatalytic CO_2 reduction. However, this result also demonstrates that the pulse dose of H_2O does not increase the CH_4 formation rate to the initial activity at 4.5 and 5.25 h (Figure 30). GC measurements show after 11.25 and 12 h reaction time (Figure 30), the CH_4 formation rate decreases again.

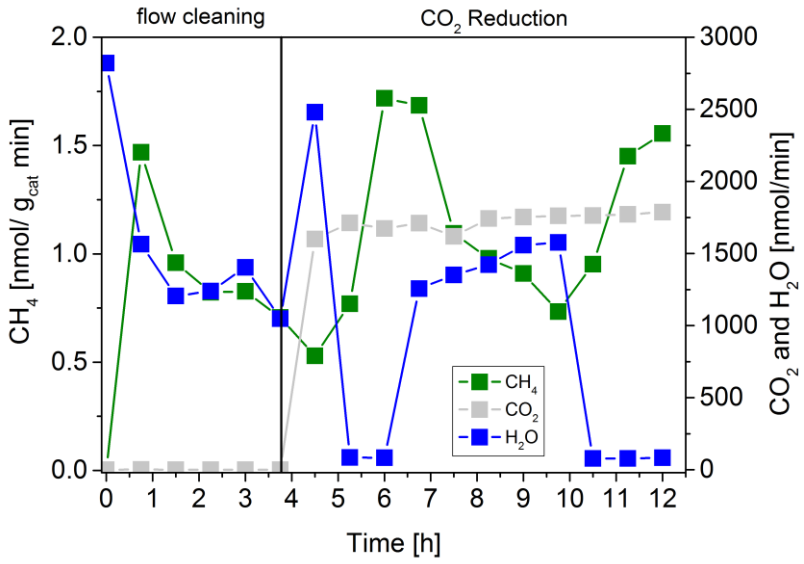

Figure 31: Photocatalytic CO_2 reduction under continuous flow conditions with alternating periods of H_2O dosing. Photocatalytic cleaning (0 to 3.75 h). CO_2 reduction (3.75 to 12 h). Continuous H_2O flow (6000 ppm amounting to 1500 nmol/min) from 0 to 4.5 h and 6.75 to 10 h. CH_4 concentrations are shown on a different scale (left axis) than the concentrations of CO_2 and H_2O.

In another experiment, photocatalytic cleaning and CO_2 reduction was run at significantly higher H_2O flow rates, to investigate if the product formation can be enhanced by higher H_2O concentrations. Figure 31 shows the experiment with alternating periods of a nominal continuous flow of 1500 nmol/min (6000 ppm) and 0 nmol/min (0 ppm) H_2O. After the cleaning procedure, CH_4 formation did not increase (4.5 h, Figure 31), on addition of both reactants H_2O and CO_2 to the reactor. After 4.5 h the saturator was set offline to stop H_2O dosing, and indeed, in the next data point at 5.25 h it can be clearly seen that the gas-phase H_2O content of the gas flow decreased significantly. At the same time the CH_4 formation significantly increases. The CH_4 formation rate further increases to about 1.75 nmol/g_{cat} min at 6 h reaction time. From 6 to 10 h H_2O dosing was continued, and H_2O flow rate increases to the nominal value of 1500 nmol/min. Simultaneously, a significant decrease of the CH_4 formation rate was observed. The product formation rate increases again as soon as the continuous H_2O dosing was turned off again after 10 h (Figure 31). This result clearly shows that a continuous flow of significant amounts of gaseous H_2O has a negative impact on the photocatalytic CO_2 reduction.

4.4 Discussion

4.4.1 Origin of Product Formation: Photoexcitation vs. Photo-induced Thermal Excitation

The experiments of this study clearly revealed the necessity of using UV light for the photocatalytic CO_2 reduction on TiO_2. Under visible light illumination, no photocatalytic activity was observed (Figure 23). In contrast pure UV light allows CH_4 formation (Figure 24). This evidences that the excitation of TiO_2 is predominantly induced by UV photons, as is expected considering that the bandgap of TiO_2 is $\geq$3 eV. Solely the UV light of the lamp spectrum delivers photons of sufficient energy to overcome the band gap of TiO_2. Thus, the transfer of electrons into the conduction band can proceed.[43,128] The visible light alone does not provide enough energy to induce the excitation of charge carriers in TiO_2. This observation, together with the lack of any product formation at 60 °C in the dark makes it seem unlikely that the reaction is predominantly photothermally induced. However, the results indicate that the mechanism of photocatalytic CO_2 reduction includes steps which are enhanced by an increased temperature, for example, caused by the evolved heat of charge carrier recombination. It might be possible that the heat of charge carrier recombination results in local heating of the surface structure of TiO_2. This could accelerate the formation of intermediates and products in the classical catalytic elementary steps, according to the common Arrhenius-type temperature dependence of reaction constants. In addition, the transport of reactants and intermediates to the active sites and desorption of the products might also be facilitated. The simple improvement of CH_4 desorption, however, cannot explain the observations.

4.4.2 Effect of Light Intensity on the Product Formation of Photocatalytic CO_2 Reduction

The results of the photocatalytic CO_2 reduction showed a clear dependence between the intensity of light and the CH_4 formation rate (Figure 26). It was further revealed that the product formation is more strongly influenced at lower light intensities than at higher light intensities. On the one hand, an improved photoexcitation owing to higher light intensities results in an increased concentration of carriers for charge transfer reactions to adsorbed species. On the other hand, the thermodynamically favored charge carrier recombination becomes a dominating effect. In this respect, the consumption of charge carriers by recombination is more strongly enhanced than the consumption by charge transfer reactions. The relative dependence of CO_2 reduction rate on light intensity thus decreases at higher light intensities. In the following paragraph the dependence of light energy on the product formation of photocatalytic CO_2 reduction are represented in a simplified kinetic model.

Simple kinetic model for CH_4 formation in photocatalytic CO_2 reduction under intermediate light intensity

In our very simplified kinetic model, it is assumed that the amount of CH_4 formed in the reaction has reached a steady state ($\frac{dp_{CH4}}{dt} = 0$). Furthermore, both the processes responsible for charge carrier generation/recombination, and CO_2 adsorption, are assumed to be in pseudo-equilibrium ($\frac{d\theta_{CO2}}{dt} = 0$; $\frac{d[e^-]}{dt} = 0$). Photoexcitation, recombination, CO_2 adsorption and desorption will all occur on much faster time scales than CH_4 formation. All steps of photocatalytic formation of CH_4 from CO_2 are summed up in just one step, which is considered to be rate-limiting.

The description of charge carrier formation is adopted from Rothenberger et al.[116] Excitation and recombination are described as:

$$TiO_2 + h\nu \xrightarrow{k_1} e^- + h^+ \xrightarrow{k_2} \text{heat} \tag{4.1}$$

The rate of photoexcitation (r_{exc}) and the rate of recombination (r_{rec}) can then be described as follows:

$$r_{exc} = k_1 I \tag{eq. 4.1}$$

$$r_{rec} = k_2 [e^-]^2 \tag{eq. 4.2}$$

In order to write Eq. (eq. 4.2) in this way, it is assumed that the concentration of photogenerated electrons and holes is equal ($[e^-] = [h^+]$) and that native charge carriers in TiO_2 can be neglected.[121]

Using Eq. (eq. 4.2), the amount of excited electrons in pseudo-equilibrium can be described as:

$$[e^-] = \sqrt{\frac{k_1}{k_2} I} \tag{eq. 4.3}$$

Adsorption and desorption of CO_2 are described according to the Langmuir isotherm (with θ_*= number of free adsorption sites):

$$CO_2 + * \overset{k_3;k_{-3}}{\longleftrightarrow} CO_2^* \tag{eq. 4.4}$$

$$r_{ads} = k_3 p_{CO_2} \theta_* \tag{eq. 4.5}$$

$$r_{des} = k_{-3} \theta_{CO_2} \tag{eq. 4.6}$$

In case of pseudo-equilibrated CO_2 adsorption, it holds that

$$\theta_{CO_2} = \frac{k_3}{k_{-3}} p_{CO_2} \theta_* = K_3 p_{CO_2} \theta_* \quad \text{(eq. 4.7)}$$

The formation of CH_4 from photogenerated electrons and adsorbed CO_2 is considered in one step. We are aware that this is an oversimplification of the true microkinetic processes. This simple model is only used to highlight the general dependence of reaction rate on light intensity, as will be shown below. The only necessary assumptions here are that the rate depends linearly on the number of photogenerated electrons, and that it depends in some way on an Arrhenius-type rate constant.

$$CO_2^* \xrightarrow{e^-;\, k_4} CH_4 \quad \text{(eq. 4.8)}$$

$$r_{CH_4} = k_4 \theta_{CO_2} [e^-] \quad \text{(eq. 4.9)}$$

Substituting Equations (eq. 4.3) and (eq. 4.7) into Equation (eq. 4.9) and slight rearrangement of terms yields:

$$r_{CH_4} = \sqrt{\frac{k_1}{k_2}} k_4 K_3 p_{CO_2} \theta_* \sqrt{I} \quad \text{(eq. 4.10)}$$

In the studies of light intensity variation, the partial pressure of CO_2 (and of H_2O) was kept constant. Neglecting a certain coverage of free sites with intermediates and products, the number of free sites can also be considered constant. Assuming that also the separate rate constants are identical in all cases, i.e. because the sample temperature is always the same, Equation (eq. 4.10) can be simplified to:

$$r_{CH_4} = k' \sqrt{I} \quad \text{(eq. 4.11)}$$

Consequently, this simplified kinetic discussion using reasonable assumptions rationalizes the square-root dependence of CH_4 formation rate on light intensity.

$$r_{CH_4} \sim \sqrt{I} \quad \text{(eq. 4.12)}$$

Under these circumstances the CH_4 formation rate should be proportional to the square root of the light intensity (eq. 4.12), owing to the predominant effect of the enhanced recombination kinetics.[118,119,129]

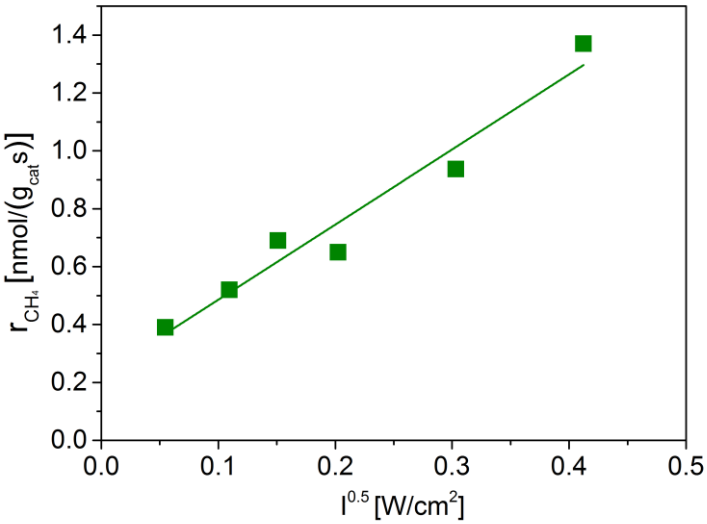

Figure 32: Photocatalytic CO_2 reduction under the influence of different light intensities. Linear fit of the CH_4 formation rate and the square root of the light intensity.

To verify the impact of enhanced charge carrier recombination on the CH_4 formation, the rate is plotted against the square root of the light intensity (Figure 32). Figure 32 indeed displays a linear tendency between the rate of CH_4 formation and the square root of the light intensity, which verifies that the charge carrier recombination downgrades the efficiency of photocatalytic CO_2 reduction at higher light intensities. The fit is a littler worse at low light intensities. This observation indicates that the square root dependence is probably not valid in a range of light intensity from 0 to 0.03 W/cm^2. Instead, it is highly probable that the rate of product formation increases linearly in the low intensity range, as is also indicated in Figure 26. In addition it is another indication that CH_4 is formed in a photo-induced process. However, a further enhancement of the rate by the light intensity should then result in conditions in which the product formation becomes mass transfer limited. Then the product formation would be independent from the light intensity.[118]

4.4.3 The Role of H_2O in the Photocatalytic CO_2 Reduction

The investigations to determine the effect of H_2O on the photocatalytic CO_2 reduction revealed a clear dependence of product formation on the H_2O content. If no H_2O is supplied to the photocatalyst the product formation decayed after a couple of hours (Figure 29). It appears realistic that the product formation came to an end as soon as the H_2O residues on the surface of the photocatalyst are consumed. The product formation is initiated again as soon as H_2O is available (Figure 30). This result verifies the participation of H_2O in the formation of CH_4. Most likely, photocatalytic H_2O oxidation represents the hydrogen (proton) delivering reaction for the formation of CH_4. However, no O_2 was detected as the product of H_2O oxidation (1.6) and CO_2 reduction (1.7). This is unexpected, because both processes should evolve O_2. Furthermore, it raises the question regarding the fate of O_2 as the second product.

Since the product analysis of this study has been performed with a GC, the presence of O_2 can only be excluded for the gas-phase of the photoreactor. On the basis of the former, the participation of H_2O oxidation in the product formation, and the absence of O_2 in the gas phase of the photoreactor, it might be possible that O_2 or O-derived species remain on the surface of the photocatalyst instead of being desorbed. Potential O-derived species could be superoxide or surface peroxyl species.[124,130-133] Another likely reason for the absence of O_2 in the gas-phase of the photoreactor could be an incomplete H_2O oxidation (4.2 and 4.3) or H_2O reduction (4.4). Reactions (4.2-4.4) represent charge transfer reactions which indeed result in the formation of a hydrogen source but O_2 is not simultaneously formed as a product. Instead OH-species and H_2O_2 could be generated, which may contribute to the formation of surface hydroxyl and peroxyl groups, respectively. The clarification of the fate of O_2 in the overall process of photocatalytic CO_2 reduction is object of our ongoing studies.

$$H_2O + h^+ \rightarrow OH^{\cdot} + H^+ \tag{4.2}$$

$$2\,H_2O + 2h^+ \rightarrow H_2O_2 + H^{\cdot} \tag{4.3}$$

$$H_2O + e^- \rightarrow OH^- + H^{\cdot} \tag{4.4}$$

However, it is also questionable why the CH_4 formation rate did not increase to the initial value after a non-quantifiable pulse of H_2O was given to the reactor. A potential reason for this observation could be that the H_2O pulse was too small. Consequently, the available amount of H_2O was not adequate to deliver enough reactants to increase CH_4 formation back to the initial rate. Likewise a potential deactivation of the photocatalyst by loss of active sites due to occupation with O_2 or O-derived species could be responsible for the lower activity. Saladin et al.[125], for instance, assumed a deactivation of TiO_2 in photocatalytic CO_2 reduction by the accumulation of O-derived species, which are unable to desorb under photocatalytic reaction conditions. As a consequence of this accumulation, these species enhance the backward reaction of CO_2 reduction, which is hydrocarbon oxidation.[125]

The experiment with a high H_2O flow rate exhibited a negative effect on the formation of CH_4, because product formation decreased under a continuous flow of 1500 nmol/min H_2O (Figure 31). A likely reason can be found in the interaction of H_2O and CO_2 with TiO_2. Both reactants may compete for adsorption sites, and thus for potential active sites. Since the binding energy of CO_2 on TiO_2 is smaller than that of H_2O,[114,134] adsorbed CO_2 may be replaced by H_2O, thus limiting the activity. Another explanation may be found in the adsorption properties of H_2O on TiO_2. It can adsorb in a molecular and dissociative manner.[127] The latter adsorption pathway results in the generation of surface hydroxyl groups.[127] Belhadj et al.[112] found an improved interaction of H_2O with TiO_2 under illumination. Under these conditions the hydrophilicity of TiO_2 is enhanced by the formation of surface hydroxyl groups.[112] These hydroxyl groups may also have an effect towards the interaction of CO_2 and TiO_2. Potentially,

the CO_2 adsorption geometry is changed by the surface hydroxyl groups in a way that its activation for a charge transfer reaction is impeded. As a consequence, less photocatalytic conversion of CO_2 takes place. As a third explanation, if a reduction of water according to equation (4.16) is involved in the formation of a hydrogen source for CH_4 formation, both reactants H_2O and CO_2 would compete for photogenerated electrons. Assuming that the transfer onto H_2O is more efficient, possibly because it is adsorbed more strongly, then considerably less electrons would be available for a transfer on CO_2. Such questions need to be clarified in future work.

Together with our previous study,[122] the inevitable limitations of bare TiO_2 in the reaction are now clear: Neither an increase in light intensity, nor in the concentration of either of the two reactants, can increase CH_4 formation. A slight increase of the reaction temperature can only lead to incremental improvements of product formation, but does not lead to order-of-magnitude effects. Furthermore, oxygen formation does not occur in any of the studied cases. Our results strongly suggest that bare commercial TiO_2 can never be an industrially viable option as photocatalyst for CO_2 reduction. On the positive side, highly promising routes for an improvement of photocatalysts for CO_2 reduction, TiO_2-based or not, are now also clearly outlined. Charge carrier recombination needs to be suppressed, so that higher light intensities can still result in a significant increase in product formation. Moreover, active sites need to be modified so they favor adsorption of CO_2 in the appropriate geometry over H_2O adsorption. Lastly, the nature of the active sites and of the reaction intermediates need to be further clarified in future studies.

4.5 Conclusions

This study reveals further evidence that the product formation of photocatalytic CO_2 reduction truly originates from CO_2 and H_2O. Product formation is strongly dependent on the availability of UV photons, verifying that the excitation of TiO_2 for CO_2 reduction is most likely a UV photon driven process. Performing the CO_2 reduction at higher temperature can increase the yield of the product CH_4. A further finding of this study revealed the dominating influence of charge carrier recombination at high light intensities. Over a certain range of low light intensities, the CH_4 formation rate can be significantly increased. At higher light intensities the charge carrier recombination is more strongly enhanced than the charge transfer reaction, so product formation can only be increased by the square root of the light intensity. The photocatalytic cleaning procedure and the CO_2 reduction can already be performed with traces of adsorbed H_2O. In contrast, a continuous flow of 1500 nmol/min H_2O results in an inhibition of the product formation. Most likely competitive adsorption phenomena between CO_2 and H_2O on TiO_2, occupation of active sites for CO_2 reduction by H_2O, changes in the adsorption geometry of CO_2, or a competition for charge carriers are responsible for this effect. Consequently photocatalytic CO_2 reduction under continuous flow conditions should be conducted with particularly small H_2O

concentrations. Significant improvements in CH_4 formation on TiO_2, however, cannot be achieved by optimization of reaction conditions alone, since improvements in the photocatalyst itself are required.

5. The Fate of O_2 in the Photocatalytic CO_2 Reduction on TiO_2

Abstract

The photocatalytic reduction of CO_2 to CH_4 by using H_2O as the oxidant presupposes the formation of O_2. Both the reduction of CO_2 and the oxidation of H_2O represent O_2 evolving processes. However, most of the studies dealing with photocatalytic CO_2 reduction are focusing on the formation of carbon related products while less attention is paid to the formation of O_2 as the by-product. It is often not included to the product analysis or it is reported to be not formed at all. On this account the present study aims to clarify the absence of O_2 in the photocatalytic CO_2 reduction on TiO_2. In the first part of this work TiO_2 has been modified with co-catalysts for H_2O oxidation, since the activity of TiO_2 for this reaction is generally low. Therefore it became possible to evaluate the effect of improved H_2O oxidation properties on the photocatalytic CO_2 reduction. The modified samples exhibited a significant activity in the H_2O splitting reaction. Both products H_2 and O_2 were formed in almost stoichiometric amounts. It is also shown that formation of H_2 is the dominating reaction of the photogenerated electrons in TiO_2. More specific it was not possible to observe any activity in CO_2 reduction as long as the H_2O splitting reaction proceeded. Most likely the electron consuming H_2 formation and an inhibiting effect of O_2 are the reasons for the absence of CH_4 formation. Experiments with bare TiO_2 under similar reaction conditions showed no activity in H_2 and O_2 formation, indicating that TiO_2 is not able to oxidize H_2O efficiently. All these results imply that the photocatalytic H_2O oxidation is not the hydrogen source for the CO_2 reduction reaction on TiO_2. Consequently a different hydrogen source must be available on TiO_2 to enable the CH_4 formation. Another part of this study reveals a consumption of O_2 by TiO_2 under photocatalytic reaction conditions. This stoichiometric reaction is potentially associated with the absence of O_2 in the CO_2 reduction reaction and at the same time represents a key factor of the photocatalytic properties of TiO_2. This study can be understood as a notice for the complexity of the reaction mechanism of the overall CO_2 reduction on TiO_2. It further outlines that the formation of CH_4 is most likely not based on a catalytic cycle of the reactants and the photocatalyst.

The main content of this chapter is published in Phys. Chem. Chem. Phys. **2019**, 10.1039/C8CP07765G as “The Fate of O_2 in Photocatalytic CO_2 Reduction on TiO_2 under Conditions of Highest Purity”, M. Dilla, A. Jakubowski, J. Strunk, R. Schlögl, S. Ristig.

5.1 Introduction

In many reports the main products of photocatalytic CO_2 reduction are CH_4, CO and methanol.[20,72,135,136] Given that CH_4 is formed from CO_2 in a photocatalytic reduction, it is necessary that the C=O double bonds are cleaved and four C-H bonds are formed. This process requires the transfer of eight electrons from TiO_2 to the carbon atom. For this reason a second reactant, which can provide these charge carriers and the source of hydrogen is needed. H_2O is the most desirable oxidant for this purpose. It is commonly believed that the process of photocatalytic H_2O oxidation on TiO_2 is associated with the transfer of four holes (h^+) to form an O_2 molecule (5.1). At the same time the bound hydrogen is liberated for a consequent hydrogenation reaction (5.1).

$$2\,H_2O + 4\,h^+ \xrightarrow{hv,\ photocatalyst} O_2 + 4\,H^+ \qquad (5.1)$$

Both processes, the reduction of CO_2 and the oxidation of H_2O produce excess oxygen as by-products. It is proposed that this excess oxygen is converted to O_2 (1.7). In the end the overall photocatalytic CO_2 reduction with H_2O results in the formation of two equivalents of O_2 per CH_4 molecule (1.7). However, with some exceptions[85-89] the research effort focuses mostly on the formation of carbon related products, probably as they are the targeted product for storing chemical energy. The formation of O_2 is often neglected, or it cannot be found at all in the products of photocatalytic CO_2 reduction[124,125]. The absence of O_2 can have several reasons, for instance, the participation in the backwards reaction (CH_4 oxidation), the replenishment of oxygen vacancies (V_{Ox}) on TiO_2[111,112] and limitations in H_2O oxidation kinetics leading to the accumulation of reaction intermediates on the catalyst surface. The latter could be related to the overpotential of H_2O oxidation on bare TiO_2.[90] Without using an external bias the activity towards H_2O oxidation might be rather low. Then it would be questionable if there is any other hydrogen source for C-H bond formation, such as surface hydroxyl groups.

In our previous studies[122,137] we performed continuous flow CO_2 reduction experiments where we demonstrated that CH_4 formation is dependent on the abundance of CO_2 and H_2O. Without dosing of H_2O, the product formation diminished after a couple of hours and initiated again as a pulse of H_2O was given into the reactor. It was concluded that the reaction proceeds initially by the contribution of physisorbed H_2O residues, which are usually available on the surface of TiO_2[126,127]. The product formation ceases once they are consumed for hydrogenation or light induced thermal desorption. Then the pulse-dosed H_2O molecules serve as the source of hydrogenation. Although H_2O appears to participate in the photoinduced CH_4 formation, it was not possible to detect any O_2 or oxygen derived species as products of H_2O oxidation. On this account the present study focuses on the clarification of the fate of O_2 as the by-product of the overall photocatalytic CO_2 reduction. Therefore P25 TiO_2 is modified with an O_2 evolution co-catalyst in order to evaluate if improved H_2O oxidation conditions have an effect towards the overall product formation of photocatalytic CO_2 reduction to CH_4. At the

same time the impact of O_2 evolution on CH_4 formation can be investigated. One of the most prominent materials for H_2O oxidation in electrochemical approaches are IrO_x and CoO_x. It has been found that these transition metal oxides exhibit an outstanding activity in this reaction because of its relatively low overpotential.[138-141] Investigations on IrO_x and CoO_x materials have shown that the activity in the oxygen evolution reaction (OER) is dependent on the concentration of lattice defects.[140,142] A study on hydrated amorphous Ir oxyhydrates[142] revealed that IrO_x species having defects in the cationic and anionic lattice structure are more active in the OER. The authors concluded that weakly bound electrophilic oxygen species play a key role in the superior activity. In order to form such electrophilic oxygen species the surrounding Ir lattice requires flexible oxidation states.[142] The electrophilic oxygen species are prone to nucleophilic attacks of H_2O. It is assumed that these species participate in the potential limiting step, namely the O-O bond formation of the OER.[142,143] Furthermore the photocatalytic activity of IrO_x as a co-catalyst for the O_2 evolution reaction has also been tested. It is proposed that photogenerated holes in TiO_2 are transferred to the IrO_x particles,[144,145] where the H_2O oxidation reaction takes place. In this way TiO_2 represents the photoabsorber and IrO_x the heterogeneous catalyst. Such IrO_x/TiO_2 materials showed an improved O_2 evolution activity compared to bare TiO_2.[145] On this account it appears to be a suitable candidate for the purpose of this work. In general it is of fundamental interest to clarify the fate of O_2 in the photocatalytic CO_2 reduction on TiO_2. This elucidation helps to verify if product formation is a true catalytic cycle. Furthermore, it contributes to a better understanding of this complicated process and assists to the development of reaction-based modification strategies for photocatalyst preparation.

5.2 Experimental

5.2.1 Sample Preparation

Sample modification of P25 with IrO_x and CoO_x was performed via photodeposition in a semi-batch reactor made from quartz glass. On-top illumination was realized by a 1000 W Hg/Xe lamp. 400 mg P25 was dispersed in 200 mL H_2O and ultra-sonicated for one minute. Then the dispersion was given into the reactor and 20 mL of methanol were added. The precursors iridium acetate or cobalt acetate were added to the dispersion amounting to a nominal loading of 0.05 wt.-% Ir and Co, respectively. The reactor was sealed and deaerated with pure He gas for 1.5 h. After purging the reactor, the He flow rate was set to 20 mL/min and the illumination was initiated. The overall deposition time was 3 h. Subsequently the dispersion was filtered and dried overnight. The obtained powder was then divided into two equal fractions. One fraction was calcined in synthetic air for 3 h at 200 °C, and the other at 400 °C, respectively, with a heating rate of 5 K/min. Reference samples without Ir and Co have been prepared by the same procedure. Calcination of the samples is the first step to remove adsorbed carbon containing species from the surface to prevent their potential contribution to the product formation leading to an overestimated activity.

5.2.2 Sample Pretreatment and Photocatalytic Activity Tests

70 mg of each sample has been tested in a CO_2 reduction experiment. As the initial calcination steps are not sufficient to remove all of the carbon-containing species from the sample, further purification has been carried out before the activity test. This pretreatment step was performed in the photoreactor set-up. A He gas flow only including H_2O was given through the reactor under illumination. The flow rate of H_2O is adjusted to ~1000 nmol/min. This pretreatment under photocatalytic reaction conditions is further termed as flow cleaning. Although such an experiment is mainly performed to purify the sample from carbonaceous impurities, it simultaneously provides conditions for photocatalytic H_2O splitting. Thus the activity in the H_2O splitting reaction is determined before CO_2 reduction is studied. GC measurements are conducted all 45 minutes to monitor the cleaning progress and the formation of H_2 and O_2. After the concentration of products from the flow cleaning procedure (CH_4 and CO_2) are sufficiently low the CO_2 reduction experiment is initiated. Therefore, the gas flow is changed from pure He to 1700 nmol/min CO_2 in He. The H_2O flow rate in the CO_2 reduction experiments is either held at ~1000 nmol/min or changed to ~25 nmol/min. From our previous study[137] we know that high H_2O flow rates can inhibit product formation. A flow of ~25 nmol/min H_2O is sufficient to observe significant product formation.

5.3 Results

5.3.1 Photocatalytic Cleaning and H_2O Splitting with IrO_x/P25

The results of photocatalytic H_2O splitting experiments with the 0.05 wt.-% IrO_x/P25 samples calcined at 400 and 200 °C, respectively are shown in Figure 33 and Figure 34. A significant H_2 formation can be observed for both samples once the illumination is started at 0 h (Figure 33 and Figure 34). It can be also seen that the H_2 formation rates scale with the flow rates of H_2O and stabilize over the course of the experiment. In contrast O_2 formation shows a different development. O_2 is only detected after 6 h of illumination in the first experiment of the 400 °C sample (Figure 33 A). For this reason a second H_2O splitting experiment with this sample is conducted (Figure 33 B). In this experiment the apparent O_2 formation rate increases strongly from 0 to 3.75 h. From 3.75 h on, the formation rate of O_2 appears to be unsteady and the ratio between the evolution of O_2 and H_2 is approximately 1:3.

The 200 °C calcined sample shows also an increase of the apparent O_2 formation rate from 0 to 3.75 h (Figure 34). Moreover, the product formation rates after 3.75 h reveals a O_2:H_2 ratio of approximately 1:2. Such a ratio is indicative for a stoichiometric product formation from H_2O splitting on the IrO_x/P25. Furthermore, it is possible to observe the simultaneous formation of both products in one high-purity reaction chamber. Overall, it is a meaningful result showing that the stoichiometric H_2O splitting in a

gas-solid process has been realized, since no external bias or any sacrificial agents were used in order to improve the formation rates of H_2 and O_2.

A B

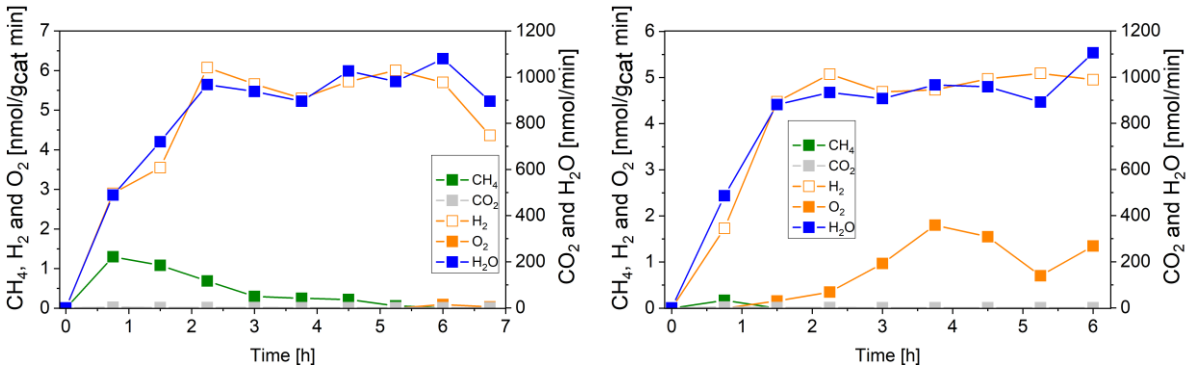

Figure 33: Photocatalytic H_2O splitting with 0.05 wt.-% IrO_x/P25 calcined at 400 °C. Irradiation time: 6.75 h. A: first experiment, B: second experiment.

From 5.25 to 6.75 h (Figure 34) the product formation becomes relatively stable so that steady-state conditions are almost reached. However, under the assumption that stoichiometric formation of both products originates from photocatalytic H_2O splitting, it becomes questionable why the apparent O_2 formation starts delayed to the H_2 formation. Another important observation is the difference in the overall activity of the two samples. It can be noticed that the 200 °C sample is about 30 times more active in H_2 formation than the 400 °C sample. Thus, the calcination temperature seems to have a distinct influence on the catalytic properties of the IrO_x/P25 samples.

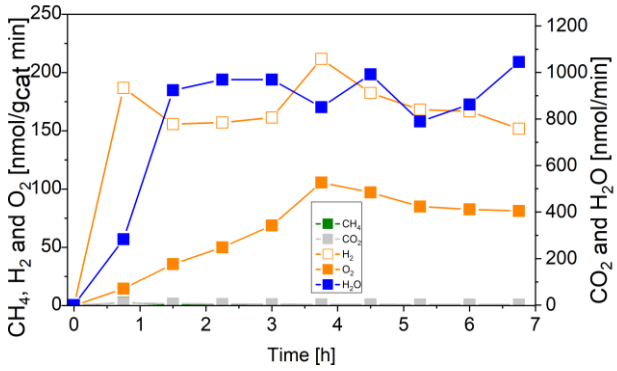

Figure 34: Photocatalytic H_2O splitting with 0.05 wt.-% IrO_x/P25 calcined at 200 °C. Irradiation time: 6.75 h.

The reference samples were also tested with respect to their performance in photocatalytic H_2O splitting. From Figure 35 A and B can be observed that the samples show no measureable activity in the formation of O_2 and H_2. The results of the modified and the reference samples, indicate that IrO_x positively influences the overall H_2O splitting reaction on P25.

A B

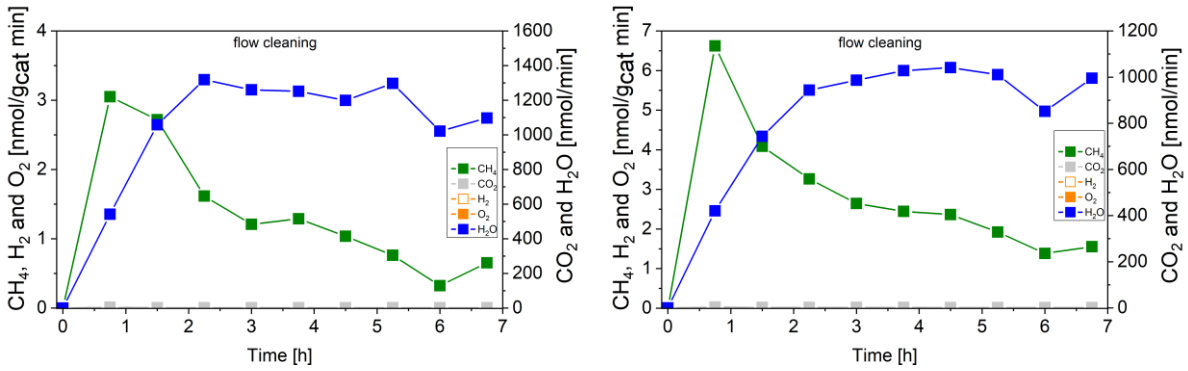

Figure 35: Photocatalytic H_2O splitting with A: P25 reference sample calcined at 200 °C. B: P25 reference sample calcined at 400 °C. Irradiation time: 6.75 h.

5.3.2 Photocatalytic Cleaning and H_2O Splitting with CoO_x/P25

A B

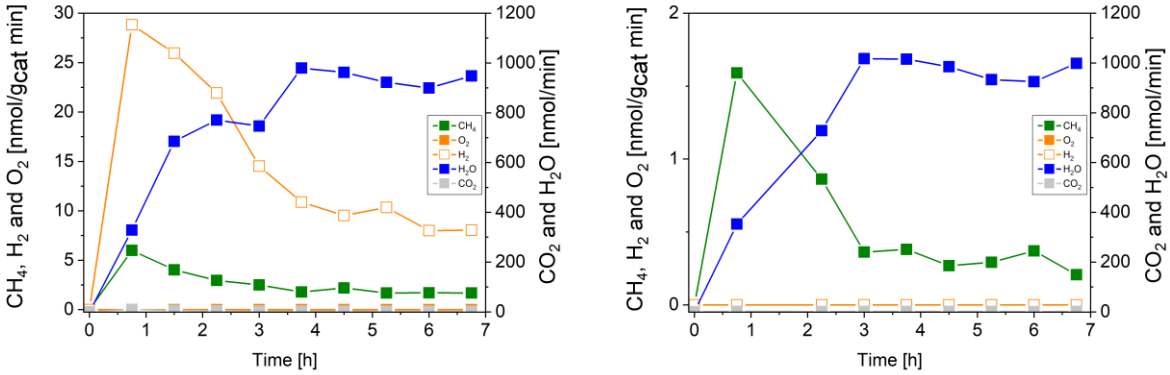

Figure 36: Photocatalytic H_2O splitting with A: 0.05 wt.-% CoOxP25 calcined at 200 °C. B: 0.05 wt.-% CoOxP25 sample calcined at 400 °C. Irradiation time: 6.75 h.

In contrast to the IrO_x modified P25 samples, the CoO_x modified samples show a significantly different activity in the photocatalytic H_2O splitting reaction. From Figure 36 A and B it can be observed that only the 200 °C calcined sample showed activity in H_2 formation. Furthermore it can be seen that the activity in H_2 formation ceases over the time of illumination (Figure 36 A), which indicates a deactivation of the CoO_x/P25 sample. Both samples, the 200 °C and 400 °C sample, did not exhibit any activity in O_2 formation. The 400 °C samples displayed no activity in the overall H_2O splitting reaction. Due to the absence of activity in O_2 formation, the samples were not further tested in the photocatalytic CO_2 reduction.

5.3.3 Photocatalytic CO_2 Reduction with IrO_x/P25

A B

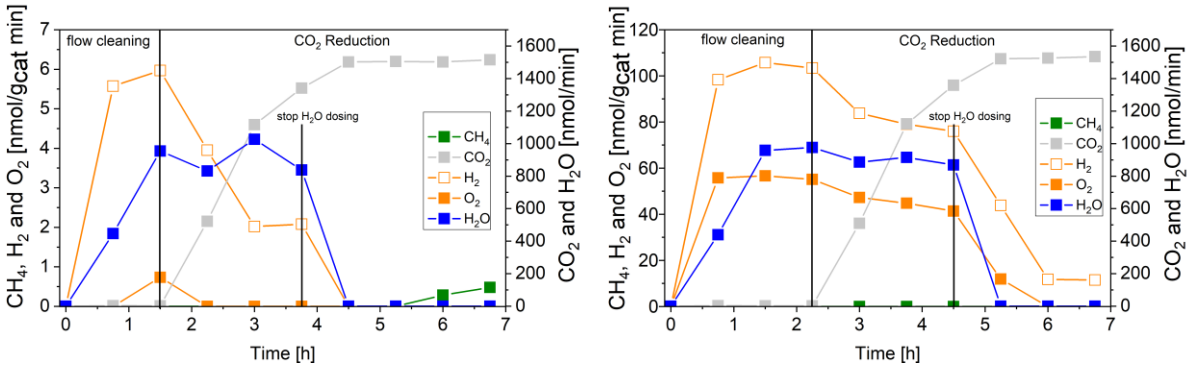

Figure 37: Photocatalytic CO_2 reduction with 0.05 wt.-% IrO_x/P25 calcined at A: 400 °C (flow cleaning from 0 to 1.5 h, CO_2 reduction from 1.5 h to 6.75 h, H_2O dosing from 0 to 3.75 h) and B: 200 °C (flow cleaning from 0 to 2.25 h, CO_2 reduction from 2.25 h to 6.75 h, H_2O dosing from 0 to 4.5 h).

Figure 37 shows results of combined flow cleaning and photocatalytic CO_2 reduction experiments with the IrO_xP25 samples. Both samples show significant activity in the formation of H_2 and O_2 before the CO_2 dosing was initiated. The formation rate of these products decreases once CO_2 is flushed through the reactor. In case of the sample calcined at 400 °C the rate of H_2 was more than halved within 3.25 h of CO_2 dosing, while O_2 was completely absent (Figure 37 A) in the products. These observations are less significant for the 200 °C sample (Figure 37 B) so that only a slight decrease of both rates was observed. However, under the applied reaction conditions it was not possible to detect CH_4 as a product of CO_2 reduction. It rather seems that CO_2 has primarily a negative impact on the H_2O splitting reaction in a way that generation of products is markedly disturbed. The dosing of H_2O was stopped after 3.25 h of CO_2 reduction, to probe if the absence of this reactant makes a difference in the overall selectivity. From Figure 37 it can be seen that the absence of H_2O in the gas flow strongly affects the H_2 and O_2 formation (Figure 37). A clear decrease of both formation rates can be seen in Figure 37. More specific, it can be noticed that no H_2 and O_2 evolution takes place for the 400 °C sample. In case of the 200 °C sample, the O_2 formation declines completely while that of H_2 drops down to a constant rate. The strong dependence of H_2 and O_2 formation from H_2O further indicates that they are actual products of photocatalytic H_2O splitting on IrO_x/P25. However, after the H_2O dosing was stopped it was possible to observe formation of CH_4, at least for the 400 °C sample. Thereby the rate increased from 5.25 to 6.75 h (Figure 37 A). In contrast the 200 °C sample showed no CH_4 formation under the applied reaction conditions.

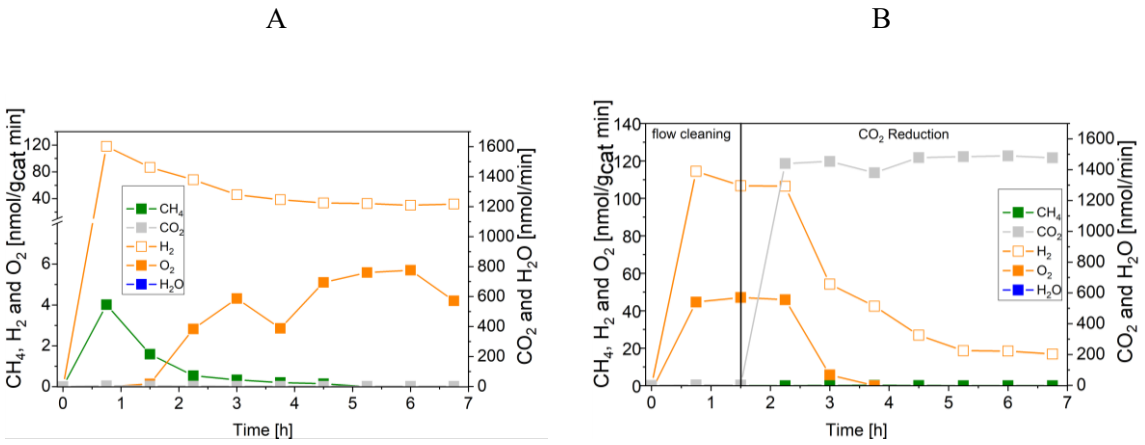

Figure 38: A: Photocatalytic H_2O splitting and cleaning with 0.05 wt.-% IrOx/P25 calcined at 200 °C. Irradiation time: 6.75 h. B: Photocatalytic CO_2 reduction with 0.05 wt.-% IrO_x/P25 calcined at 200 °C (flow cleaning from 0 to 1.5 h, CO_2 reduction from 1.5 h to 6.75 h, ~25 nmol/min H_2O dosing from 0 to 6.75 h).

The intensive dosing of H_2O during activity studies could result in an accumulation of this reactant on the surface of TiO_2 based photocatalysts, which can limit its activity in CO_2 reduction.[137] In order to investigate this potential limitation, a similar experiment with the 200 °C sample was carried out with a reduced H_2O flow rate of ~25 nmol/min. With these conditions bare P25 showed the highest CO_2 reduction activity in our previous studies. The results of the flow cleaning and CO_2 reduction experiments are displayed in Figure 38 A and B, respectively, and reveal a significant activity in the H_2 and O_2 formation with the reduced amounts of H_2O. After adding CO_2 to the gas flow the apparent O_2 formation ceases completely, while H_2 formation decreases to a stable rate. It was again not possible to detect any CH_4 formation (Figure 38 B).

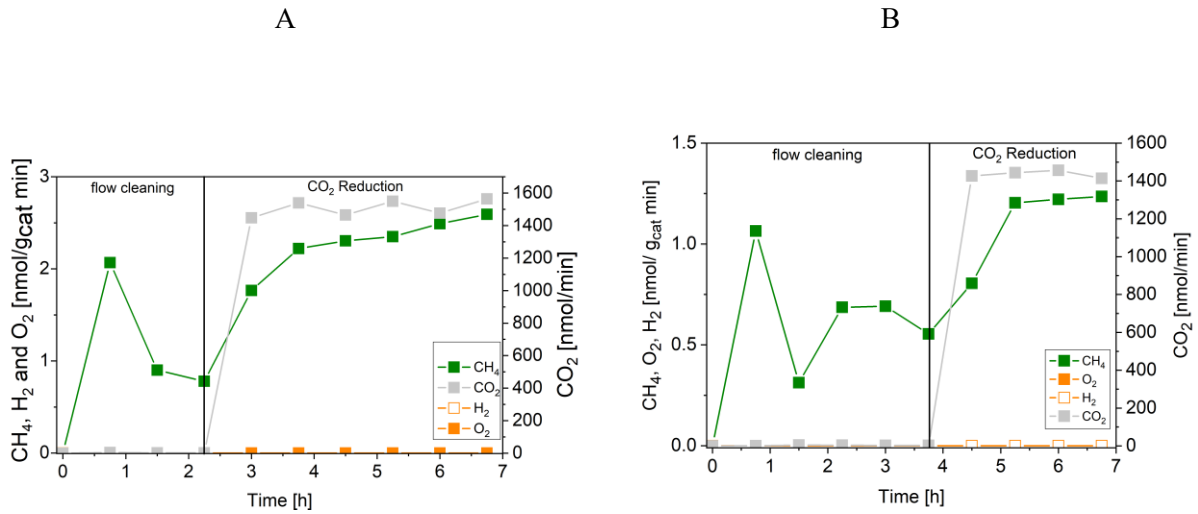

Figure 39: Photocatalytic CO_2 reduction with A: P25 reference sample calcined at 200 °C (flow cleaning from 0 to 2.25 h, CO_2 reduction from 2.25 h to 6.75 h, ~25 nmol/min H_2O dosing from 0 to 6.75 h) and B: P25 reference sample calcined at 400 °C (flow cleaning from 0 to 3.75 h, CO_2 reduction from 3.75 h to 6.75 h, ~25 nmol/min H_2O dosing from 0 to 6.75 h).

The pure P25 references, without IrO_x or CoO_x, showed significant activity in CH_4 formation when CO_2 was given to the reactor (Figure 39 A and B). The activity of the sample calcined at 200 °C (Figure 39A) was higher than that of the 400 °C sample (Figure 39 B). This observation is similar to the activity of the IrO_x/P25 samples in H_2O splitting (Figure 33 and Figure 34). The P25 reference samples however exhibited no activity in H_2 and O_2 formation at all. These findings are in accordance with our previous studies on photocatalytic CO_2 reduction with P25.[122,137] In a consecutive experiment with the P25 references it was investigated if a similarly delayed initiation of O_2 evolution can be observed during CH_4 formation, as it was observed for the IrO_x/P25 samples. Therefore a combined flow cleaning and CO_2 reduction experiment was carried out with the sample calcined at 400 °C (Figure 40) for an extended period of 18 h. To prevent an inhibition of CH_4 formation by extensive accumulation or a complete lack of H_2O, repetitive pulse dosing of H_2O was performed in order to provide suitable conditions to run CH_4 formation over an appropriate period of time. It can be obviously seen in Figure 40 that after about 6 h the pulses of H_2O initially decrease the rate of CH_4 formation. However, a significant increase of the CH_4 formation can be observed in each of the subsequent GC analysis cycles. In total it was possible to observe CH_4 formation over a period of 14.25 h (Figure 40). Under the applied reaction conditions the CH_4 formation rate decreases over the course of the CO_2 reduction experiment. There was no activity left after 17.75 h (Figure 40). As no delayed O_2 formation could be detected during the experiment it seems that, in contrast to the H_2O splitting experiments on IrO_x/P25, bare P25 does not release any molecular oxygen in a similar range of time.

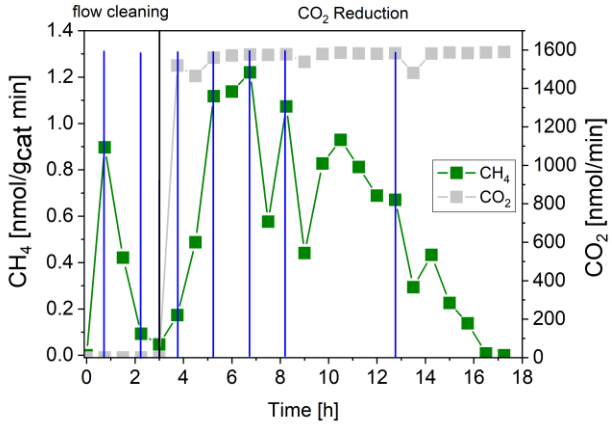

Figure 40: Photocatalytic CO_2 reduction with P25 calcined at 400 °C (flow cleaning from 0 to 3 h, CO_2 reduction from 3 h to 17.75 h, pulse dosing of H_2O (blue dashes).

On IrO_x/P25 the H_2O splitting reaction appeared to be the dominating photocatalytic process under all applied reaction conditions which seemed to inhibit the photocatalytic reduction of CO_2. The formation of CH_4 was only possible, when there was no activity in O_2 and H_2 formation. If the sample was not modified with the co-catalyst, CH_4 formation was observed but no O_2 could be found as the by-product of CO_2 reduction and H_2O oxidation. The unmodified samples showed no activity in the H_2O splitting reaction.

5.4 Discussion

5.4.1 Photocatalytic Cleaning and H_2O Splitting on IrO_x/P25

The IrO_x modified P25 samples showed a noticeable activity in the formation of H_2 and O_2. Due to the strong dependence of the activity from the dosing of H_2O and the O_2:H_2 ratio of approximately 1:2, it is assumed that the product formation originates from photocatalytic H_2O splitting (5.3). However, it is questionable how the product formation is realized on IrO_x/P25 and which charge carrier dynamic processes are involved. A hypothetical approach to explain the activity of IrO_x/P25 can be based on the two main functions of a photocatalyst. In this sense TiO_2 represents the photoabsorber, where mobile charge carriers are generated under absorption of UV photons. Some of the photogenerated h^+ escape from recombination and migrate to the IrO_x particles, where they catalyze the oxidation of H_2O to O_2 (5.1). In this way IrO_x represents the function of the heterogeneous catalyst. The separation of charge carriers over the interface of TiO_2 and IrO_x enhances their lifetime, thus it is beneficial for the light efficiency of the overall H_2O splitting reaction (5.3). The H^+ formed from H_2O oxidation (5.1) are then reduced to H_2 gas (5.2). This reaction proceeds by the photogenerated e^- on TiO_2. For this purpose TiO_2 must expose sites which can transfer electrons. It appears that such sites are available and their accessibility maintains even under continuous flow conditions and accumulation of H_2O on the surface of TiO_2, since the activity of H_2 formation is almost stable during the H_2O splitting experiments.

$$2\,H^+ + 2\,e^- \longrightarrow H_2 \qquad E^0 = 0\,V \qquad (5.2)$$

$$2\,H_2O \longrightarrow 2\,H_2 + O_2 \qquad (5.3)$$

With respect to H_2 formation, the catalytic functionality is thus inherent to TiO_2, as has been observed earlier, and a modification with a co-catalyst does not seem to be needed.[146]

5.4.2 Photocatalytic Cleaning and H_2O Splitting on CoO_x/P25

According to the hypothetical approach in the previous chapter to explain the activity of IrO_x/P25 it is expected that the H_2O oxidation reaction proceeds on CoO_x and the formation of H_2 on TiO_2. In Figure 36 it was shown that only the sample calcined at 200 °C showed activity in H_2 formation. However, the fact that H_2 was formed indicates that a hydrogen source has been provided by photocatalytic H_2O oxidation. The interface between TiO_2 and CoO_x can potentially cause an insufficient hole transfer between the photoabsorber and the co-catalyst which lowers the activity of H_2O oxidation. Furthermore the reaction pathway of photocatalytic H_2O oxidation on CoO_x will be different compared to IrO_x. Therefore it is possible that specific steps in the overall reaction mechanism cannot be activated sufficiently to allow an efficient O_2 formation. As a consequence H_2O is only oxidized partly, so that the resulting oxygen derived intermediates remain on CoO_x, without being further oxidized to O_2 gas.

In this way the oxygen derived intermediates might prevent further oxidation of H_2O, which lowers the activity over time as it was observed in Figure 36 A.

5.4.3 Evaluation of Improved H_2O Oxidation Conditions on the Photocatalytic CO_2 Reduction

The CO_2 reduction experiments with the IrO_x/P25 samples displayed no measurable activity in CH_4 formation as long as O_2 and H_2 are formed. This observation is in stark contrast to the reference samples. It is highly probable that the improved H_2O splitting conditions by the IrO_x modification are responsible for the absence of CH_4 formation. In the following it will be elucidated in which ways the H_2O oxidation reaction might affect the CO_2 reduction reaction. The oxidation of H_2O to O_2 is often represented by four single step reactions (5.4-5.7).[83,90,123,147] Each of these steps comprises the transfer of one h^+ and the generation of hydroxyl- (5.4), oxygen adatom- (5.5) and peroxyl-species (5.6) as intermediates. Especially the hydroxyl and peroxyl species are highly reactive oxygen species and have potential to promote the backward reaction of CO_2 reduction, which is hydrocarbon oxidation.

$$H_2O + h^+ \longrightarrow OH_{ads} + H^+ \tag{5.4}$$

$$OH_{ads} + h^+ \longrightarrow O_{ads} + H^+ \tag{5.5}$$

$$H_2O + O_{ads} + h^+ \longrightarrow OOH_{ads} + H^+ \tag{5.6}$$

$$OOH_{ads} + h^+ \longrightarrow O_2 + H^+ \tag{5.7}$$

Another explanation for the absence of CH_4 formation could be based on a competition for charge carriers. For instance the reduction of O_2 (1.11) and the generation of H_2 (5.2) are also electron consuming reactions. It is questionable which of these processes is associated with the lowest barrier and is thus more likely to proceed. Therefore the redox potentials of the particular reactions are regarded. For a reaction with CO_2 the commonly proposed one electron transfer[17] is considered to be the rate limiting step. The comparison of the redox potentials reveals that CO_2 reduction (1.8) is the thermodynamically least favored process.[21,91,148] It needs to be stressed that reaction (1.8) is virtually not possible on any semiconducting material.[17] This one electron transfer can only proceed if, for instance, a specific interaction between CO_2 and TiO_2 lowers the barrier of reaction (1.8) so that the redox potential of the photogenerated electrons is more negative. As a consequence of the extreme stability of CO_2 it is highly probable that the photogenerated charge carriers are more likely consumed by H_2 evolution and O_2 reduction, so that less electrons available for reduction of CO_2. Hence the activity of TiO_2 in CH_4 formation could be negatively influenced.

The absence of CH_4 formation in the presence of a highly active co-catalyst for O_2 evolution due to reactive oxygen species and competitive charge transfer reaction appears to be plausible. What makes the results of the IrO_x/P25 sample significantly more interesting is the activity in the H_2 formation as a consequence of the improved H_2O oxidation properties, together with the delayed O_2 formation rate in the initial phase of the flow cleaning experiments. The obtained results provide specific information about the photocatalytic properties, which can be used to explain product formation of photocatalytic CO_2 reduction on TiO_2. On this account the results of the reference samples will be interpreted under consideration of the results from IrO_x/P25. In contrast to the IrO_x modified samples, the reference P25 samples exhibited a significant activity in the CH_4 formation. At the same time there was no observable activity in the H_2O splitting reaction. In general, the photocatalytic H_2O oxidation is thermodynamically possible on bare TiO_2. Kinetic barriers in the overall reaction cycle might result in a very small apparent rate when no co-catalyst is used. Nevertheless, the H_2O oxidation reaction is expected to deliver the hydrogen for CH_4 formation, and the product formation will be hardly possible without it. In the proposed elementary steps of H_2O oxidation (5.4-5.7) it can be seen that each single charge transfer reaction results formally in the formation of an H^+, which could be used for hydrogenation. Already the first charge transfer (5.4) liberates H^+. Even if the final step of O_2 evolution (5.7) would be kinetically limited, so that H_2O oxidation is occurring only partially then at least the hydrogen source is generated. From the results with the IrO_x/P25 samples it can be concluded that such a source of hydrogen is rapidly reduced to H_2. However, on bare TiO_2 we did not observe H_2 formation, so it is doubtful if any step of H_2O oxidation occurs under the applied reaction conditions. In this case a different source of protons than photocatalytic H_2O oxidation needs to participate in C-H bond formation.

5.4.4 Balancing the Absent Amount of O_2 in Photocatalytic Reaction with IrO_x/P25 and P25

The results with IrO_x/P25 (Figure 33, Figure 34 and Figure 37) indicated that not all O_2 produced from H_2O oxidation was detected over the course of the experiment. In case of CO_2 reduction on P25 it was even not possible to detect any O_2. For this reason the deficient amount of O_2 was determined for the IrO_x/P25 and P25 samples calcined at 400 °C. At first the absent amount of O_2 is calculated for IrO_x/P25. For this purpose the overall H_2 formation and the O_2:H_2 ratio of 1:2 as proposed in reaction 5.2 are used. The difference between the theoretically expected (O_2 theoretical) and the detected amount (O_2 detected) corresponds to the amount of O_2 which was not found (O_2 absent) in the gas-phase of the photoreactor (Table 3). In order to realize a reliable comparison to the absent amount of O_2 in CO_2 reduction, it would be necessary to run the reaction until stoichiometric formation of both products can be observed too. However, the CH_4 formation ceased after 14.25 h of CO_2 reduction (Figure 40). Consequently it is solely possible to determine the theoretically expected amount of O_2 to this point of time. The calculation was performed under consideration of the stoichiometry in reaction (1.7). Thereby the molar amount of O_2 corresponds to twice the molar amount of CH_4 (Table 4).

Table 3: Calculation of absent O_2 in the flow cleaning experiments with the 0.05 wt.-% IrO_x/P25 (400°C).

	Molar amount [nmol]
H_2	247
O_2 theoretical	123.5
O_2 detected	20
O_2 absent	103.5

The comparison of the balances (Table 3 and Table 4) exhibits that the absent amounts of O_2 in both the H_2O splitting reaction with IrO_x/P25 (Figure 33) and the CO_2 reduction with bare P25 (Figure 40) are at least in the same order of magnitude. On this account it appears realistic that the observed phenomena are based on the same effect. The present study uses a GC as the analytical device so that only the gas phase of the photoreactor can be analyzed. Hence, the absence of O_2 in the analysis is either indicative for the absence of its formation or the consumption by the sample. The obtained results are the basis to hypothesize the fate of oxygen in photocatalytic reaction on TiO_2.

Table 4: Calculation of absent O_2 in the flow cleaning experiments with P25 (400°C).

	Molar amount [nmol]
CH_4	39
O_2 absent	78

5.4.5 Hypothetical Statement to the Photocatalytic Activity of TiO_2 in Photocatalytic CO_2 Reduction

The results of the present study revealed that CH_4 formation only proceeds when no H_2O is oxidized and the by-product O_2 is absent in the gas-phase. This correlation is in conflict with the proposed reaction equation 1.7. For this reason a hypothetical approach explaining the product formation of photocatalytic CO_2 reduction on the basis of the obtained results is proposed. It has been suggested that O_2 is consumed by TiO_2. One feasible way for such consumption is the replenishment of V_{OX}. From experimental studies[149-151] it is known that O_2 dissociates and can undergo reactions with V_{OX} on the surface of TiO_2 under room temperature conditions. Since all experiments of this study were performed under such

conditions and the amount of absent O_2 is very small, it is proposed that the replenishment of V_{OX} may be associated with the fate of this by-product. The obtained results of the IrO_x/P25 samples showed that O_2 formation started delayed to the H_2 formation. Over the course of the reaction both formation rates converged to the stoichiometric ratio of H_2O splitting. The replenishment of V_{OX} may be the reason why fractions of O_2 were temporarily not detectable in the gas phase. Once all defects are healed the release of the entire amount of O_2 from the surface of the photocatalyst initiates. From this point of time the stoichiometric ratio of H_2O splitting was observed.

The overall CO_2 reduction is proposed to include two processes forming O_2. On the one hand side the formation of CH_4 by reduction of CO_2, on the other hand side the oxidation of H_2O to generate the source of hydrogen for C-H bond formation. Given that vacant positions are responsible for the absence of O_2, it can be hypothesized that these point defects are strongly associated with the photocatalytic activity of TiO_2. In one of our studies[122] it was verified that the presence of O_2 in the gas-phase of the reaction gas atmosphere induces an inhibition of CH_4 formation. Furthermore oxygen-derived species from CO_2 reduction are also suspected to affect the CH_4 formation negatively. On this account a replenishment of V_{OX} might avoid that O_2 and oxygen-derived intermediates inhibit the CH_4 formation. This represents an important factor explaining the activity of TiO_2 in photocatalytic CO_2 reduction. A further meaningful observation of this work was that bare P25 showed obviously no activity in H_2O complete oxidation to O_2, wherefore it is questionable if any step of this reaction is occurring under the applied reaction conditions. Under this circumstance, a different source than photocatalytic H_2O oxidation might be responsible for liberation of hydrogen. Nonetheless, the CH_4 formation has been proven to be dependent on the presence of H_2O.[137] For this reason an alternative pathway for liberation of the hydrogen in H_2O should be considered. In general, surface hydroxyl groups are naturally present on the surface of TiO_2 and can be formed by dissociative adsorption of H_2O in a V_{OX} (5.8). The surface OH-groups represent hydrogen-containing species which are available in high concentration. If they would be sufficiently Brönsted acidic to hydrogenate, for instance carbonaceous radicals as intermediates from CO_2 reduction, they could participate in product formation. Additionally, the dissociative H_2O adsorption illustrates a pathway which is consistent with the dependency of CH_4 formation from H_2O and the absence of O_2 formation.

$$H_2O + V_{OX} + O_{br} \longrightarrow 2\,OH_{br} \tag{5.8}$$

Anyway, the irreversible replenishment of vacant positions by excess oxygen from CO_2 or H_2O is an example for a stoichiometric reaction of the photocatalyst. Most likely the photocatalytic activity will be influenced strongly as soon as all vacancies are healed. As a consequence, the excess oxygen cannot undergo a reaction with TiO_2 and contributes to the oxidation of intermediates and CH_4 formed in CO_2 reduction. The observed termination of the CH_4 formation in the CO_2 reduction after 14.25 h (Figure 40) could be indicative for this hypothesis. It must be noted that the observations made here are no

verification for the participation of V_{OX} in photocatalytic reaction on TiO_2. However, they indicate that the overall CH_4 formation is presumably not based on a complete catalytic cycle including both the photocatalytic CO_2 reduction and H_2O oxidation.

5.5 Conclusions

In this study the absence of gaseous O_2 as the by-product of photocatalytic CO_2 reduction was investigated. Therefore we modified P25 with IrO_x and CoO_x as co-catalysts for H_2O oxidation, and tested the obtained materials in the photocatalytic CO_2 reduction and H_2O splitting. Furthermore, the effect of improved H_2O oxidation properties on the gas-phase photocatalytic CO_2 reduction was studied. The IrO_x/P25 samples exhibited a significant activity in the overall photocatalytic H_2O splitting. It was possible to detect both products H_2 and O_2 in nearly stoichiometric amounts. Thereby no sacrificial agents were used. The photocatalytic CO_2 reduction experiments with the IrO_x/P25 samples revealed that CH_4 formation is only possible when no activity in H_2 and O_2 formation was observed. Competition for charge carriers by H_2 formation and the backward reaction of CO_2 reduction due to the presence of highly reactive oxygen species formed on IrO_x appear to be responsible for the absence of CH_4 formation. The fact that photogenerated electrons are favorably consumed by H_2 formation, but this product is not formed on bare TiO_2 strongly indicates that H_2O oxidation is not the source of hydrogen for C-H bond formation in CO_2 reduction. Furthermore, the results of the H_2O splitting experiments on IrO_x/P25 showed that O_2 formation started delayed to the H_2 formation. This observation is a strong indication for consumption of O_2 and O-derived species by TiO_2 under photocatalytic reaction conditions. A quantification of the missing amounts showed that a consumption of O_2 by TiO_2 could be responsible for the absence of this by-product in the CO_2 reduction reaction. Under this circumstance TiO_2 undergoes a stoichiometric reaction and the CH_4 formation is not a true catalytic cycle and runs only as long as TiO_2 can consume oxygen. In addition the inhibiting effect of O_2 on the product formation of CO_2 reduction reveals that the consumption of this by-product is essential for the activity of TiO_2 in this reaction. Only then the inhibiting effect of O_2 and O-derived species in the photocatalytic CO_2 reduction is prevented.

6. Judging the Feasibility of TiO_2 as Photocatalyst for Chemical Energy Conversion by Quantitative Reactivity Determinants

Abstract

In this study we assess the general applicability of the widely used P25-TiO_2 in gas-phase photocatalytic CO_2 reduction based on experimentally determined reactivity descriptors from classical heterogeneous catalysis (productivity) and photochemistry (apparent quantum yield / AQY). A comparison of the results with reports on the use of P25 for thermodynamically more feasible reactions and our own previous studies on P25-TiO_2 as photocatalyst imply that the catalytic functionality of this material, rather than its properties as photoabsorber, limits its applicability in the heterogeneous photocatalytic CO_2 reduction in the gas phase. The AQY of IrO_x/TiO_2 in overall water splitting in a similar high-purity gas-solid process was four times as high, but still far from commercial viability.

The main content of this chapter is published in Phys. Chem. Chem. Phys. **2019**, 10.1039/c9cp00981g as "Judging the Feasibility of TiO_2 as Photocatalyst for Chemical Energy Conversion by Quantitative Reactivity Determinants", M. Dilla, N.G. Moustakas, A. E. Becerikli, T. Peppel, A. Springer, R. Schlögl, J. Strunk and S. Ristig.

6.1 Introduction

Within the last decades photocatalysis has attracted lots of attention because it bears potential to contribute to the development of novel strategies for renewable energy sources. TiO_2 is still the most frequently applied semiconductor in a manifold of different reactions, mainly due to its sufficiently wide band gap (>3.0 eV), its availability and its physical and chemical stability.[71] A commercially available TiO_2 composite consisting of approximately 20% rutile and 80% anatase (P25, Evonik Industries) is often considered as the standard or benchmark material in photocatalytic research.[17] One of the most prominent photocatalytic reactions on semiconducting materials is the reduction of CO_2 to CH_4 utilizing H_2O splitting as hydrogen source (1.7).

Many groups have carried out important and detailed research on this very complex reaction following the pioneering work of Inoue et al.,[62] including mechanistic studies and investigations of the structure-activity relationship,[63,86,96,152-156] effects of co-catalysts, doping, substrates and composites.[157-164] Unfortunately, despite years of research on photocatalytic conversion of CO_2 on TiO_2, the exact mechanism of CH_4 formation is still unknown and the formation rates are generally low, ranging from a few nmol g_{cat}^{-1} h^{-1}, especially regarding pure P25-TiO_2, to an order of µmol g_{cat}^{-1} h^{-1} for modified TiO_2-based materials.[17] The tininess of product formation contributes to the complexity of this reaction, as it makes the analytics very difficult and allows only a few techniques, such as highly specialised GCs. Regarding the almost 40 years of high-quality research, the question may arise why it was not possible to achieve a major breakthrough in terms of catalytic efficiency and detailed understanding of CO_2 reduction on the molecular level up to now.

Our groups have also devoted considerable research effort on this research topic with the main focus on carrying out the reaction under high-purity conditions in the absence of carbon-containing impurities. As main conclusions from our work we were able to prove true CH_4 formation from CO_2 as a reactant, although we were never able to detect gas-phase oxygen as a by-product (1.7) with pure P25-TiO_2 as the photocatalyst.[72,122] The variation of reactant concentration and light intensity revealed that the formation of CH_4 actually results from a photo-induced process on TiO_2 and that maximum CH_4 formation was achieved at low reactant concentrations. We have yet to demonstrate the possibility to obtain quantitative activity determinants under high-purity conditions, enabling a final conclusion on the potential of P25-TiO_2 in photocatalytic CO_2 reduction. In accordance with earlier work[12,165] it seems desirable to apply different quantitative descriptors. The apparent quantum yield, as outlined below, is an appropriate measure to describe the light-based efficiency of the process, but it does not take into account the applied photocatalyst quantity. On the other hand, typical measures from heterogeneous catalysis, such as the productivity, do not consider light intensity or light absorption.

The rate of a photocatalytic reaction is strongly influenced by the intensity and energy of the incident light beam, the charge carrier dynamics and the illuminated portion of surface area.[166] As a consequence the validity of comparing rate constants of photocatalysts (at a given temperature and pressure) will be limited. To circumvent this, a generally accepted approximation is to describe the activity of a photocatalyst by regarding the quantum yield (QY).[12] The QY is defined as the ratio between the amount of charge carriers consumed by product formation and the amount of photons absorbed by the photocatalyst (eq. 6.1) which consequently excite an electron-hole-pair. These charge carriers will be consumed by the photochemical process, if they escape from recombination and arrive at the active sites on the surface of the photocatalyst where they undergo a charge transfer reaction with an adsorbed reactant.

$$\mathrm{QY} = \frac{\mathrm{N_{consumed\ charge\ carrier}}}{\mathrm{N_{Absorbed\ photons}}} \qquad \text{(eq. 6.1)}$$

$$\mathrm{AQY} = \frac{\mathrm{N_{consumed\ charge\ carrier}}}{\mathrm{N_{Incident\ photons}}} \qquad \text{(eq. 6.2)}$$

The number of the consumed charge carriers can be directly deduced from the amount of formed products. A calculation of the absorbed photons is only possible if the incident, reflected and scattered photons can be quantified,[166] which is rarely the case. In order to avoid this fundamental problem it became popular to use instead the amount of incident photons.[167-169] A determination of the latter can be performed by an actinometrical measurement of the light source. The ratio between the amount of consumed charge carriers and the amount of incident photons is termed the apparent quantum yield (AQY) (eq. 6.2) or apparent photonic yield.[166] AQY a as measure for the efficiency of a photocatalyst should be determined in a range where the product formation rate no longer depends on the catalyst mass. This ensures optimum light absorption.[170] However, when considering the term ‘efficiency’ from the viewpoint of classical heterogeneous catalysis, AQY is not ideal because it does not take into account the applied photocatalyst quantity or the ideal illumination of the latter.[165]

In classical heterogeneous catalysis, the comparison of different catalysts is often performed on the basis of massrelated production rates in μmol g^{-1} h^{-1} as a measure for the productivity of a certain catalyst. For photocatalytic reactions, calculation of this quantity requires that the entire sample mass is exposed to light and thus in principle able to participate in the reaction.

A critical point in the literature dealing with CO_2 reduction in both, the QY and the productivity estimation, is the ambiguity if the experiments were performed in absence of carbonaceous impurities. It is important to notice that in reactions with such low product yields particular caution has to be exercised concerning impurities on the photocatalyst, as adsorbents from prior air contact or remains from syntheses can contribute to the products formed during the reaction.[171-173] Thus, it is clear that

both determinations are meaningless without adequate purification steps before the CO_2 reduction experiment, as products formed from such species overestimate the number of consumed charge carriers and the amount of formed products. Due to an insufficient removal of carbonaceous species, the sensitivity of the photochemical performance of TiO_2 to the illumination properties and the diverse approaches of performing QY analysis, it is obvious that the obtained values often differ by orders of magnitude.[39,174]

In this work, both reactivity determinants, the AQY and the productivity, are determined under suitable conditions for each quantity. Thin films deposited on glass surfaces were used to study the effect of the deposited mass to the production of hydrocarbons. We show that all of the deposited titania in these films participates in the photoreaction which allows an accurate determination of the productivity. Due to the low product yields, these experiments had to be performed under batch conditions. Under steady CH_4 formation in continuous flow we show an approach to determine the AQY of powdered bare TiO_2 (P25) in the gas-phase photocatalytic CO_2 reduction. Furthermore the AQY of IrO_x modified P25 (IrO_x/P25) in the gas-phase photocatalytic H_2O splitting was analysed under similar flow conditions. For the first time the AQY of both, the CO_2 reduction and H_2O splitting is determined under exclusion of contaminants in order to ensure a proper analysis of the activity of P25 and IrO_x/P25.

Based on the results presented here, we strongly suggest that P25-TiO_2 is not suitable as photocatalyst for gas-phase CO_2-reduction because (i) the reaction is most likely not a full catalytic cycle with the oxygen probably being consumed by titania and (ii) both, productivity and AQY are far below any commercial viability.

6.2 Experimental

All experiments in this work were carried out in two similar high purity photoreactor set-ups described in detail by Mei et al.[102] For the batch experiments, a Shimadzu Tracera GC 2010 plus gas chromatograph equipped with a barrier ionization discharge detector (BID) and a flame ionization detector (FID) was used to quantify CO_2, O_2, H_2O, CH_4 and higher hydrocarbons in the single-digit ppm range, as well as H_2 and CO from ≥ 20 ppm. Illumination in the CO_2 reduction experiments was carried out with a 10 W 365 nm LED (SeoulViOSys), operated at 7.2 V and 0.92 A with a total output intensity of 755 mW cm^{-2} (Thorlabs PM100USB actinometer with a S405C measuring cell).

For the flow experiments, a Shimadzu Tracera GC 2010 Plus, equipped with a barrier discharge ionization detector (BID) was used which allows quantifying CO_2, CH_4, H_2O, H_2 and O_2 in the 0.1 ppm range. A detection of CO, CH_3OH, C_2H_6, C_3H_8 is also feasible. Illumination of the samples for the approximation of the AQY was realised with a 365 nm^2 W high-power LED, operated at 3.5 V and 0.5 A with a total output intensity of 185 mW cm^{-2} (Thorlabs PM100D actinometer with a S305C measuring

cell). Monochromatic LED light sources allow a straightforward determination of the incident photons which can be calculated from the light intensity hitting the sample surface. A transmittivity of the reactor lid window of 86 % at 365 nm was accounted for in the calculation of the AQY.

6.2.1 Preparation of P25-TiO_2 Thin Films

To remove any loosely bound carbon-containing impurities the P25 powder (Evonik Industries) was calcined in synthetic air at 400 °C for 3 h prior to use. All thin films were deposited on a 2.5 X 2.5 cm surface of a microscope glass slide. The glass slides were cleaned with a Hellmanex® III cleaning solution, rinsed with de-ionised H_2O and then ultrasonicated for 30 min at room temperature (Elmasonic S 60 H). For thin films prepared by doctor blading a P25-TiO_2 paste was prepared according to Ito et al.[175] with slight modifications. Briefly, 10 mL EtOH were added to a solution of ethyl cellulose (3.5 g, ~50 cP, 10 wt.-% in EtOH), P25 (0.8 g) and terpineol (6.5 g, mixture of isomers) in a 50 mL round-bottom flask. The mixture was thoroughly sonicated for 45 min at room temperature in an ultrasonic bath (Elmasonic S 60 H). Afterwards, the solvent was removed stepwise with a rotary evaporator (final T = 40 °C; final p = 7 mbar). The resulting suspension (~10 wt.-% P25) was used directly for doctor blading.

For thin films prepared by the air-brush technique, a solution of 0.5 g of P25 in 100 ml de-ionised H_2O was sprayed on the surface of the microscope slides. The glass substrates were put on a hot plate at 250 °C to quickly evaporate sprayed H_2O leaving behind a P25 coating. In order to get films of different thickness, different deposition times were applied.

After deposition, all thin films were calcined at 300 °C for 3 h to increase the adhesion of the powder to the glass surface and to remove the solvents and other C-containing species from the surface of the samples. SEM images of the films were collected using a Merlin VP compact (Zeiss, Oberkochen, Germany). To estimate the amount of deposited P25, the thin films were mechanically removed from the glass substrates after the CO_2 reduction experiments and the received solid was quantified gravimetrically.

6.2.2 Removal of Carbonaceous Species, Photocatalytic CO_2 Reduction with P25 and Approximation of the AQY

70 mg of P25 were used for the approximation of the AQY in the photocatalytic CO_2 reduction in flow mode. The sample was calcined at 400 °C for 3 h in synthetic air prior to use. After calcination the sample was further cleaned from residual carbon-containing species before the CO_2 reduction was performed. This cleaning step was performed in the photoreactor set-up under continuous flow conditions and at ambient pressure. H_2O enriched He 6.0 (99.9999 % He) was flushed (5 mL/min) through the reactor while a 200 W Hg/Xe light source (Oriel Instruments) irradiated the sample. This

polychromatic light source was used in order to clean the sample quickly. A GC measurement was performed every 45 minutes to monitor the cleaning progress. As soon as the concentrations of the products were sufficiently low, the purification step was terminated. After purging out the gasphase in the reactor, the CO_2 reduction reaction was initiated. The reactant gas, a diluted CO_2 in He mixture (7000 ppm CO_2 in He 6.0) was passed through the reactor with a flow rate of 5 mL/min.

For the batch experiments, 15.000 ppm CO_2 in He 6.0 and 6000 ppm H_2O filled the reactor up to a final pressure of 1500 mbar. Every 45 min a sample was collected to identify the products of the CO_2 reduction over the course of 6 h. All results were normalised to take into consideration the resulting pressure drop from each sampling event.

6.2.3 Preparation of IrO_x/P25 and Approximation of AQY in H_2O Splitting

The iridium modified sample was prepared by photodeposition in a semi-batch quartz glass reactor. Iridium acetate was used as the precursor for the modification of P25. The nominal loading of iridium was set to 0.05 wt.%. On-top illumination was realised by a 1000 W Hg/Xe lamp (LOT quantum design). After 3 h of photodeposition, the illumination was stopped. The obtained powder was dried overnight and calcined at 400 °C for 3 h. For the AQY analysis of photocatalytic H_2O splitting, 70 mg of the 0.05 wt.% IrO_x/P25 were used. Dosing of the reactant H_2O was performed from stainless-steel cups, which are temperature-controlled. The temperature of the saturator was adjusted to set the H_2O concentration in the gas flow to ~1000 nmol/min. The flow rate of the reactant gas flow was also set to 5 mL/min.

6.3 Results and Discussion

6.3.1 Determination of the CH_4 Productivity using TiO_2 Thin Films

In order to study the effect of the mass of the P25 photocatalyst in CO_2 reduction under high-purity conditions, three films were synthesised either by doctor blading (DB) or airbrush technique (AB: air brush; TAB: thick air brush). The latter was employed as it does not require any organic solvents to deposit the P25 particles on the glass surface. The SEM images (Figure 41) exemplarily illustrate that the TAB film exhibits a rather uniform distribution of the P25 material. This is not the case for the AB sample. In order to produce thinner and more uniform films doctor blading was used. Even though the used paste includes organic solvents, the calcination of the deposited film and the extensive photocatalytic cleaning of the samples inside the reactor ensure that any remaining carbon-containing impurities are successfully removed. In the case of the DB and TAB samples, a calculation of the average film thickness was possible (Table 5). Due to the short airbrush deposition time, the AB film was not uniform exhibiting thicker and thinner domains of deposited P25 (Figure 41).

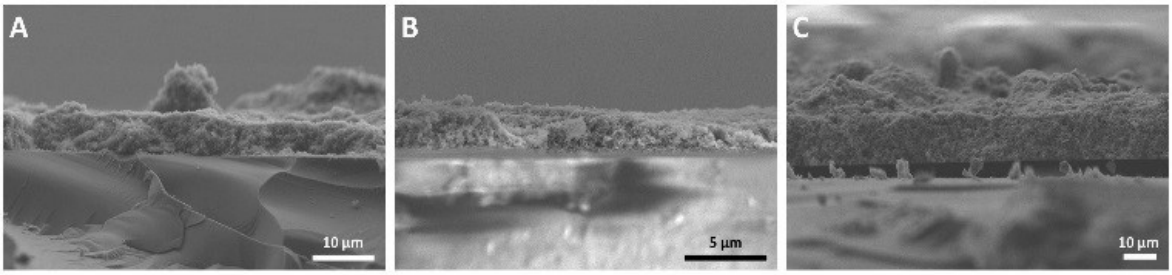

Figure 41: SEM images for the three tested films DB (A, left), AB (B, middle), TAB (C, right).

Thus, an accurate calculation of the AB film thickness was not possible. Based on the mass of the deposited P25 (Table 5) and the fact that the geometric dimensions were the same for all three films (2.5 x 2.5 cm), it can be assumed that the average film thickness of the AB sample is higher than that of DB and lower than the one of the TAB film.

Each one of the films was subjected to photocatalytic CO_2 reduction experiments in batch mode. Excessive cleaning took place inside the reactor until the sample was considered sufficiently clean (no or negligibly low amounts of C-containing impurities). The main product formed in all three cases was CH_4 while only traces of ethane were identified for the AB and TAB films. The CH_4 yields for the three tested films are presented in Figure 42. After the end of the experiments, the deposited P25 photocatalyst was mechanically removed to quantify the respective deposited masses. Under equal conditions, P25 in powder form (50 mg) was tested as a reference (Figure 42). All results from the batch experiments are summed up in Table 5.

Table 5: Average thickness and deposited mass for the three tested films and calculation of the respective CH_4 yield of photocatalytic CO_2 reduction.

Sample	Average film thickness [µm]	Mass [mg]	CH_4 Yield [µmol]	CH_4 Productivity [µmol g_{cat}^{-1} h^{-1}]
DB	5.4	1.6	$1.5 \cdot 10^{-3}$	0.103
AB	-	3.5	$2.7 \cdot 10^{-2}$	0.861
TAB	19.9	6.5	$1.3 \cdot 10^{-1}$	2.227
TiO_2 (P25) powder	-	50.0	$3.4 \cdot 10^{-1}$	0.781

Based on these results, a calculation of the CH_4 productivity (µmol g_{cat}^{-1} h^{-1}) is possible. As it can be seen from Table 5 there is a linear increase in the deposited mass of the three films (approximate ratio of 1:2:4 DB:AB:TAB) while the CH_4 productivity also increases linearly (Figure 43). The linear correlation evidences that indeed all of the deposited titania in the three films participates in the reaction.[165]

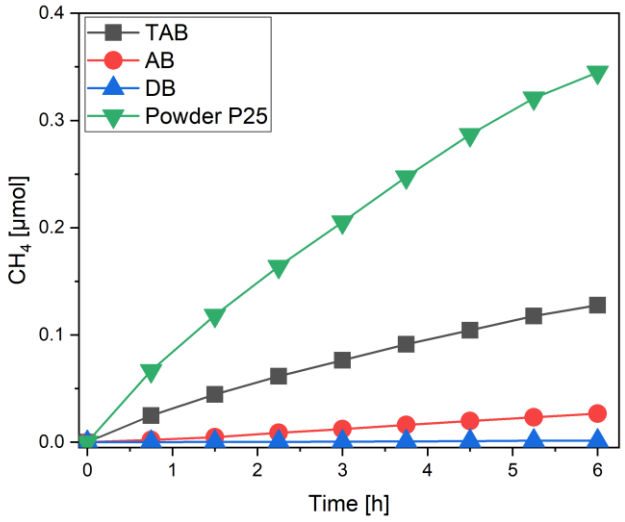

Figure 42: CH_4 yield for the DB, AB and TAB thin films. P25 powder was used under the same conditions as the reference.

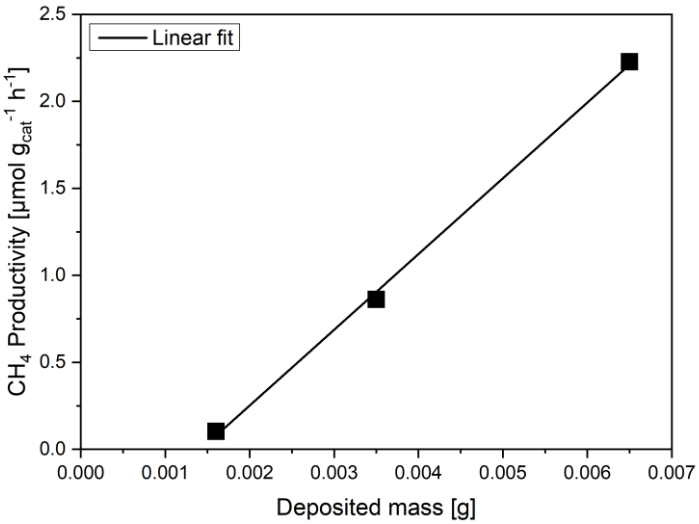

Figure 43: Linear fit of the CH_4 productivity in the CO_2 reduction experiments with the thin film samples.

It is expected, though, that after a certain film thickness and consequently deposited mass is reached, the increase in the CH_4 productivity should be marginal or non-existent.[170] Either the reactants CO_2 and H_2O will not be able to reach the lower layers of the film, or scattering and absorption phenomena will hinder the light from irradiating the entire film. The TAB has a much higher CH_4 productivity than the other three measured samples, including the powder sample with roughly eightfold titania mass. Based on the observed correlation, we can estimate the necessary titania mass of a film to reach the CH_4 yield (µmol) of the powdered P25, amounting to approximately 10 mg on the same 2.5 x 2.5 cm glass substrate. Thus it is clear that a major part of the powdered P25 is inactive in these experiments. The results also show that the mass of all three films is still below a certain threshold where the product yield is independent of the mass of the used photocatalyst. This is not an appropriate basis for the calculation of AQYs.[170] It should be also noted that no gas-phase O_2 was observed in any of the tested samples, inconsistent with the predicted stoichiometry of 1.7 but consistent with our previous observations.[122]

As in batch mode the reactants and the products of the CO_2 reduction remain in the reactor until the experiment ends, produced CH_4 molecules and other intermediate C-containing species could re-adsorb to the surface of the photocatalyst or react again in further cycles. The adsorbed CH_4 molecules could also facilitate the adsorption or reaction of more CO_2 molecules, thus improving the production of more C-containing molecules.[72] For the aforementioned reasons, it is necessary to perform CO_2 reduction experiments under flow conditions where formed hydrocarbons are continuously removed from the reaction chamber, allowing the calculation of more reliable AQYs. As demonstrated above, the mass of the used P25 will not be relevant, as long as it is above 10 mg. In order to compare the results to our own previous flow mode experiments, we decided to use 70 mg of P25.

6.3.2 Approximation of the AQY of P25 in Photocatalytic CO_2 Reduction

The photocatalytic CO_2 reduction with P25 was tested in a combined experiment with two reaction steps. In the first step carbonaceous impurities were removed and in the second step the activity in CO_2 reduction was studied to determine the AQY. Only such a procedure can guarantee that product formation is depending solely on the presence of CO_2. As described in our previous study[122] the detection of CH_4 and CO_2 during the first three hours results from the cleaning procedure. The consistent observation in our previous studies[122,137] was that a residual CH_4 baseline could not be avoided, even after extended cleaning procedures. The only potential reason for this observation not previously excluded is a diffusion of carbonaceous impurities from the bulk of P25. Figure 44 A-C display the result of blank experiments which were conducted to disprove this hypothesis. In all three cases P25 was photocatalytically cleaned for a certain period of time, followed by a dark period to allow diffusion of carbonaceous species from the bulk to the surface, before the photocatalytic cleaning was continued. In the dark period, the He gas flow of 5 mL/min was maintained. After the dark period, the illumination was started again, but in contrast to the activity test in Figure 43 without dosing of CO_2.

A

B

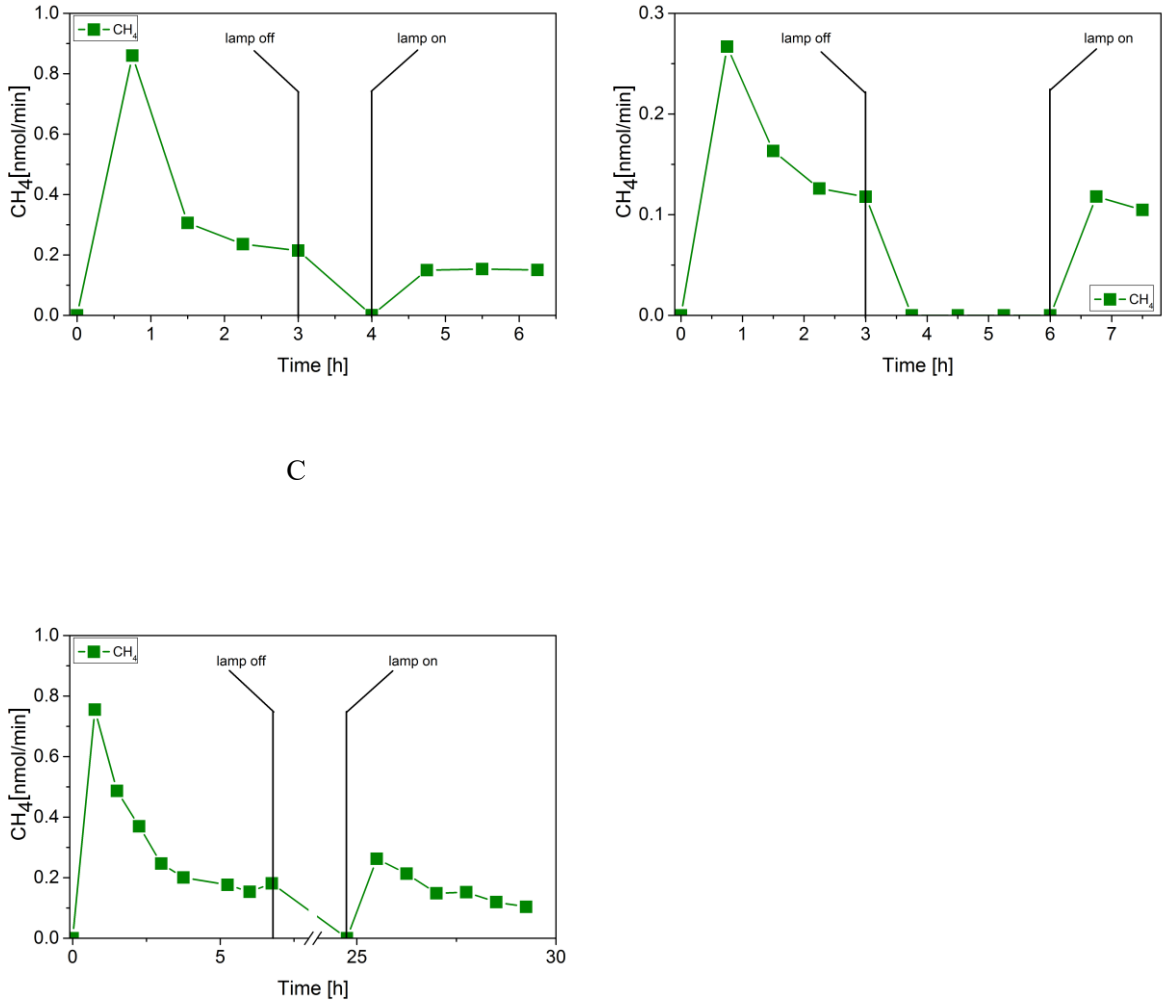

C

Figure 44: Removal of carbonaceous impurities with intermediate illumination interruptions, A: 3 h cleaning, 1 h without illumination, resuming cleaning; B: 3 h cleaning, 3 h without illumination, resuming cleaning, C: 6 h cleaning, 18 h without illumination, resume cleaning

The CH_4 formation increases only to the same baseline rate as observed before turning off the illumination (Figure 44 A and B). This result illustrates that no carbonaceous impurities from the bulk are diffusing to the surface of P25 when the light was turned off. Hence, a contribution of impurities from the bulk to the activity in CH_4 formation during the CO_2 reduction experiment in Figure 43 can be ruled out. Even when pausing the illumination for 18 h, only a slight increase of the CH_4 formation rate can be observed (Figure 44 C).

Regarding the results presented above the CH_4 formed after initiating the photocatalytic CO_2 reduction experiment at 3.75 h (Figure 45) truly originates from CO_2 as carbon source. A formation of other carbon

containing products such as CO, CH_3OH, C_2H_6, C_3H_6, which are frequently mentioned as products of the photocatalytic CO_2 reduction was not observed. Figure 45 shows that the CH_4 formation rate increased from 3.75 to 6 h. A stable CH_4 formation rate was observed after 6 h. Since the application of the high-purity reactor was essential for this work, the limited interaction between the reactant gas mixture and the solid P25 in the overflow geometry had to be accepted. As a consequence, the complete mixing of CH_4 in the gas flow to detect a stable formation rate is likely delayed.

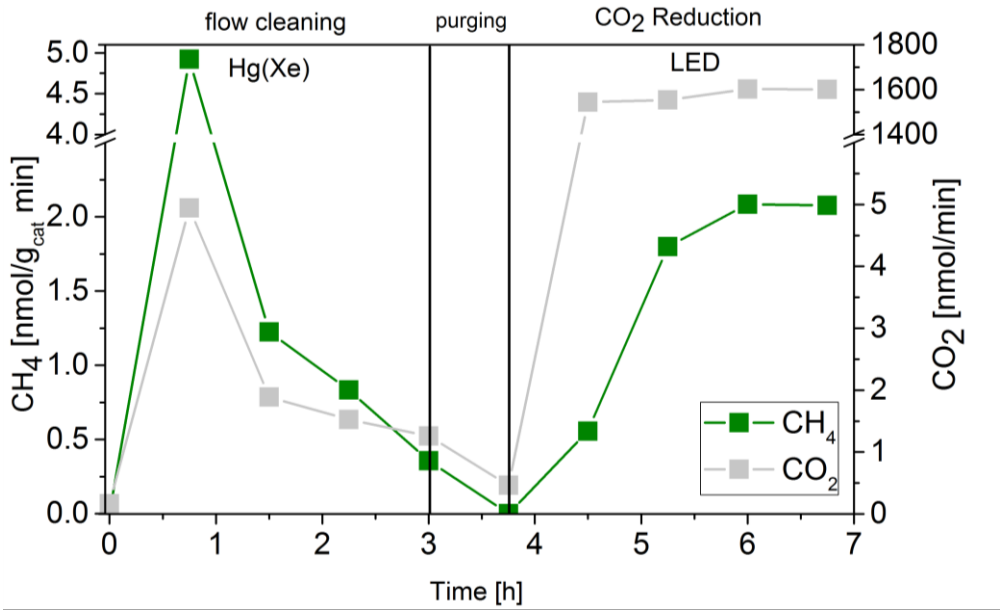

Figure 45: Approximation of the apparent quantum yield of P25 in the photocatalytic CO_2 reduction. Photocatalytic cleaning with Hg(Xe) lamp (0-3 h). Purging with He (3-3.75 h), no illumination. Photocatalytic CO_2 reduction (3.75-6.75 h) with 2 W LED (365 nm).

The stable formation rate of CH_4 was used as the basis for the AQY determination. The formation of CH_4 from CO_2 requires that two C-O double bonds are cleaved and 4 C-H bonds are formed. In this process eight electrons need to be transferred to the carbon atom. On this account the factor eight was used in the numerator of eq. 6.3 to obtain the number of electrons from the molar amount of CH_4 formed.

$$AQY_{P25\ (CH_4)} = \frac{8 \cdot n(CH_4)}{N_{Incident\ photons}} \qquad \text{(eq. 6.3)}$$

The obtained AQY of $6.5 \cdot 10^{-4}$ % in this study implies that only a minimal amount of the energy provided by the illumination source is utilised for the product formation of CO_2 reduction. In Table 6 the value for the AQY of CO_2 reduction is compared with those of other studies dealing with TiO_2. The AQY determined in this study is up to three orders of magnitude smaller (Table 6). A potential reason for this difference can be found in the high-purity conditions of the reactor set-up and the extensive cleaning procedure prior to the activity study. In this way a contribution of products from carbonaceous impurities

is avoided. As a consequence, the overall amount of CH_4 formed is relatively small, but it can be guaranteed that all of it originates from a reaction with CO_2.

Table 6: Comparison of the AQY of photocatalytic CO_2 reduction on TiO_2 from literature and this work.

Photocatalyst	AQY / %	Reference
TiO_2 (Anatase)	$4.8 \cdot 10^{-3}$	He et al.[176]
TiO_2	$1.5 \cdot 10^{-2}$	Yaghoubi et al.[177]
TiO_2 (oxygen deficient)	$3.1 \cdot 10^{-1}$	Liu et al.[39]
TiO_2 (P25)	$6.5 \cdot 10^{-4}$	This work

Furthermore, comparing the AQY of CO_2 reduction with studies on thermodynamically more favoured reactions, such as the decomposition of less stable organic compounds on TiO_2, for instance phenol,[178] methylene blue[179] or PCBs[180] shows that the values can reach 1 % up to 20 %. The fact that the AQY reaches higher values in these reactions when TiO_2 is used as the photocatalyst implies that a significant amount of electrons and holes is available for charge transfer reactions. This indicates that TiO_2 sufficiently functions as photoabsorber and creates charge carriers, but that is not a suitable catalyst for the formation of CH_4 in gas-phase CO_2 reduction, either because suitable active sites are lacking, or because most charge carriers lack a sufficient thermodynamic driving force to create relevant intermediates.

An additional shortcoming of P25 identified in our previous studies[72,122,137] is its inability to liberate gaseous O_2 as the stoichiometric by-product. The often-represented reaction (1.7) supposes the formation of CH_4 and O_2 in a 1:2 ratio. However, under the applied reaction conditions, it was not possible to detect any O_2. The formation of O_2 is often neglected in the literature. It is either not analysed or cannot be found in the products of photocatalytic CO_2 reduction.[124,125] With some exceptions[85-88,181] the research effort is focused on the formation of carbon related products, since they are the desired products for storing chemical energy.

6.3.3 Approximation of the AQY of IrO_x/P25 in Photocatalytic H_2O Splitting

The absence of O_2 can have various reasons: (i) the consumption of O-derived species in the backward reaction (CH_4 oxidation), (ii) limitations in H_2O oxidation kinetics, so that the reaction stops at adsorbed intermediates, or (iii) the replenishment of defects, namely oxygen vacancies (V_{OX}) on TiO_2[111,112]. This

leads to the suggestion that the oxidation half reaction in photocatalytic CO_2 reduction on P25-TiO_2 does not occur. Instead, reactions that consume oxygen take place that are not of catalytic but of stoichiometric nature. In the previous chapter we performed studies on Ir-modified P25 in CO_2 reduction and H_2O splitting. In contrast to the pure P25 overall H_2O splitting is possible with such a system. Consequently, using IrO_x/P25 gives us the opportunity to comparatively study the AQY of a reaction not limited by a stoichiometric counter reaction.

Figure 46 demonstrates that IrO_x/P25 shows activity in the overall H_2O splitting reaction. Both products, H_2 and O_2 can detected in a ratio of almost 2:1, according to 5.3.

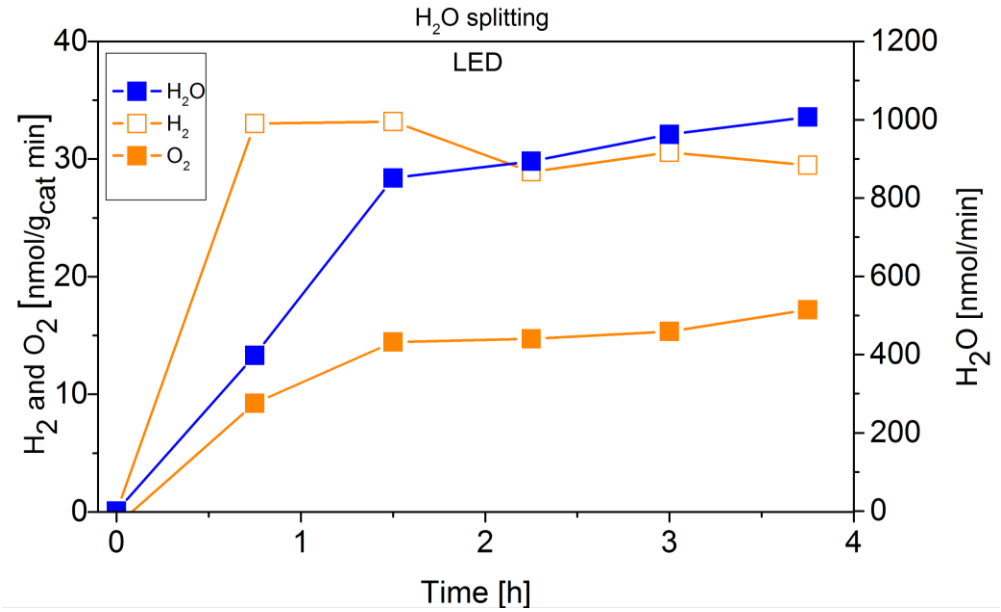

Figure 46: Approximation of the apparent quantum yield of 0.05 wt.% IrO_x/P25 in the photocatalytic H_2O splitting reaction. Illumination with 2 W LED (365 nm).

A more detailed analysis of the H_2O splitting experiment in Figure 46 shows that the O_2 formation rate increases within the first 2.25 h, while the H_2 formation rate is almost stable from the beginning. This observation is a strong indication that a certain amount of evolved O_2 remains on or in TiO_2. The missing amount of O_2 according to the stoichiometric ratio in 5.3 has been calculated to 410 nmol. Assuming that V_{OX} would be responsible for a complete consumption of the missing O_2 in the H_2O splitting experiment, at least 820 nmol V_{OX} are required. In case of the 70 mg of TiO_2, only ~ 0.1 % of lattice oxygen positions need to be vacant. On this account, the stoichiometric reaction of surface defects may be an important function in the activity of CO_2 reduction.

Using the stable and stoichiometric values of O_2 and H_2 formation rates, an AQY of $2.5 \cdot 10^{-3}$ % is obtained. Although this value is almost four times as high as the AQY of CO_2 reduction, it is still small.

It is important to note, that this value has also been obtained under high-purity conditions, so a falsifying influence of carbonaceous impurities acting as sacrificial reagents can be excluded.

6.4 Conclusions

As central outcome of this work, reliable values for AQY and productivity of P25-TiO_2 in photocatalytic CO_2 reduction have been obtained. Thin films composed of less than 10 mg titania are presumably fully illuminated, so that all of the TiO_2 contributes to the product formation and reliable values for the productivity can be obtained. Applying a larger amount of P25 allows determination of reliable AQY values. The resulting values and a comparison with thermodynamically more feasible reactions imply that the absorption functionality of P25 would allow higher yields, but the catalytic function is not suitable for CO_2 reduction reaction. Implementing the same procedure for overall H_2O splitting with IrO_x/TiO_2 reveals a four times higher AQY value. Additionally, a small amount of O_2 missing in comparison to the expected 2:1 ratio (H_2:O_2) provides further indication that a stoichiometric reaction consuming oxygen species might play an important role in photocatalytic CO_2 reduction.

7. Development of a Tubular Continuous Flow Reactor for the Photocatalytic CO_2 Reduction on TiO_2

Abstract

This work describes the development of a self-made, low-cost tubular reactor for the gas-phase photocatalytic CO_2 reduction on TiO_2. Such a reactor geometry allows preparing a fixed bed of the solid photocatalyst in the inside of the tube. The resulting flow conditions cause an intensive interaction between the reactants in the gas-phase and the photocatalyst. This approach is used to test the scalability of tubular reactors for the photocatalytic CO_2 reduction. Furthermore, the effect of an improved gas-solid interaction between the reactants and fixed photocatalyst particles is investigated.

The main content of this chapter is published in Photochem. Photobiol. Sci. **2019,** 18, 314-318 as "Development of a Tubular Continuous Flow Reactor for the Photocatalytic CO_2 Reduction on TiO_2", M. Dilla, A. E. Becerikli, R. Schlögl, S. Ristig

7.1 Introduction

In order to prove if the photocatalytic CO_2 reduction proceeds, a reactor set-up needs to be developed which allows performing light induced experiments under optimal conditions. For such a design the illuminated fraction of the surface area should be maximized to realize adequate excitation of the photocatalyst, since the penetration depth of UV light with a wavelength of, for instance, 355 nm into TiO_2 (anatase) is stated as ~ 280 nm[182] which is extremely low. In this way only a very small fraction of TiO_2 will be excited by photons. Another important prerequisite is that experiments can be performed under optimal mass transport conditions of reactants and products, necessitating an intensive interaction between the gas-phase and the solid photocatalyst. One approach to meet these demands is the construction of a reactor with tubular geometry. A successful application of such a reactor design in photocatalytic research has already been reported for the oxidation of, for instance, organic compounds[183-185] in liquid phase or NO_2[186]in the gas phase, employing quartz glass[184-186] and fluorinated-ethylene-propylene (FEP)[183] as reactor materials. There are however no reports on the application of a tubular reactor geometry for photocatalytic gas phase CO_2 reduction on solid state photocatalysts, e.g. TiO_2. The feasibility to design such a reactor and utilize it for studying this highly complex reaction is reported here for the first time. To achieve reaction conditions of highest purity, an experimental procedure was developed for the removal of carbonaceous impurities from the surface of the sample prior to testing the photocatalytic activity in CO_2 reduction. This is crucial, as residual impurities can contribute to the product formation in the CO_2 reduction reaction, which leads to a significant overestimation of the activity. Only after successful removal it can be guaranteed that product formation originates from the reactants. With this set-up it was possible to conduct photocatalytic CO_2 reduction on TiO_2 with intensive interaction of the reactants and the solid photocatalyst under high-purity conditions.

7.2 The Reactor Material and the LED Bar

For this design it is mandatory that the material of the tubular reactor is transparent and chemically stable under illumination with UV light as well as mechanically flexible. Furthermore, the diameter of the tube must be as small as possible to increase the illuminated portion of the photocatalyst surface. One material which seems to fulfill these requirements is fluorinated ethylene propylene (FEP). The FEP tube chosen for the approach presented here has an inner diameter of 2.1 mm. To realize illumination of the photocatalyst with a centered light source, the FEP tube was wrapped around a self-made high intensity UV-LED bar. The UV light source consists of a square aluminum bar with three high power UV-LEDs (365 nm) on each side of the bar, amounting to a total of 12 UV-LEDs with a combined output power of 10 W (Figure 47).

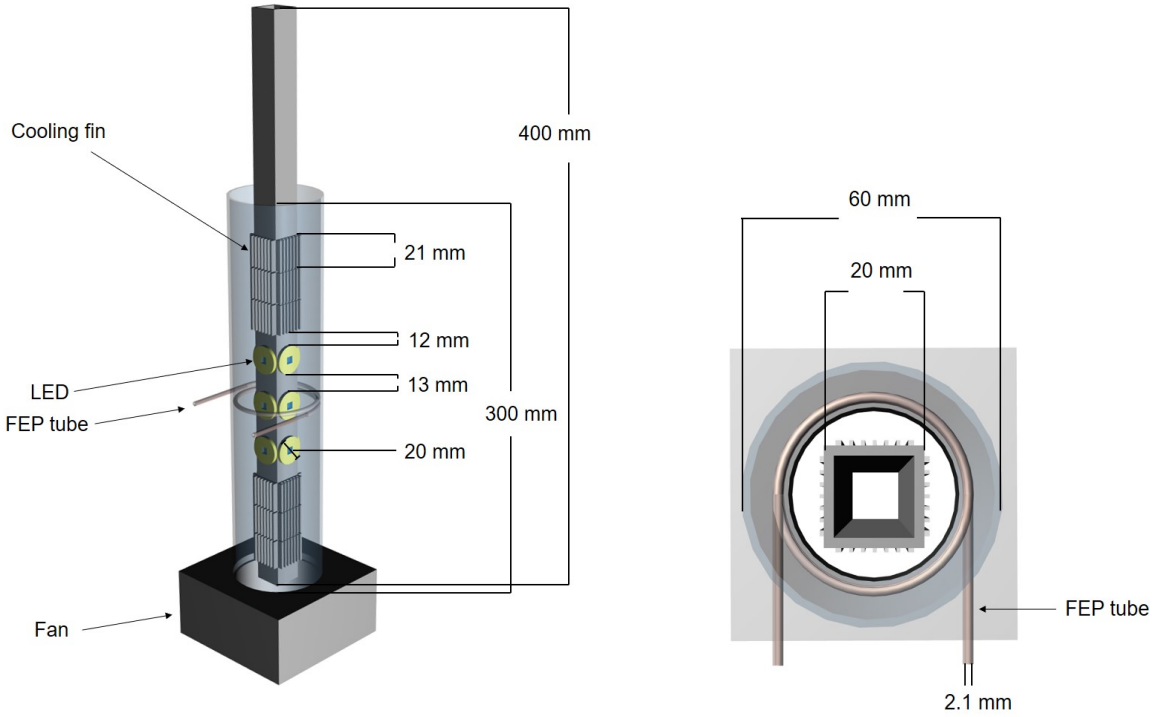

Figure 47: Illustration of the self-made high intensity UV-LED bar equipped with a fan and attached cooling fins. Left side: Front view. Right side: On-top view.

The tubular reactor is wrapped equidistantly to the UV-LED bar along the inner wall of the PTFE (Figure 47). The inlet of the reactor is connected to the gas supply to realize purging with He 6.0 (99.9999 % purity) and dosing of the reactant gas mixture (7000 ppm CO_2 in He 6.0). The outlet of the reactor is connected to a Shimadzu Tracera GC 2010 Plus. This GC is equipped with a barrier discharge ionization detector (BID), which allows quantifying CO_2, CO, CH_4, C_2H_6, H_2O, O_2 and H_2 in the 0.1 ppm range. Based on this high sensitivity, the BID is a suitable analytical device for an application in continuous-flow photocatalytic CO_2 reduction. Swagelok fittings were used for all tube connections.

7.3 The UV Stability and Diffusion Properties of FEP

To verify that the FEP tube does not release any carbon containing species upon UV light irradiation which can be misleadingly counted as products, a blank experiment with an empty tube reactor was performed (Figure 48 A). After flushing out the remaining atmospheric air inside the reactor with He (50 mL/min), the flow rate was decreased to 5 mL/min (0 h, Figure 48 A). Then the gas flow was held for 0.75 h. In this period of time the concentration of CO_2 and O_2 increased. From 0.75 to 1.5 h the He flow rate was increased to 10 mL/min and a decrease in the concentration of both species was observed as a consequence of the higher dilution with inert gas. In the following, the gas flow was decreased again to 5 mL/min. It can be seen that the concentration of CO_2 and O_2 from 0.75 h can be reproduced at 2.25 h (Figure 48 A). Due to the absence of illumination it is assumed that environmental CO_2 and O_2 diffused through the tube walls. Starting from 2.25 h the UV illumination was initiated. No significant release of

CO_2 and CH_4 was observed under the influence of UV light. Furthermore, the presence of CO, H_2 and C_2H_6 (not shown in Figure 48 A) can be excluded. This result shows that the FEP tube is physicochemically stable against UV light irradiation, thus its use is suitable for the purpose of this work. However, since we know from our previous work[122] that O_2 inhibits the photocatalytic CO_2 reduction, it was decided to study the diffusion properties of the FEP tube in detail. More specifically the amount of incoming O_2 as a function of the tube length was analyzed. It is obvious from Figure 48 B that the concentration of O_2 increases linearly with the length of the reactor. An increase of the O_2 concentration by 0.33 ppm/cm of reactor was determined from the slope of the linear fit (Figure 48 B, red line). Most likely diffusion of O_2 from air is the reason for this observation.

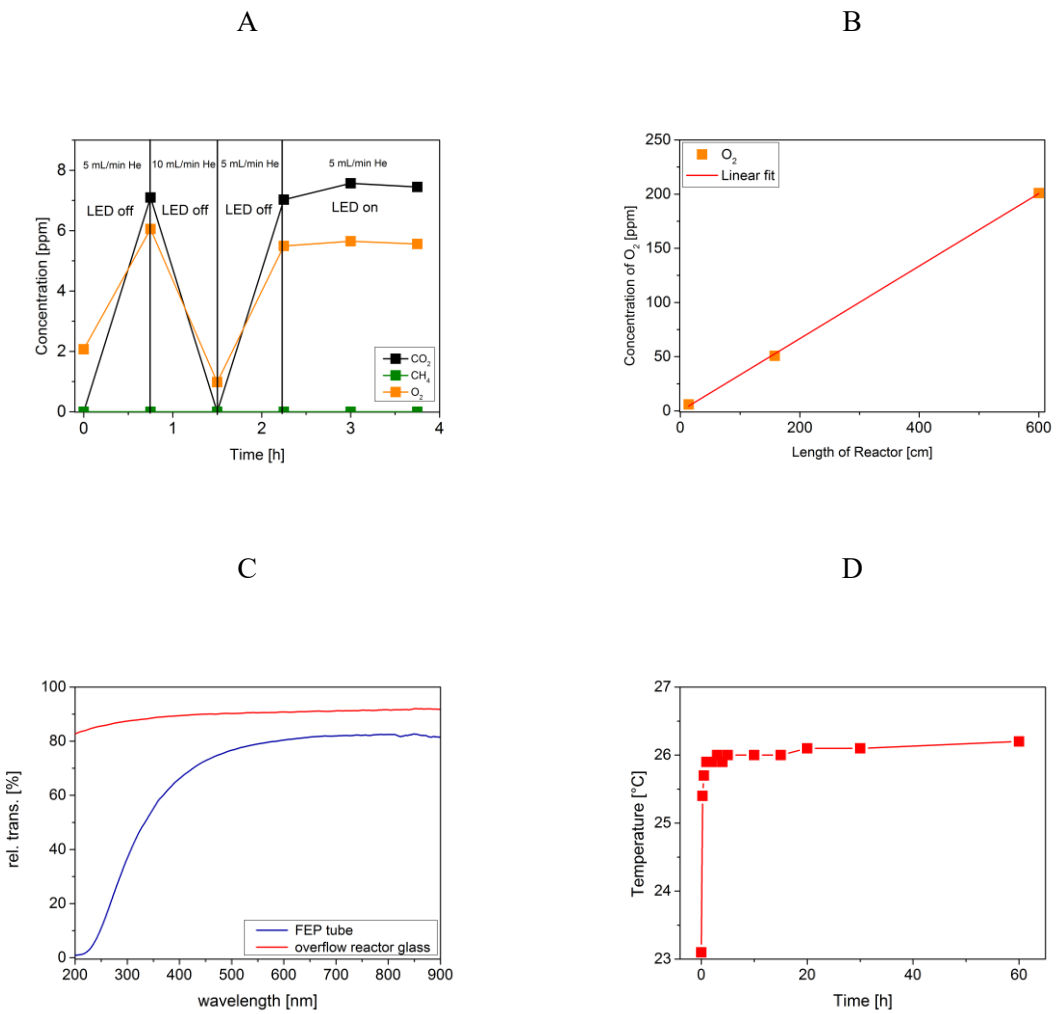

Figure 48: A: Stability of the FEP tube under illumination with UV light. Illumination takes place from 2.25 h to 3.75 h. B: Concentration of atmospheric O_2 diffused into the tube as a function of the tube length. C: relative transmission of the FEP tube and the overflow reactor lid. D: Temperature profile inside the fixed bed of P25 in the FEP tube during illumination with the LED bar.

To verify the UV-transparency of the reactor material, the relative transmission of the FEP tube was determined via UV-Vis spectroscopy (Figure 48 C, blue line). At 365 nm, the emitted wavelength of the UV-LEDs, the relative transmission is 60 %. This indicates that a significant fraction of the light

intensity does not reach the photocatalysts surface, likely due to absorption and scattering phenomena. As the absorption of photons by the FEP tube could result in heating of the reactor, the temperature inside the tube under photocatalytic reaction conditions was determined, since thermal energy was found to influence the activity in CO_2 reduction on TiO_2[137]. Consequently, a thermocouple was placed in a fixed bed of TiO_2 (P25) in the FEP tube. In the temperature profile in Figure 48 D it can be seen that the temperature inside the reactor increases from 23.1 to 26.2 °C under the applied illumination conditions. Hence, the air stream inside the PTFE tube seems to be sufficient to keep the reactor temperature close to room temperature.

7.4 Photocatalytic CO_2 Reduction with P25 - Scalability of FEP Tube Reactors

After verification of the suitability of the reactor material and setting the optimum experimental conditions at which the set-up can be used for the photocatalytic CO_2 reduction, two tube reactors were prepared with P25 as photocatalyst. Previously, the P25 sample was calcined at 400 °C for 3 h. This pretreatment allows a first oxidative removing of carbonaceous impurities. The sample was pressed and sieved and the mesh size 0.28 mm fraction was filled into the tube using a small funnel. A small plug of glass wool at the reactor outlet and inlet kept the fixed bed in the reactor. For testing the set-up, reactors with lengths of 14 and 26 cm were prepared and filled with 223 and 680 mg of P25, respectively. In Figure 49 the formation of CH_4 in the cleaning procedure and the CO_2 reduction with the 26 cm reactor is shown exemplarily.

To flush out the remaining air inside the FEP tube, the reactor was purged with He (50 mL/min) for 30 min. Subsequently, remaining carbonaceous impurities were removed during the flow cleaning procedure (5 mL He/min) under UV irradiation (Figure 49). Since the powder was in contact with ambient air during the sample filling, the P25 sample was expected to be covered by multilayers of physisorbed water.[98] GC measurements were carried out every 45 min to monitor the cleaning progress. The duration of the cleaning procedure depends on the concentration of carbon-containing species on the photocatalyst. The products of the cleaning procedure are CH_4 and CO_2. As shown in our previous reports,[122] CH_4 originates from hydrogenation of carbon-containing impurities and from the photocatalytic reduction of trace amounts of CO_2 in the He purging gas. Apart from 0.5 ppm CO_2 in the He purge gas, the observed CO_2 might also originate from the oxidation of carbon-containing species or from desorption of carbonates. In this case however, no CO_2 formation is observed (Figure 49).

The photocatalytic CO_2 reduction experiment is started as soon as the CH_4 concentration is almost constant. Then it is assumed that all carbonaceous species are removed and CH_4 is formed from CO_2 in the He purge gas. For both reactors the CO_2 reduction is initiated after 3 h of photocatalytic cleaning

(Figure 49) by changing the gas flow from pure He to the reactant gas mixture (7000 ppm CO_2 in He). The flow rate of 5 mL/min is maintained and the UV illumination is continued without interruption. No additional H_2O is dosed to the reactor since we verified in previous experiments that continuous dosing of H_2O can lower the activity of P25 in the CO_2 reduction reaction due to competitive adsorption phenomena and occupation of active sites.[137] The present amounts of H_2O on P25 are sufficient to run the CO_2 reduction for the desired timeframe.[137] It becomes obvious from Figure 49 that the CH_4 flow rate increases when CO_2 is dosed to the tubular reactor.

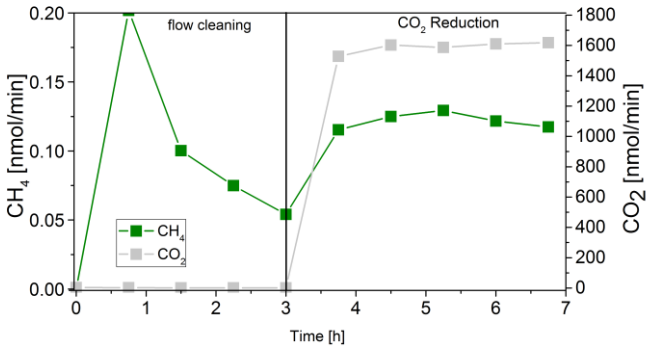

Figure 49: Photocatalytic cleaning and CO_2 reduction with P25 in the tubular continuous flow reactor. B: Reactor length 26 cm, 680 mg P25; photocatalytic cleaning (0 to 3 h); photocatalytic CO_2 reduction (3 to 6.75 h).

In Table 7 the overall formation rates of CH_4 with the 14 and 26 cm reactor are shown. Since the activity of the photocatalytic reaction is dependent on the amount of exposed surface area, it becomes obvious that the activity scales with the length of the reactor and the amount of TiO_2, respectively. The results also show that there is no increased inhibitive effect which scales with the reactor length and thus the higher amounts of O_2. In both experiments with the tubular reactors it was not possible to detect any formation of O_2 as the by-product of photocatalytic CO_2 reduction. Therefore, it is possible that O_2 and O-derived species as products and intermediates of the CO_2 reduction reaction remain on the surface of TiO_2 instead of being desorbed. Consequently, they can contribute to the oxidation of CH_4, occupation of active sites or competition for charge carriers with CO_2. These effects might lower the overall activity in the photocatalytic CO_2 reduction reaction.

Table 7: Summary of CH_4 formation rates in the tube reactors.

	14 cm reactor	26 cm reactor
Overall CH_4 formation rate $[\mathrm{nmol \cdot h^{-1}}]$	1.4	3.6
O_2 concentration (end of the reactor) [ppm]	4.7	13

7.5 The Effect of Gas-Solid-Interaction on the Photocatalytic CO_2 Reduction

To investigate the performance of the tubular reactor setup, photocatalytic CO_2 reduction was also conducted with an overflow reactor. The results are then compared to those from the 14 cm reactor. A detailed description of the overflow reactor geometry was made by Mei et al.[102] In this reactor the reactants only pass the surface of the fixed bed resulting in a significantly less intensive interaction between the gas-phase and the photocatalyst. Due to the O_2 permeability of the FEP tube it was decided to use the experimental results obtained with the smaller tube for a comparison with the overflow reactor. In this way similar reaction conditions are established, except for the gas-solid interaction. This comparison is the basis for an evaluation of the effect of the gas-solid interaction on the activity of photocatalytic CO_2 reduction on TiO_2.

Table 8: Comparison of the overall formation rates of CH_4 in the photocatalytic CO_2 reduction with the 14 cm tube reactor and an overflow reactor geometry.

	Tube reactor	Overflow reactor
r_{CH_4} $[\mathrm{nmol \cdot cm^{-2} \cdot h^{-1}}]$	0.42	0.26
r_{CH_4} $[\mathrm{nmol \cdot g_{cat}^{-1} \cdot h^{-1}}]$	6.3	23

In Table 8 the obtained formation rates of CH_4 from both different reactor designs are shown. The rates are related to the mass of P25 (g_{cat}) and the geometric illuminated area to evaluate the effect of the illumination conditions and the gas-solid interaction, respectively. It can be clearly seen that the overflow reactor shows a higher CH_4 formation rate related to the mass of P25 (Table 8). Most likely a large mass fraction of P25 inside the tube is not illuminated due to the small penetration depth of UV light, the tubular geometry and the arrangement of illumination. Consequently, only a minor amount of

photocatalyst is excited. This result clearly shows that the activity in the photocatalytic CO_2 reduction reaction is strongly dependent on the illuminated fraction of the surface area. For comparison of the rates related to the geometric illuminated area it needs to be stressed that the transmission of the overflow reactor lid (89 % at 365 nm, Figure 48 C) exceeds that of the FEP reactor. Although the same kind of UV LED is used for the two reactor types, the light intensity impinging on the exposed surface of the photocatalyst will be lower for the FEP reactor. Still, the comparison of the rates related to the geometric illuminated area reveals a higher activity for the tubular reactor, although the light intensity is lower. It verifies that the improved gas-solid interaction in the tubular reactor is beneficial for the activity in photocatalytic CO_2 reduction.

7.6 Conclusions

To summarize, this study shows the successful development of a scalable tubular reactor for the gas-phase photocatalytic CO_2 reduction on TiO_2. For the first time, it was possible to report the formation of CH_4 as the main product of this highly complex process by using such a reactor geometry and conditions of highest purity. For the development of new reactor geometries for the photocatalytic CO_2 reduction it is essential that the illuminated fraction of photocatalyst is maximized and the interaction of the reactants in the gas-phase with the photocatalyst is intensive. In general, a tubular reactor geometry is an appropriate choice to overcome the abovementioned problems. However, with respect to the O_2 diffusion properties, FEP as material appears to be less applicable for the scalability as a photoreactor for the photocatalytic CO_2 reduction, as an inhibition of the product formation due to increased amounts of O_2 in the reactor might occur for elongated reactors. A suggested alternative could be quartz glass, as it is transparent to UV light and prevents the diffusion of O_2 into the reactor from the environment. The utilization of quartz capillaries would provide intensive gas-solid interaction and the small inner diameter would improve the illumination conditions. Furthermore, the reactor can be arranged in a centered geometry relative to the light source. This will result in the illumination of the whole tube and an improved UV excitation of the photocatalyst.

8. Final Conclusions and Prospects

In this work the photocatalytic CO_2 reduction was investigated from two perspectives. On the one hand side reaction engineering work was performed to develop appropriate experimental approaches and reactor geometries to gain knowledge about the requirements and limitations of the product formation. On the other hand side it was investigated if the product formation on TiO_2 is based on a photocatalytic cycle with the reactants CO_2 and H_2O. In this context it was intended to clarify the absence of O_2 as the by-product of CO_2 reduction and H_2O oxidation.

In the initial part of the thesis, the development of experimental conditions to perform CO_2 reduction experiments under continuous flow conditions and the highest possible purity was described. For this purpose a reactor system which was originally designed for gas-phase photocatalytic reaction under batch condition was used. The resulting overflow reactor geometry and the acquired operation procedures for the removal of carbonaceous impurities and the activity test were the basis for most of the experiments in this work. Furthermore, a measuring protocol for the approximation of the AQY in photocatalytic CO_2 reduction has been developed. For the AQY investigations and the tubular reactor design appropriate LED light sources were built to realize specific illumination conditions for each experiment. The tubular reactor design was built to allow an intensive interaction between the components in the gas-phase and the solid photocatalyst. With these two reactor geometries it became possible to verify the relevance of a large illuminated surface area and an intensive interaction between the reactants and the photocatalyst to achieve high product formation rates. The activity studies with bare TiO_2 demonstrated a strong correlation between the CH_4 formation rate and the availability of the reactants. This observation proved that the product formation is based on a reaction with CO_2 and H_2O. The contribution of impurities in CH_4 formation can be ruled out due to the high purity of the reaction conditions. However, formation of O_2 as the by-product of photocatalytic CO_2 reduction and H_2O oxidation was not observed on bare TiO_2. Experiments with external dosing of O_2 pulses revealed an inhibiting effect on the CH_4 formation. Furthermore it was shown that the formation rate of CH_4 is dependent on the energy and intensity of the incident light beam. The product formation rate can only be increased by the square root of the light intensity, as a consequence of the growing influence of the charge carrier recombination reaction. Another important finding is the dependence of product formation from UV photons. In absence of UV light no CH_4 was formed. Nevertheless, UV light and additional visible light or external heat can improve the activity in CO_2 reduction, indicating that a thermal component exists in the product formation mechanism. The approximation of the AQY further revealed that the concentration of available charge carriers on the surface of the photocatalyst is potentially not the reason for the generally low activity of TiO_2 in photocatalytic CO_2 reduction. Due to the extreme stability of the reactants CO_2 and H_2O, it appears more likely that at least one step in the overall reaction mechanism of the product formation is rate limiting. A modification with IrO_x, as a co-

catalyst for H_2O oxidation, gave further insights into the photocatalytic properties of bare TiO_2 and the absence of O_2 in CO_2 reduction. IrO_x modified TiO_2 samples showed significant activity in photocatalytic H_2O splitting. A formation of both products, H_2 and O_2 in stoichiometric amounts was apparent. Photocatalytic CO_2 reduction experiments with IrO_x/P25 samples exhibited the H_2 formation as the favored charge transfer reaction of the photogenerated electrons in TiO_2. Thus, the competitive H_2 formation, the presence of O_2 and highly reactive oxygen species are most likely the reason for the absence of CH_4 formation. However, the fact that bare TiO_2 shows obviously no activity in H_2 and O_2 formation, but a significant activity in the CH_4 formation is a strong indication that the photocatalytic H_2O oxidation is not the source of hydrogen in the C-H bond formation in the CO_2 reduction reaction. Under this circumstance, a different source than H_2O oxidation, for instance surface hydroxyl groups, must deliver hydrogen for CH_4 formation. A further meaningful observation of this work is the indication that TiO_2 consumes oxygen under photocatalytic reaction conditions. Under this circumstance, TiO_2 is associated with the absence of O_2 in the CO_2 reduction and the delayed initiation of the O_2 formation in the H_2O splitting experiments with IrO_x/P25. In this way the consumption of O_2 represents an important factor of the photocatalytic activity. Consequently, TiO_2 undergoes a stoichiometric reaction with reaction products, meaning the reduction of CO_2 is not based on a catalytic cycle.

In summary this work can be understood as an insight into the complexity of a photocatalytic reaction. Furthermore, it demonstrates the tremendous effort and the related challenges of performing reliable experiments to scrutinize the validity of elementary assumptions in photocatalytic CO_2 reduction. Indeed the overall results of the present study reveal the CH_4 formation to be a light induced process originating from CO_2. H_2O seems to be also relevant for the product formation, but the liberation of the hydrogen source does not seem to be based on a photocatalytic reaction. However, the indications that bare TiO_2 performs stoichiometric reaction and H_2O oxidation is obviously not involved in the CH_4 formation are in strong conflict with the often-represented reaction equation (1.7) of CO_2 reduction. This fundamental assumption seems to be wrong and prefigures that an approach of only using TiO_2 does not work for the conversion of such extremely stable molecules. Therefore novel strategies for chemical energy storage by CO_2 reduction based on light induced or light assisted reaction need to be developed and tested. It is desirable that such a system is capable of performing both the CO_2 reduction and the H_2O oxidation in a catalytic cycle. At the same time the hydrogen source is supposed to be directly used for hydrogenation. If H_2 is generated, then a catalytic functionality to utilize this gas for hydrogenation needs to be available as well. Furthermore, the by-product O_2 must be removed to prevent the inhibiting effect towards CH_4 formation. Thus, it is questionable if a system based on H_2O as the oxidant and hydrogen source can be realized by only one photocatalyst in a single pot synthesis. The numerous requirements a photocatalyst needs to satisfy, and the limited usability of standard analytical methods due to the low activity of the current systems make the investigation of the overall photophysical and chemical processes

complicated. In addition, the content of information obtained with reactor set-ups as they are used, for instance, in this work only allow investigations on the overall reaction rates under the influence of different reaction parameters. In other words, the scope of information from such experimental approaches is limited and possibly not sufficient to make progress in understanding the complete reaction mechanism. However, the development of novel reactor designs assisted by spectroscopic techniques might bear an option for studying details of light induced reaction processes on TiO_2. EPR spectroscopy is a common technique for the analysis of species with unpaired electrons, as for instance Ti^{3+} species. Such an approach is capable of monitoring changes in the concentration of Ti^{3+} species under the influence of the photocatalytic reaction. If V_{OX} in vicinity of Ti^{3+} species are consumed by oxygen from CO_2 reduction or the dissociative adsorption of H_2O, changes in the corresponding signal will be detected. In this way the option of a stoichiometric reaction by TiO_2 under photocatalytic reaction conditions could be verified. Another surface sensitive technique which could be used is high resolution electron energy loss spectroscopy (HREELS). This method is based on the inelastic scattering of electrons on a surface. HREELS is suitable for the detection of surface OH-groups on TiO_2. The analysis of the OH-group concentration and changes of their concentration under the influence of photocatalytic reaction conditions can be carried out. Thus, the potential contribution of these species as a hydrogen source in CH_4 formation could be studied. The major challenge in the development of such experimental designs will be the low intensity of the relevant signals and the sensitivity of the spectrometer. Furthermore, an experimental design for the investigation of the thermal effect on the photocatalytic CO_2 reduction should be developed, so that the rate of product formation at temperatures above 100 °C can be studied. In this way, the influence of the product desorption as the overall rate limiting step can be evaluated. In addition, the effect of H_2O and the influence of its evaporation on the product formation can be investigated.

In terms of the challenges of CO_2 reduction it needs to be considered which performance a photocatalyst must have to exceed the energy conversion efficiency of solar cells and wind power systems. As an example, the combination of performing electrocatalytic reactions driven by ecological power would represent an alternative. However, independent of the approach, it is essential that the CO_2 reduction reaction is understood in detail. For this goal, it is mandatory to focus the prospective research on the overall reaction mechanism of the CO_2 reduction. Only the knowledge of the elementary steps will allow progress in the chemical energy storage based on CO_2 reduction.

Finally, we should keep in mind that the evolution of the natural photosynthesis of plants took more than three billion years. Compared to that, the four decades of research in the field of photocatalytic CO_2 reduction are a negligible period of time. On these grounds, it can be expected that there is potential to realize a successful artificial pathway in the future.

9. Bibliography

[1] BMWI, "Available from: http://www.bmwi.de/Redaktion/DE/Infografiken/Energie/Energiedaten/Energiegewinnung-und-Energieverbrauch/energiedaten-energiegewinnung-verbrauch-03.html", *23.02.2018*.

[2] BP, *BP Statistical Review of World Energy 2017,* **2017**.

[3] P. Falkowski, R. J. Scholes, E. Boyle, J. Canadell, D. Canfield, J. Elser, N. Gruber, K. Hibbard, *Science* **2000**, *2000*, 291.

[4] C. Le Quéré, R. J. Andres, T. Boden, T. Conway, R. A. Houghton, J. I. House, G. Marland, G. P. Peters, G. van der Werf, A. Ahlström et al., *Earth Syst. Sci. Data Discuss.* **2012**, *5*, 1107.

[5] Earth System Research Laboratory – Global Monitoring Division, "Trends in Atmospheric Carbon Dioxide; Recent Monthly Average Manua Loa carbon dioxide (http://www.esrl.noaa.gov/gmd/ccgg/trends/)", **2017**.

[6] R. Schlögl (Ed.) *Chemical energy storage*, de Gruyter, Berlin, **2013**.

[7] P. McKendry, *Bioresours. Technol.* **2002**, *2002*, 37.

[8] W. Kremers, J. Thiele, F. Wahl in *Neue Wege der Energieversorgung* (Eds.: W. Kremers, J. Thiele, F. Wahl), Vieweg+Teubner Verlag, Wiesbaden, **1982**.

[9] J. Renn, R. Schlögl, H.-P. Zenner, *Herausforderung Energie*, Gesellschaft Deutscher Naturforscher und Ärzte e.V., Berlin, **2011**.

[10] P. W. Atkins, J. de Paula, *Physical Chemistry*, Oxford University Press, Oxford, **2014**.

[11] J. Nowotny, *Oxide semiconductors for solar energy conversion*. *Titanium dioxide*, CRC Press, Boca Raton, **2012**.

[12] H. Kisch, D. Bahnemann, *Phys. Chem. Lett* **2015**, *6*, 1907.

[13] J. Li, N. Wu, *Catal. Sci. Technol.* **2015**, *5*, 1360.

[14] S. R. Morrison, *Electrochemistry at semiconductor and oxidized metal electrodes*, Springer, New York, **2011**.

[15] Y. Pleskov, *Semiconductor Photoelectrochemistry*, Springer, New York, **2012**.

[16] R. Beranek, *Ad. Phys.* **2011**, *2011*, 1.

[17] S. N. Habisreutinger, L. Schmidt-Mende, J. K. Stolarczyk, *Angew. Chem. Int. Ed.* **2013**, *52*, 7372.

[18] P. V. Kamat, *J. Phys. Chem. Lett* **2012**, *3*, 663.

[19] J. C. Colmenares, Y.-J. Xu (Eds.) *Green chemistry and sustainable technology*, Springer, Heidelberg, New York, Dordrecht, London, **2016**.

[20] J. Schneider, M. Matsuoka, M. Takeuchi, J. Zhang, Y. Horiuchi, M. Anpo, D. W. Bahnemann, *Chem. Rev.* **2014**, *114*, 9919.

[21] R. van de Krol, M. Grätzel (Eds.) *Photoelectrochemical Hydrogen Production*, Springer, Heidelberg, **2012**.

[22] A. Di Paola, M. Bellardita, L. Palmisano, *Catalysts* **2013**, *3*, 36.

[23] M. Anpo, J. M. Thomas, *Chem. Comm.* **2006**, 3273.

[24] U. Diebold, *Surf. Sci. Rep* **2003**, *48*, 53.

[25] M. Rande, *Proc. Natl. Acad. Sci.* **2002**, *2002*, 6476.

[26] V. Sammelselg, A. Rosental, A. Tarre, L. Niinisto, K. Ilmonen, L.-S. Johansson , T. Uustare, *App. Surf. Sci.* **1996**, *134*, 78.

[27] H. Chang, P. J. Huang, *J. Raman Spectrosc.* **1998**, *29*, 97.

[28] A. F. Holleman, E. Wiberg, N. Wiberg, *Lehrbuch der anorganischen Chemie*, de Gruyter, Berlin, **2007**.

[29] S. Kelly, F. H. Pollak, M. Tomkiewicz, *J. Phys. Chem. B* **1997**, *1997*, 2730.

[30] T. Ohsaka, F. Izumi and Y. Fujiki, *J. Raman Spectrosc.* **1978**, *1978*, 321.

[31] J. Zhang, M. Li, Z. Feng, J. Chen, C. Li, *J. Phys. Chem. B* **2006**, *110*, 927.

[32] B. Ohtani, O. O. Prieto-Mahaney, D. Li, R. Abe, *J. Photochem. Photobiol. A.: Chem.* **2010**, *216*, 179.

[33] R. I. Bickley, T. Gonzalez-Carreno, J. S. Lees, L. Palmisano, R. J. D. Tilley, *J. Solid State Chem* **1991**, *1991*, 178.

[34] T. Ohno, K. Sarukawa, K. Tokieda, M. Matsumura, *J. Catal.* **2001**, *203*, 82.

[35] Z. Zhang, C.-C. Wang, R. Zakaria, J. Y. Ying, *J. Phys. Chem. B* **1998**, *1998*, 10871.

[36] A. K. Datye, G. Riegel, J. R. Bolton, M. Huang, M. R. Prairie, *J. Solid State Chem* **1995**, *1995*, 236.

[37] C. Di Valentin, G. Pacchioni, A. Selloni, *J. Phys. Chem. C* **2009**, *113*, 20543.

[38] L. Liu, *Aerosol Air Qual. Res.* **2014**, *14*, 453.

[39] L. Liu, Y. Jiang, H. Zhao, J. Chen, J. Cheng, K. Yang, Y. Li, *ACS Catal.* **2016**, *6*, 1097.

[40] X. Xin, T. Xu, L. Wang, C. Wang, *Sci. Rep* **2016**, *6*, 23684.

[41] M. Setvin, U. Aschauer, P. Scheiber, Y.-F. Li, W. Hou, M. Schmid, A. Selloni, U. Diebold, *Science* **2013**, *2013*, 988.

[42] B. Ohtani, *Catalysts* **2013**, *3*, 942.

[43] C. Di Valentin, A. Selloni, *J. Phys. Chem. Lett.* **2011**, *2*, 2223.

[44] D. Lawless, N. Serpone, and D. Meisel, *J. Phys. Chem.* **1991**, *1991*, 5166.

[45] Z. Zhang, J. T. Yates, *J. Phys. Chem. Lett.* **2010**, *1*, 2185.

[46] L. Li, P. A. Salvador, G. S. Rohrer, *Nanoscale* **2014**, *6*, 24.

[47] Z. Zhang, J. T. Yates, *Chem. Rev.* **2012**, *112*, 5520.

[48] L. Kavan, M. Grätzel, S. E. Gilbert, C. Klemenz, and H. J. Scheel, *J. Am. Chem. Soc.* **1996**, *1996*, 6716.

[49] M. Xu, Y. Gao, E. M. Moreno, M. Kunst, M. Muhler, Y. Wang, H. Idriss, C. Wöll, *Phys. Rev. Lett* **2011**, *106*, 138302.

[50] Y. Yamada, Y. Kanemitsu, *Appl. Phys. Lett.* **2012**, *101*, 133907.

[51] G. Li, K. A. Gray, *Chem. Phys.* **2007**, *339*, 173.

[52] D. C. Hurum, A. G. Agrios, S. E. Crist, K. A. Gray, T. Rajh, M. C. Thurnauer, *J. Electron. Spectrosc. Relat. Phenom.* **2006**, *150*, 155.

[53] H. Nakajima, T. Mori, Q. Shen, T. Toyoda, *J. Chem. Phys.* **2005**, *409*, 81.

[54] D. C. Hurum, A. G. Agrios, K. A. Gray, T. Rajh, M. C. Thurnauer, *J. Phys. Chem. B* **2003**, *107*, 4545.

[55] S. C. Roy, O. K. Varghese, M. Paulose, C. A. Grimes, *ACS nano* **2010**, *4*, 1259.

[56] J. Barber, *Chem. Soc. Rev.* **2009**, *38*, 185.

[57] N. Cox, D. A. Pantazis, F. Neese, W. Lubitz, *Acc. Chem. Res* **2013**, *46*, 1588.

[58] C. A. Raines, *Photosynth. Res.* **2003**, *2003*, 1.

[59] A. Krapp, W. P. Quick, and M. Stitt, *Planta* **1991**, *1991*, 58.

[60] M. Pahle, B. Knopf, O. Edenhofer, *GAIA* **2012**, *21*, 284.

[61] G. Zhao, X. Huang, X. Wang, X. Wang, *J. Mater. Chem. A* **2017**, *5*, 21625.

[62] T. Inoue, A. Fujishima, S. Konishi, K. Honda, *Nature* **1979**, *1979*, 637.

[63] N. M. Dimitrijevic, I. A. Shkrob, D. J. Gosztola, T. Rajh, *J. Phys. Chem. C* **2012**, *116*, 878.

[64] I. A. Shkrob, T. W. Marin, H. He, P. Zapol, *J. Phys. Chem. C* **2012**, *116*, 9450.

[65] C.-C. Yang, J. Vernimmen, V. Meynen, P. Cool, G. Mul, *J. Catal.* **2011**, *284*, 1.

[66] S. G. Kumar, L. G. Devi, *J. Phys. Chem. A* **2011**, *115*, 13211.

[67] M. Che, J. C. Vedrine, *Characterization of Solid Materials and Heterogeneous Catalysts*. *From Structure to Surface Reactivity*, Wiley, Weinheim, **2012**.

[68] B. Tian, J. Zhang, T. Tong, F. Chen, *App. Catal. B* **2008**, *79*, 394.

[69] D. B. Ingram, P. Christopher, J. L. Bauer, S. Linic, *ACS Catal.* **2011**, *1*, 1441.

[70] M. Dilla, A. Pougin, J. Strunk, *J. Energy Chem.* **2016**, *26*, 277.

[71] E. V. Kondratenko, G. Mul, J. Baltrusaitis, G. O. Larrazábal, J. Pérez-Ramírez, *Energy Environ. Sci.* **2013**, *6*, 3112.

[72] A. Pougin, M. Dilla, J. Strunk, *Phys. Chem. Chem. Phys.* **2016**, 10809.

[73] S. Sato, T. Arai, T. Morikawa, *Inorg. Chem.* **2015**, *54*, 5105.

[74] L.-J. Guo, Y.-J. Wang, T. He, *Chem Rec* **2016**, *16*, 1918.

[75] J. Raskó and F. Solymosi, *J. Phys. Chem.* **1994**, *1994*, 7147.

[76] M. Gattrell, N. Gupta, A. Co, *J. Electroanal. Chem.* **2006**, *594*, 1.

[77] V. P. Indrakanti, H. H. Schobert, J. D. Kubicki, *Energy Fuels* **2009**, *23*, 5247.

[78] H.-J. Freund, M. W. Roberts, *Surf. Sci. Rep* **1996**, *1996*, 225.

[79] L.-M. Liu, P. Crawford, P. Hu, *Prog. Surf. Sci* **2009**, *84*, 155.

[80] P. Salvador, *Prog. Surf. Sci* **2011**, *86*, 41.

[81] R. Nakamura, Y. Nakato, *J. Am. Chem. Soc.* **2004**, *126*, 1290.

[82] A. Imanishi, T. Okamura, N. Ohashi, R. Nakamura, Y. Nakato, *J. Am. Chem. Soc.* **2007**, *2007*, 11569.

[83] Y.-F. Li, A. Selloni, *ACS Catal.* **2016**, *6*, 4769.

[84] C. Amatore, J.-M. Savéant, *J. Am. Chem. Soc.* **1981**, *1981*, 5021.

[85] J.-C. Wang, L. Zhang, W.-X. Fang, J. Ren, Y.-Y. Li, H.-C. Yao, J.-S. Wang, Z.-J. Li, *ACS Appl. Mater. & interfaces* **2015**, *7*, 8631.

[86] L. Liu, H. Zhao, J. M. Andino, Y. Li, *ACS Catal.* **2012**, *2*, 1817.

[87] K. Iizuka, T. Wato, Y. Miseki, K. Saito, A. Kudo, *J. Am. Chem. Soc.* **2011**, *133*, 20863.

[88] E. Korovin, D. Selishchev, D. Kozlov, *Top. Catal.* **2016**, *59*, 1292.

[89] K. Teramura, S. Iguchi, Y. Mizuno, T. Shishido, T. Tanaka, *Angew. Chem.* **2012**, *124*, 8132.

[90] J. Rossmeisl, Z.-W. Qu, H. Zhu, G.-J. Kroes, J. K. Nørskov, *J. Electroanal. Chem.* **2007**, *607*, 83.

[91] J. Petlicki, T. G. M. van den Ven, *Faraday Trans* **1998**, *1998*, 2763.

[92] W. Göpel, G. Rocker, and R. Feierabend, *Phys. Rev. B* **1983**, *1983*, 3427.

[93] E. Carter, A. F. Carley, D. M. Murphy, *J. Phys. Chem. C* **2007**, *111*, 10630.

[94] K-I. Ishibashi, Y. Nosaka, K. Hashimoto, A. Fujishima, *J. Phys. Chem. B* **1998**, *102*, 2117.

[95] R. Nakamura, A. Imanishi, K. Murakoshi, Y. Nakato, *J. Am. Chem. Soc.* **2003**, *125*, 7443.

[96] C.-C. Yang, Y.-H. Yu, B. van der Linden, J. C. S. Wu, G. Mul, *J. Am. Chem. Soc.* **2010**, *132*, 8398.

[97] http://webbook.nist.gov/cgi/cbook.cgi?ID=C7732185&Mask=4&, *12.01.2018*.

[98] M. A. Bañares, I. E. Wachs, *J. Raman Spectrosc.* **2002**, *33*, 359.

[99] N. M. Dimitrijevic, B. K. Vijayan, O. G. Poluektov, T. Rajh, K. A. Gray, H. He, P. Zapol, *J. Am. Chem. Soc.* **2011**, *133*, 3964.

[100] D. Lee, Y. Kanai, *J. Am. Chem. Soc.* **2012**, *134*, 20266.

[101] M. Anpo, H. Yamashita, Y. Ichibashi, S. Ehara, *J. of Electroanal. Chem.* **1995**, *1995*, 21.

[102] B. Mei, A. Pougin, J. Strunk, *J. Catal.* **2013**, *306*, 184.

[103] M. Salaices, B. Serrano, H.I. de Lasa, *Chem. Eng. J.* **2002**, *90*, 219.

[104] C. Zhao, A. Krall, H. Zhao, Q. Zhang, Y. Li, *Int. J. Hydrog. Energy* **2012**, *37*, 9967.

[105] Y. Li, W.-N. Wang, Z. Zhan, M.-H. Woo, C.-Y. Wu, P. Biswas, *App. Catal. B* **2010**, *100*, 386.

[106] R. Cai, Y. Kubota, T. Shuin, H. Sakai, K. Hashimoto, and A. Fujishima, *Cancer Res.* **1992**, *1992*, 2346.

[107] M. A. Fox, M. T. Dulay, *Chem. Rev.* **1993**, *1993*, 341.

[108] K. Yamakawa, Y. Sato, K. Fukutani, *J. Chem. Phys.* **2016**, *144*, 154703.

[109] L. Mino, G. Spoto, A. M. Ferrari, *J. Phys. Chem. C* **2014**, *118*, 25016.

[110] T. L. Thompson, O. Diwald, J. T. Yates, *J. Phys. Chem. B* **2003**, *107*, 11700.

[111] Z. Dohnálek, J. Kim, O. Bondarchuk, J. M. White, B. D. Kay, *J. Phys. Chem. B* **2006**, *110*, 6229.

[112] H. Belhadj, A. Hakki, P. K. J. Robertson, D. W. Bahnemann, *Phys. Chem. Chem. Phys.* **2015**, *17*, 22940.

[113] W. Lin, H. Han, H. Frei, *J. Phys. Chem. B* **2004**, *108*, 18269.

[114] H. He, P. Zapol, L. A. Curtiss, *J. Phys. Chem. C* **2010**, *114*, 21474.

[115] B. Ohtani, *J. Photoch. Photobiol. C* **2010**, *11*, 157.

[116] G. Rothenberger, J. Moser, M. Gratzel, N. Serpone, D. K. Sharmaf, *J. Am. Chem. Soc.* **1985**, *1985*, 8054.

[117] B. Ohtani, *PCCP* **2014**, *16*, 1788.

[118] D. F. Ollis, E. Pelizzetti, N. Serpone, *Environ. Sci. Technol.* **1991**, *1991*, 1523.

[119] T. Sauer, G. Cesconeto Neto, H.J. José, R.F.P.M. Moreira, *J. Photochem. Photobiol. A.: Chem.* **2002**, *149*, 147.

[120] J.-C. D'Ollvelra, G. Ai-Sayyed, P. Pichat, *Environ. Sci. Technol.* **1990**, *1990*, 990.

[121] Y. Li, S. Sun, M. Ma, Y. Ouyang, W. Yan, *Chem. Eng. J.* **2008**, *142*, 147.

[122] M. Dilla, R. Schlögl, J. Strunk, *ChemCatChem* **2017**, 696.

[123] Y.-F. Li, Z.-P. Liu, L. Liu, W. Gao, *J. Am. Chem. Soc.* **2010**, *132*, 13008.

[124] J. Tang, J. R. Durrant, D. R. Klug, *J. Am. Chem. Soc.* **2008**, *130*, 13885.

[125] F. Saladin, I. Alxneit, *Faraday Trans.* **1997**, *1997*, 4159.

[126] R. L. Kurtz, R. Stockbauer, T. E. Madey, E. Roman, J. L. De Segovia, *Surf. Sci.* **1989**, *1989*, 178.

[127] D. A. Panayotov, J. T. Yates, *Chem. Phys. Lett.* **2005**, *410*, 11.

[128] R. M. Navarro Yerga, M. C. Alvarez Galvan, F. del Valle, Villoria de la Mano, Jose A, J. L. G. Fierro, *ChemSusChem* **2009**, *2*, 471.

[129] P. Mazierski, J. Nadolna, W. Lisowski, M. J. Winiarski, M. Gazda, M. Nischk, T. Klimczuk, A. Zaleska-Medynska, *Catal. Today* **2017**, *284*, 19.

[130] M. Buchalska, M. Kobielusz, A. Matuszek, M. Pacia, S. Wojtyła, W. Macyk, *ACS Catal.* **2015**, 7424.

[131] V. M. Daskalaki, P. Panagiotopoulou, D. I. Kondarides, *Chem. Eng. J.* **2011**, *170*, 433.

[132] E. Tsuji, K.-i. Fukui, A. Imanishi, *Electrochem. Commun.* **2011**, 787.

[133] Y. Oosawa, M. Grätzel, *J. Am. Chem. Soc.* **1988**, *1988*, 197.

[134] R. S. Smith, Z. Li, L. Chen, Z. Dohnalek, B. D. Kay, *J. Phys. Chem. B* **2014**, *118*, 8054.

[135] M. Anpo, H. Yamashita, Y. Ichihashi, Y. Fujii, and M. Honda, *J. Phys. Chem. B* **1997**, *1997*, 2632.

[136] N. G. Moustakas, J. Strunk, *Chem. Eur. J.* **2018**, 12739.

[137] M. Dilla, A. Mateblowski, S. Ristig, J. Strunk, *ChemCatChem* **2017**, *6*, 4345.

[138] C. C. L. McCrory, S. Jung, J. C. Peters, T. F. Jaramillo, *J. Am. Chem. Soc.* **2013**, *135*, 16977.

[139] F. A. Frame, T. K. Townsend, R. L. Chamousis, E. M. Sabio, T. Dittrich, N. D. Browning, F. E. Osterloh, *J. Am. Chem. Soc.* **2011**, *133*, 7264.

[140] Z. Cai, Y. Bi, E. Hu, W. Liu, N. Dwarica, Y. Tian, X. Li, Y. Kuang, Y. Li, X.-Q. Yang et al., *Adv. Energy Mater.* **2017**, *355*, 1701694.

[141] H. Tüysüz, Y. J. Hwang, S. B. Khan, A. M. Asiri, P. Yang, *Nano Res.* **2013**, *6*, 47.

[142] V. Pfeifer, T. E. Jones, S. Wrabetz, C. Massué, J. J. Velasco Vélez, R. Arrigo, M. Scherzer, S. Piccinin, M. Hävecker, A. Knop-Gericke et al., *Chem. Sci.* **2016**, *7*, 6791.

[143] V. Pfeifer, T. E. Jones, J. J. Velasco Vélez, R. Arrigo, S. Piccinin, M. Hävecker, A. Knop-Gericke, R. Schlögl, *Chem. Sci.* **2017**, *8*, 2143.

[144] B. H. Meekins, P. V. Kamat, *J. Phys. Chem. Lett.* **2011**, 2304.

[145] W.-H. Ryu, Y. W. Lee, Y. S. Nam, D.-Y. Youn, C. B. Park, I.-D. Kim, *J. Mater. Chem. A* **2014**, *2*, 5610.

[146] Y. K. Kho, A. Iwase, W. Y. Teoh, L. Mädler, A. Kudo, R. Amal, *J. Phys. Chem. C* **2010**, *114*, 2821.

[147] Á. Valdés, Z.-W. Qu, G.-J. Kroes, J. Rossmeisl, J. K. Nørskov, *J. Phys. Chem. C* **2008**, *112*, 9872.

[148] W. H. Koppenol and J. D. Rush, *J. Phys. Chem.* **1997**, *1997*, 4429.

[149] S. Tan, Y. Ji, Y. Zhao, A. Zhao, B. Wang, J. Yang, J. G. Hou, *J. Am. Chem. Soc.* **2011**, *133*, 2002.

[150] Y. Du, Z. Dohnalek, I. Lyubinetsky, *J. Phys. Chem. C* **2008**, *112*, 2649.

[151] M. A. Henderson, W. S. Epling, C. H. F. Peden, C. L. Perkins, *J. Phys. Chem. B* **2003**, *107*, 534.

[152] K. Mori, H. Yamashita, M. Anpo, *RSC Adv.* **2012**, *2*, 3165.

[153] J. Yu, J. Low, W. Xiao, P. Zhou, M. Jaroniec, *J. Am. Chem. Soc.* **2014**, *136*, 8839.

[154] A. Derylo-Marczewska, W. Gac, N. Popivnyak, G. Zukocinski, S. Pasieczna, *Catal. Today* **2006**, *114*, 293.

[155] C. P. Sajan, S. Wageh, A. A. Al-Ghamdi, J. Yu, S. Cao, *Nano Res.* **2016**, *9*, 3.

[156] K. Kočí, K. Matějů, L. Obalová, S. Krejčíková, Z. Lacný, D. Plachá, L. Čapek, A. Hospodková, O. Šolcová, *App. Catal. B* **2010**, *96*, 239.

[157] Y. T. Liang, B. K. Vijayan, K. A. Gray, M. C. Hersam, *Nano letters* **2011**, *11*, 2865.

[158] S. Neatu, J. A. Macia-Agullo, P. Concepcion, H. Garcia, *JACS* **2014**, *136*, 15969.

[159] I.-H. Tseng, J. C.S. Wu, H.-Y. Chou, *J. Catal.* **2004**, *221*, 432.

[160] W. Hou, W. H. Hung, P. Pavaskar, A. Goeppert, M. Aykol, S. B. Cronin, *ACS Catal.* **2011**, *1*, 929.

[161] Q. Zhai, S. Xie, W. Fan, Q. Zhang, Y. Wang, W. Deng, Y. Wang, *Angew. Chem. Int. Ed.* **2013**, *52*, 5776.

[162] L. Zhang, H. Liu, X. Huang, X. Sun, Z. Jiang, R. Schlögl, D. Su, *Angew. Chem. Int. Ed.* **2015**, *54*, 15823.

[163] X. Liu, J. Iocozzia, Y. Wang, X. Cui, Y. Chen, S. Zhao, Z. Li, Z. Lin, *Energy Environ. Sci.* **2017**, *10*, 402.

[164] W.-J. Ong, L.-L. Tan, S.-P. Chai, S.-T. Yong, A. R. Mohamed, *Nano Res.* **2014**, *7*, 1528.

[165] T. Maschmeyer, M. Che, *Angew. Chem. Int. Ed.* **2010**, *49*, 1536.

[166] N. Serpone, *J. Photochem. Photobiol. A.: Chem.* **1997**, *104*, 1.

[167] N. Serpone, R. Terzian, D. Lawless, P. Kennepohl, G. Sauvé, *J. Photochem. Photobiol. A.: Chem.* **1993**, *1993*, 11.

[168] N. Serpone, G. Sauvé, R. Koch, H. Tahiri, P. Pichat, P. Piccinini, E. Pelizzetti, H. Hidaka, *J. Photochem. Photobiol. A.: Chem.* **1996**, *1996*, 191.

[169] M. R. Hoffmann, S. T. Martin, W. Choi, D. W. Bahnemann, *Chem. Rev.* **1995**, *95*, 69.

[170] H. Kisch, *Angew. Chem. Int. Ed.* **2010**, *49*, 9588-9590.

[171] T. Yui, A. Kan, C. Saitoh, K. Koike, T. Ibusuki, O. Ishitani, *ACS Appl. Mater. & interfaces* **2011**, *3*, 2594.

[172] A. Cybula, M. Klein, A. Zaleska, *App. Catal. B* **2015**, *164*, 433.

[173] I. Grigioni, M. V. Dozzi, M. Bernareggi, G. L. Chiarello, E. Selli, *Catal. Today* **2017**, *281*, 214.

[174] T.-V. Nguyen, J. C.S. Wu, *Appl. Catal., A* **2008**, *335*, 112.

[175] S. Ito, T. N. Murakami, P. Comte, P. Liska, C. Grätzel, M. K. Nazeeruddin, M. Grätzel, *Thin Solid Films* **2008**, *516*, 4613.

[176] Z. He, J. Tang, J. Shen, J. Chen, S. Song, *Appl. Surf. Sci.* **2016**, *364*, 416.

[177] H. Yaghoubi, Z. Li, Y. Chen, H. T. Ngo, V. R. Bhethanabotla, B. Joseph, S. Ma, R. Schlaf, A. Takshi, *ACS Catal.* **2014**, *5*, 327.

[178] V. Loddo, M. Addamo, V. Augugliaro, L. Palmisano, M. Schiavello, E. Garrone, *AIChE J.* **2006**, *52*, 2565.

[179] B. Serrano, H. de Lasa, *Ind. Eng. Chem. Res.* **1997**, *36*, 4705.

[180] C. C. Wong, W. Chu, *Chemosphere* **2003**, *50*, 981.

[181] K. Teramura, S. Iguchi, Y. Mizuno, T. Shishido, T. Tanaka, *Angew. Chem. Int. Ed.* **2012**, *51*, 8008.

[182] H. Kim, R.C.Y. Auyeung, M. Ollinger, G. P. Kushto, Z. H. Kafafi, A. Piqué, *Appl. Phys. A* **2006**, *83*, 73.

[183] D. Dan, R. C. Sandford, P. J. Worsfold, *The Analyst* **2005**, *130*, 227.

[184] Y.-C. Kim, S. Sasaki, K. Yano, K. Ikebukuro, K. Hashimoto, I. Karube, *Anal. Chem.* **2002**, *74*, 3858.

[185] F. Moulis, J. Krýsa, *Res. Chem. Intermed.* **2015**, *41*, 9233.

[186] K. Chaisiwamongkhol, N. Manoyen, K. Suttiponparnit, D. Nacapricha, S. M. Smith, K. Uraisin, *Microchem. J.* **2017**, *135*, 199.

10. Eidesstattliche Erklärung

Hiermit versichere ich, die vorliegende Arbeit mit dem Titel

„Fundamental Studies of Photocatalytic CO_2 Reduction on TiO_2“

selbständig verfasst und keine außer den angegebenen Hilfsmitteln und Quellen verwendet zu haben. Sowohl inhaltlich als auch wörtlich entnommene Stellen wurden als solche kenntlich gemacht.

Zudem erkläre ich, dass diese Arbeit nicht in dieser oder einer ähnlichen Form bei einer anderen Fakultät eingereicht wurde.

Martin Dilla

Essen, im April 2019

11. Curriculum vitae

Der Lebenslauf ist in der Online-Version aus Gründen des Datenschutzes nicht enthalten.

Scientific Contribution

Publications:

Paper
A. Pougin, **M. Dilla**, J. Strunk, "Identification and exclusion of intermediates of photocatalytic CO_2 reduction on TiO_2 under conditions of highest purity", Phys. *Chem. Chem. Phys.* **2016**, 18, 10809.

Paper
M. Dilla, A. Pougin, J. Strunk, "Evaluation of the plasmonic effect of Au and Ag on Ti-based photocatalysts in the reduction of CO_2 to CH_4", *J. Energy Chem.* **2016**, 2, 277.

Paper
M. Dilla, R. Schlögl, J. Strunk, "Photocatalytic CO_2 Reduction Under Continuous Flow High-Purity Conditions: Quantitative Evaluation of CH_4 Formation in the Steady-State", *ChemCatChem* **2017**, 9, 696.

Paper
M. Dilla, A. Matekblowski, S. Ristig, J. Strunk, "Photocatalytic CO_2 Reduction under Continuous Flow High-Purity Conditions: Influence of Light Intensity and H_2O Concentration", *ChemCatChem* **2017**, 9, 4345.

Paper
A. Pougin, G. Dodekatos, **M. Dilla**, H. Tüysüz, J. Strunk, "Au@TiO_2 Core-Shell Composites for the Photocatalytic Reduction of CO_2", *Chem. Eur. J.*, **2018**, 24, 12416-12425

Paper
M. Dilla, A. Jakubowski, S. Ristig, J. Strunk, R. Schlögl
The Fate of O_2 in Photocatalytic CO_2 Reduction on TiO_2 under Conditions of Highest Purity,
Phys. Chem. Chem. Phys. **2019**, 10.1039/C8CP07765G

Paper
M. Dilla, N.G. Moustakas, A.E. Becerikli, T. Peppel, A. Springer, R. Schlögl, J. Strunk, S. Ristig
Judging the Feasibility of TiO_2 as Photocatalyst for Chemical Energy Conversion by Quantitative Reactivity Determinants, *Phys. Chem. Chem. Phys.* **2019**, 10.1039/c9cp00981g

Communication
M. Dilla, A. E. Becerikli, A. Jakuboswki, R. Schlögl, S. Ristig, "Development of a Tubular Continuous Flow Reactor for the Photocatalytic CO_2 Reduction on TiO_2", *Photochem. Photobiol. Sci.*, **2019**, 18, 314-318

Oral presentations:

M. Dilla, N.G. Moustakas, N. Cibura, F. Katsaros, A.G. Kontos, J. Strunk, P. Falaras, "Core-Shell TiO_2 Photocatalysts for Exceptionally Efficient CO_2 Conversion to CH_4 under High Purity Conditions", The first international conference on new photocatalytic materials for environment, energy sustainability (NPM-1), Göttingen, **2016**.

M. Dilla, R. Schlögl, J. Strunk, "Fundamental studies of photocatalytic CO_2 reduction", 50. Tagung Deutscher Katalytiker, Weimar, **2017**.

M. Dilla, R. Schlögl, J. Strunk, "Fundamental Investigations of photocatalytic CO_2 reduction with TiO_2 under continuous flow conditions", Europacat, Florence, **2017**.

M. Dilla, A. Mateblowski, S. Ristig, J. Strunk, "Photocatalytic CO_2 Reduction under Continuous Flow High-Purity Conditions: Influence of Light Intensity and H_2O Concentration", Catalysis for Sustainable Chemical Energy Conversion (CSCEC), Duisburg, **2017**.

Poster presentations:

A. Pougin, **M. Dilla**, J. Strunk, "Intermediates in photocatalytic CO_2 reduction on Ti-based photocatalysts", 49. Tagung Deutscher Katalytiker, Weimar, **2016**.

A. Pougin, **M. Dilla**, J. Strunk, "Intermediates in photocatalytic CO_2 reduction on Ti-based photocatalysts", Manfred-Eigen-Gespräche, Mülheim a.d. Ruhr, **2016**.

M. Dilla, S. Ristig, R. Schlögl, J. Strunk, "Influence of reactant concentration and light intensity on methane yields in continuous-flow photocatalytic CO_2 reduction", 6th International Conference on Semiconductor Photocatalysis, Oldenburg, **2017**.

M. Dilla, S. Ristig, R. Schlögl, J. Strunk," New insights into the fate of O_2 in the photocatalytic CO_2 reduction with IrO_xTiO_2", 51. Tagung Deutscher Katalytiker, Weimar, **2018**.